Propeller selection based on real weather conditions

Maxime Steelandt

Thesis to obtain the Master of Science Degree in

Master of Science in Electromechanical Engineering (Maritime Engineering)

Advisor(s)/Supervisor(s): Prof. Evert Lataire (Ugent)
Prof. Carlos Guedes Soares (Técnico)
Dr. Roberto Vettor (Técnico)
Dr. Maxim Candries (Ugent)

Examination Committee

Chairperson: Prof. Yordan Garbatov
Advisor: Dr. Roberto Vettor
Member of the Committee: Dr. Serge Sutulo

2019 - 2020

Preface

In light of this master's dissertation, a special word of thank should be given to a number of people:

First, I would like to thank my advisor doctor Roberto Vettor for guiding and helping me. Especially for reading my texts deep at night, answering all my questions on Skype, being flexible and helping me managing my tight deadlines.

Further, I am thankful for the opportunity given by Ghent University and Instituto Superior Técnico Lisboa to do my final master year abroad and do my thesis in collaboration with both universities. This would not have been possible without professor Evert Lataire and all the other people involved in the Erasmus program. Furthermore, I would like to thank him and doctor Maxim Candries for their advice and fast replies on my emails.

Besides both universities, I am very grateful to my parents for support, motivation, removing the grammar mistakes and providing me the opportunity and the means to study at the Ghent University and abroad.

On a more personal level, there are a few people without who I probably would not have gotten here. My friends and brother at home that although being miles away were always ready for a call to motivate me especially Simon, Evelyne, Ben and Celest. But also my friends in Lisbon to go for a run and listen to my frustrations, invite me for dinner, having video call,...

Last but not least, I could never thank enough this one person without this would never been possible. Tobias, without your support and laptop, I would never been able to finish this thesis on time. Thank you!

Abstract

The maritime industry is one of the biggest consumers of fossil fuels. In 2018, the IMO (International Maritime Organisation)[1] made a long term strategy to reduce the annual amount of greenhouse gas emissions by 50% by 2050. So, the study of energy efficient ships and the factors affecting them is of paramount importance. The choice of propeller is key in order to have a ship with good efficiency. In modern shipbuilding the propeller is optimised as if the ship is sailing in still water, although most ships will barely sail in still water.

Therefore, an alternative propeller selection procedure for the Wageningen B-series propeller was developed and discussed. This selection procedure optimises the delivered efficiency in waves. The efficiency calculation is based on the simulation of the ship and propeller sailing in waves and takes into account ventilation, varying added resistance and varying wake. The last two factors were calculated by the 'quasi' regular wave approach that was proposed in [2].

The proposed selection procedure was performed for the KVLCC2 tanker and S175 container ship in several sea states. The selected propellers were compared to the propellers selected by the still water method. The differences were small and the increase of performance negligible. However, the differences could be explained by the increase of the average advance speed and the added resistance. Furthermore it was concluded that to reduce the risk of cavitation the average added resistance could be taken into account for the propeller selection in still water.

Keywords: Wageningen B-series, propeller selection, propulsion in waves, irregular waves

Resumo

A indústria marítima é um dos maiores consumidores de combustíveis fósseis. Em 2018, a IMO (Organização Marítima Internacional)[1] definiu uma estratégia a longo prazo para reduzir a quantidade anual de emissões de gases com efeito de estufa em 50% até 2050. Assim, o estudo dos navios eficientes do ponto de vista energético e dos factores que os afectam é da maior importância. A escolha do hélice é uma componente chave para ter um navio com boa eficiência. Na construção naval moderna o hélice é optimizado com o navio a navegar em águas paradas, embora a maioria dos navios mal navegue em águas paradas.

Por conseguinte, foi desenvolvido e discutido um procedimento alternativo de selecção do hélice para o hélice da série B da Wageningen. Este procedimento de selecção optimiza a eficiência do desempenho em ondas. Este cálculo da eficiência baseia-se na simulação do navio e do hélice a navegar em ondas e tem em conta a ventilação, a resistência acrescida variável e a velocidade de avanço variável. Os dois últimos factores foram calculados pela abordagem 'quasi' de ondas regulares que foi proposta em [2].

O procedimento de selecção proposto foi realizado para o navio-tanque KVLCC2 e o porta-contentores S175 em vários estados do mar. Os hélices seleccionados foram comparados com os hélices seleccionadas pelo método da água parada. As diferenças foram pequenas e o aumento do desempenho negligenciável. No entanto, as diferenças podiam ser explicadas pelo aumento da velocidade média de avanço ou pela perda de velocidade devido à resistência acrescida. Além disso, concluiu-se que, para reduzir a cavitação, a resistência média acrescentada poderia ser tida em conta para a selecção do hélice em água parada.

Contents

Abstract iii

Resumo v

Extended abstract vii

List of Tables xxi

List of Figures xxiii

Nomenclature xxvii

1 Introduction 1
- 1.1 Motivation . . . 1
- 1.2 Topic overview and objectives . . . 1
- 1.3 Structure of the dissertation . . . 2

2 Literature study 5
- 2.1 Ship resistance . . . 5
  - 2.1.1 Still water resistance . . . 5
    - 2.1.1.1 Bare hull resistance by ITTC 1978 . . . 5
    - 2.1.1.2 Holtrop and Mennen's method . . . 6
    - 2.1.1.3 Hollenbach´s method . . . 7
  - 2.1.2 Added resistance . . . 8
    - 2.1.2.1 Far-field method . . . 8
    - 2.1.2.2 Near-field method . . . 9
- 2.2 Ship motions . . . 9
  - 2.2.1 Strip theory . . . 10
  - 2.2.2 Time-domain Rankine method . . . 10
- 2.3 Propeller . . . 11
  - 2.3.1 B-series diagrams and still water propeller selection . . . 12
    - 2.3.1.1 Classic Wageningen diagrams . . . 13
    - 2.3.1.2 Efficiency maps . . . 16
  - 2.3.2 Cavitation . . . 16
    - 2.3.2.1 The phenomenon . . . 16
    - 2.3.2.2 Criteria . . . 18
  - 2.3.3 Propeller in waves . . . 20
    - 2.3.3.1 Dynamic loading . . . 20

2.3.3.2 Changing wake . . . 21
2.3.3.3 Ventilation . . . 21

3 Methodology **25**
3.1 Global power flow . . . 25
3.2 Main principle of the selection procedure . . . 26
3.3 Setup: define ship and environment . . . 27
3.3.1 Ship characteristics . . . 28
3.3.2 Boundary conditions of propeller and initial guess . . . 28
3.3.3 Sailing route . . . 28
3.3.4 Discussion of the ship characteristic calculation . . . 29
3.4 Still water propeller selection . . . 30
3.5 Propeller selection in waves . . . 31
3.5.1 Wave related input . . . 31
3.5.2 Average speed estimation . . . 31
3.5.3 Processing simulation output . . . 33
3.6 Simulation of the ship in a sea state . . . 33
3.6.1 Initialisation . . . 34
3.6.2 Simulation . . . 34
3.6.2.1 Wave parameters . . . 34
3.6.2.2 Ship motion parameters . . . 36
3.6.2.3 Thrust influencing parameters . . . 36
3.6.2.4 Ship working point . . . 37

4 Validation of the simulation code **39**
4.1 Verification of the Oosterveld polynomials . . . 39
4.2 Verification of the RAO . . . 39
4.3 Verification of the wake variation . . . 41
4.4 Verification of the still water resistance . . . 42
4.5 Verification of the added resistance in regular waves . . . 42
4.6 Verification of the torque . . . 43
4.7 Simulations in irregular sea . . . 44
4.7.1 Ventilation in irregular seas . . . 45
4.7.2 Discussion of ship's speed and delivered efficiency . . . 46

5 Propeller selection **51**
5.1 Propeller selection for the KVLLC2 . . . 51
5.1.1 Still water selection for the KVLCC2 . . . 52
5.1.2 Propeller selection of the KVLCC2 for specific sea states . . . 52
5.2 Propeller selection for the S175 . . . 53
5.2.1 Still water selection for the S175 . . . 54
5.2.2 Propeller selection of the S175 for specific sea states . . . 54

6 Conclusion **61**

Bibliography **62**

A Profile summary **67**

B Flowcharts with names of the Matlab code **69**

C Most important Matlab codes **73**

List of Tables

4.1 Ship particulars of the KVLCC2 39
4.2 Comparison of increase in mean propeller inflow due to pitch in head waves using formula and experiments 41
4.3 Comparison of the added resistance for $\lambda/L_{PP} = 0.6$ 43
4.4 Comparison between the several simulation runs and simulation periods 46

5.1 Comparison of the propeller selected by the 'fmincon'-function and by a simple Matlab code 52
5.2 Propellers selected for the KVLCC2 with still water resistance boundary conditions 53
5.3 Ship particulars of the S175 53
5.4 Sea states of the DNV North Atlantic scatter diagram with a probability of occurrence higher than 5% 56
5.5 Propellers selected for the S175 with still water resistance boundary conditions 56
5.6 Characteristics of the propeller selected for still water taking into account the average added resistance in SS2 (ADP) and propellers selected for SS2 with boundary condition including the average added resistance (SS2.1P and SS2.2P) 58

List of Figures

1.1 The effects of waves on ship propulsion 2

2.1 Ship resistance comparison for different methods for a ship of 169m [3] 8
2.2 Comparison of vertical motions: Wigley III, $Fn = 0.2$, head waves (a) Heave motion RAO and (b) Pitch motion RAO [4] 11
2.3 Comparison of vertical motions: S175 containership, $Fn = 0.25$, head waves (a) Heave motion RAO and (b) Pitch motion RAO [4] 11
2.4 Comparison of added resistance on Wigley III model: $Fn = 0.2$, head waves (a) Strip method and (b) Rankine panel method and Cartesian grid method [4] 12
2.5 Comparison of added resistance on Wigley III model: $Fn = 0.3$, head waves (a) Strip method and (b) Rankine panel method and Cartesian grid method [4] 12
2.6 Comparison of added resistance on Series 60 $C_B = 0.7$ model: $Fn = 0.222$, head waves (a) Strip method and (b) Rankine panel method and Cartesian grid method [4] 13
2.7 Comparison of added resistance on Series 60 $C_B = 0.8$ model: $Fn = 0.15$, head waves (a) Strip method and (b) Rankine panel method and Cartesian grid method [4] 13
2.8 Open water diagram for propeller B4-70. The Reynolds number is $2.72\ 10^5$ for the original data, otherwise $2\ 10^6$ [5] 14
2.9 $B_P - \delta$ diagram for propeller B4-70 [6] 15
2.10 P-J and T-J efficiency maps of the B3-50 found in [5] based on the Oosterveld polynomials [7] 17
2.11 Legend regarding P-J and T-J efficiency maps (fig. 2.10) [5] 18
2.12 Burrill cavitation diagram for uniform flow found in [8] 19
2.13 Example of a cavitation bucket diagram [8] 20
2.14 Comparison of the thrust and torque of an open propeller during ventilation [9] 23

3.1 Schematic overview of the power, efficiency and forces in a propulsion system 25
3.2 Flowchart of the propeller selection procedure in waves 26
3.3 Example of how η_0 and J found for B4-43.2 with a pitch ratio of 0.47 with the Oosterveld polynomials 29
3.4 Coordinate system (OX´Y´, Earth fixed coordinate system; oxy, ship fixed coordinate system; χ, wave encounter angle/heading [10] 29
3.5 Flowchart of the function that calculates the delivered efficiency 32
3.6 Flowchart of the simulation of the ship and propeller 35

4.1 Comparison between by code generated polynomials (left) and polynomials shown in [5](right) for the Wageningen B4-70 40
4.2 Comparison of the RAO of pitch amplitude used in the simulation (left) and used in [11](right) 40

4.3 Comparison of the RAO of relative motion amplitude used in the simulation (left) and used in [11](right) . . . 41
4.4 Comparison of the RAO of relative motion phase angle used in the simulation (left) and used in [11](right) . . . 41
4.5 Simulations of the fluctuating wake in regular waves with an amplitude of 3 meters . . . 42
4.6 Distribution of the EHP difference (%) over different speeds at design load [12] . . . 43
4.7 Comparison of the torque by the simulation code (left) and torque of the reference simulation (right) [11] for $\lambda/L_{PP} = 0.6$ . . . 44
4.8 Comparison of the torque by the simulation code (left) and torque of the reference simulation (right) [11] for $\lambda/L_{PP} = 1.1$ . . . 44
4.9 Comparison of the torque by the simulation code (left) and torque of the reference simulation (right) [11] for $\lambda/L_{PP} = 1.6$ . . . 45
4.10 Five runs in several sea states for an engine speed of $100rpm$ and the a $B4-432$ with $P/D = 0.47$ and $D = 9.86$ propeller during 120 minutes . . . 47
4.11 Ventilation loss factor in SS4 and SS5 for an engine speed of $100rpm$ and the a $B4-432$ with $P/D = 0.47$ and $D = 9.86$ propeller during 120 minutes . . . 47
4.12 Close-up of the orange run in SS5 of figure 4.11($H_s = 12.5m$ and $T_p = 12.5s$) . . . 48
4.13 Very deep close-up of the orange run in SS5 of figure 4.11($H_s = 12.5m$ and $T_p = 12.5s$) . 49
4.14 20 minute moving averages of the ship's speed . . . 49

5.1 Function value for each iteration for the propeller selection for the KVLCC2 in still water(a) and in SS2 (b) . . . 52
5.2 Speed of the S175 and the $B5-69.1$ propeller with $P/D = 0.981$ and $D = 6m$ during 120 minutes in SS2 and SS3 . . . 54
5.3 Moving averages of the ship's speed in SS3 . . . 55
5.4 Illustration of the effect by a lower pitch for the S175 . . . 57
5.5 Illustration of the effect by a lower expanded blade ratio for the S175 . . . 57
5.6 Open water curves for ADP and SS2.1P and their average advance coefficients . . . 59
5.7 Open water curves for ADP and SS2.3P and their average advance coefficients . . . 60

A.1 Profile summary of the most time consuming functions during a 120 minute simulation in average sea state . . . 67

B.1 Flowchart corresponding to figure 3.2 and representing matlab code: *'main_prop_select_waves.m'* 69
B.2 Flowchart corresponding to figure 3.5 and representing matlab code: *'calc_eta_D_and_more.m'* 70
B.3 Flowchart corresponding to figure 3.6 and representing matlab code: *'simulate.m'* . . . 71

Nomenclature

α	coefficient representing the effect of wave amplitude decrease at the stern	$[-]$
β_T	thrust loss factor	$[-]$
χ	wave encounter angle/heading	$[rad]$
$\Delta\omega$	frequency step size	$[s]$
$\Delta\overline{p}$	pressure increase due to pitching	$[Pa]$
Δt	time step size	$[rad/s]$
Δ	weight of the ship	$[ton]$
δ	inverse advance coefficient	$[-]$
ϵ	error margin	$[-]$
η_0	open water efficiency	$[-]$
$\eta_{D,r}$	delivered route specific efficiency	$[-]$
$\eta_{D,s}$	delivered sea specific efficiency	$[-]$
$\eta_{D,z}$	delivered zone specific efficiency	$[-]$
η_D	delivered efficiency	$[-]$
η_G	gearing efficiency	$[-]$
η_M	mechanical efficiency	$[-]$
η_S	shaft efficiency	$[-]$
η_T	total efficiency	$[-]$
λ	wave length	$[m]$
ν	kinematic viscosity	$[m^2/s]$
ω	wave frequency	$[rad/s]$
ω_e	encounter wave frequency	$[rad/s]$
ϕ	phase between different waves of different frequencies	$[rad]$
φ	phase of complex motion amplitude	$[rad]$
Φ_{AW}	dimensioned added resistance coefficient	$[N/m^2]$
ρ	density of water	$[kg/m^3]$
σ	cavitation number	$[-]$
σ_{AW}	added wave resistance coefficient	$[-]$
τ_C	non-dimensional propeller load	$[-]$
ζ_1	phase of surge	$[rad]$
ζ_A	amplitude of the stern wave in still water	$[m]$

A_0	propeller disk area	$[m^2]$
A_E	expanded propeller blade area	$[m^2]$
A_E/A_0	expanded blade area ratio	$[-]$
A_P	projected blade area	$[m^2]$
A_w	wave amplitude	$[m]$
B	breath of the ship	$[m]$
C_B	block coefficient	$[-]$
C_i	resistance coefficient	$[-]$
C_P	prismatic coefficient	$[-]$
d	draft of the ship	$[m]$
D	propeller diameter	$[m]$
d_A	draft of the ship at aft perpendicular	$[m]$
d_F	draft of the ship at fore perpendicular	$[m]$
D_{hub}	propeller hub diameter	$[m]$
E	height of propeller shaft above the base line	$[m]$
Fn	Froude number	$[-]$
g	gravitational acceleration	$[m/s^2]$
h_{prop}	propeller shaft submergence	$[m]$
H_s	specific wave height	$[m]$
H_w	instantaneous wave height	$[m]$
J	advance coefficient	$[-]$
k	wave number	$[-]$
K_{Q0}	open water polynomial torque coefficient	$[-]$
K_{T0}	open water polynomial thrust coefficient	$[-]$
K_Q	torque coefficient	$[-]$
K_T	common thrust coefficient	$[-]$
L_{OS}	ship length over surface	$[m]$
L_{PP}	ship length between perpendiculars	$[m]$
L_{WL}	ship length on waterline	$[m]$
L_R	ship length on run	$[m]$
M	modelled surge mass	$[kg]$
m	mass of the ship	$[kg]$
m_{11}	added mass in surge	$[kg]$
N	rotational propeller speed	$[rad/s]$
n	rotational propeller speed	$[rps]$
N_{it}	number of iterations	$[-]$
P	propeller pitch	$[m]$
P/D	pitch ratio	$[-]$
p_0	total static pressure	$[Pa]$
p_a	atmospheric pressure	$[Pa]$
P_B	brake power	$[W]$
P_D	delivered power by the shaft	$[W]$
P_E	effective power	$[W]$
P_I	indicated power	$[W]$
P_S	shaft power	$[W]$
p_s	probability of a sea state	$[-]$

P_T	delivered thrust power by the propeller	$[W]$
p_v	vapour pressure	$[Pa]$
Q	propeller torque	$[N/m]$
q	stagnation pressure	$[Pa]$
Q_{eff}	effective torque	$[N/m]$
Q_0	open water propeller torque	$[N/m]$
R	propeller radius	$[m]$
R_{Add}	added resistance	$[N]$
R_{TS}	still water resistance	$[N]$
R_T	total ship resistance	$[N]$
$RAO_{RM,P}$	RAO of the relative motion amplitude of the propeller hub	$[m/m]$
$RAO_{VM,P}$	RAO of the vertical motion at the propeller hub	$[m/m]$
RAO_i	RAO of motion i, i is a motion of choice	$[m/m]$ or $[rad/m]$
Re	Reynolds number	$[-]$
$S_{RM,prop}$	response spectrum of the relative motion amplitude of the propeller hub	$[m^2s]$
S_w	wave spectrum	$[m^2s]$
T	propeller thrust	$[N$
t	time	$[s]$
t_c	computation time	$[min]$
T_{eff}	effective thrust	$[N]$
T_0	open water propeller thrust	$[N$
T_p	peak period	$[s]$
t_s	thrust reduction factor in still water	$[-]$
t_z	time to sail in a zone	$[s]$
U	ship speed	$[m/s]$
U_a	advance velocity	$[m/s]$
U_S	service speed	$[m/s]$
V_0	relative propeller inflow velocity	$[m/s]$
w_s	wake fraction in still water	$[-]$
X	X-position of the ship in stationary reference frame	$[m]$
x_P	x coordinate of the propeller hub	$[m]$
X_z	distance to sail in a zone	$[m]$
y_P	y coordinate of the propeller hub	$[m]$
Z	number of blades	$[-]$
z_i	motion amplitude of i	$[m]$ or $[rad]$
z_P	z coordinate of the propeller hub	$[m]$

Chapter 1

Introduction

1.1 Motivation

The world today is using more resources than it can produce in a year. In 2019, all the resources available for the year were used by the 29th of July[13]. This is the so called overshoot day. Because of our growing conscience that this is not sustainable, the call for energy efficient devices is high and the world's leading research institutes are focusing on increasing efficiency in all of their facets. It is very important to utilise the energy resources with utmost care or the future world will end up with a deficiency of them. Furthermore the use of fossil fuels causes a lot of pollution, especially in ships, where more polluted fuels and less filters are used. The maritime industry, as one of the biggest consumers of fossil fuels, has been alerted to this fact. In 2018, the IMO (International Maritime Organisation)[1] made a long term strategy to reduce the annual amount of greenhouse gas emissions by 50% by 2050. So, the study of energy efficient ships and the factors affecting them is of paramount importance.

Most ships these days use a single open propeller with constant pitch in combination with a diesel engine as means of propulsion. The choice of propeller is key in order to have a ship with good efficiency. In modern shipbuilding the propeller is optimised as if the ship is sailing in still water, although most ships will barely sail in still water. The effect of waves on the propeller is yet to be clearly understood. However, it has been observed that the propeller reacts to the time varying flow field encountered in waves, and it would be useful to consider the effect of waves on the propeller already in the design stage. In case of propeller emergence, when the propeller is coming close to the water, the propeller thrust and torque drop significantly. Furthermore, the resistance of the ship varies when the ship is encountering waves. Some research has already been conducted regarding those influences and some models were proposed. Yet, these models have not been implemented in the selection procedure of a propeller. Using this knowledge in the selection of propellers in waves could help to reach the goals set by the IMO.

1.2 Topic overview and objectives

In this thesis an alternative propeller selection procedure for single open propellers with constant pitch is developed and discussed. In this procedure the focus is put on the hydrodynamic aspects of the propeller. However, some other aspects are not considered such as the increase of ship resistance of its service life. The selection is carried out for the Wageningen B-series propellers with the help of the built-in Matlab function *'fmincon'* which optimises the delivered efficiency in waves. The delivered

efficiency in waves is calculated by a custom built Matlab function. This function simulates the ship and propeller sailing in waves in time and space domain and takes into account several effects of waves on the propulsion. An overview of the effects of waves on the performance is shown in figure 1.1. The effects shown in grey are not modelled in the proposed selection method due to their complexity and sometimes limited influence. The varying wake and added resistance are calculated by the 'quasi' regular wave approach as proposed in [2]. Inspiration of the time domain simulation is taken from [11], which is also the main reference used to validate the simulation code.

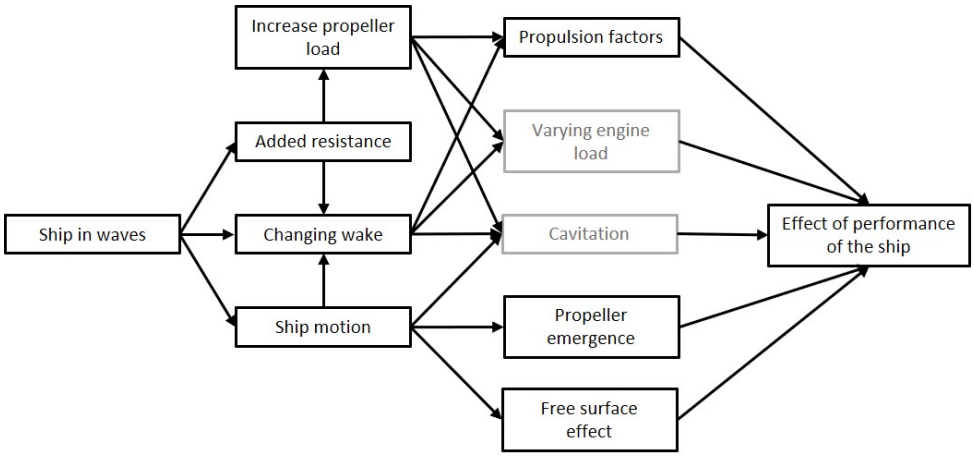

Figure 1.1: The effects of waves on ship propulsion

The selection, and thus also the simulation, is made in such way that it can run for regular or irregular waves. Furthermore, the simulation also works for a sequence of different wave profiles to allow the selection based on a scatter diagram. In order to execute the selection code the ships characteristics are required. These are calculated by a code developed at CENTEC which has been used previously used in [14] and [15]. This code computes three types of characteristics:

- **Still water resistance** according to [16]
- **Ship motions in the frequency domain** according to the strip theory as formulated in [17].
- **Added resistance in head and bow waves** according to the far-field theory as formulated in [18].

This alternative selection procedure is used to select the optimal propeller for the KVLCC2 tanker and the S175 container-ship for different sea states. These propellers are compared to the optimal in still water. The aim of this alternative selection procedure is to increase the real life efficiency of the ship.

1.3 Structure of the dissertation

The dissertation has four main parts and a conclusion. These main parts are the literature study, methodology and validation of the simulation code and propeller selection.

The studied literature is first of the four chapters. In this chapter the different elements of the power flow are discussed. The discussion is focused on how they are influenced by the waves and how they can be modelled. These different models are compared by their advantages, disadvantages and usage.

Based on the literature, an alternative propeller selection procedure is proposed. This is covered in chapter 3, where the proposed procedure is also further clarified and implemented in a Matlab code.

In the following chapter (ch. 4) the code is validated by comparing simulation results of the KVLCC2 to results found in the literature.

In chapter 5 the propeller selection procedure is applied for several irregular sea states for the KVLCC2 and the S175. For latter, a propeller is also selected based on the DnV North Atlantic scatter diagram. Conclusions and recommendations are given in chapter 6.

Chapter 2

Literature study

In the literature study three key elements of the ship-propeller performance in waves are studied: ship resistance, ship behaviour in waves and propeller.

2.1 Ship resistance

The resistance of a ship is more or less proportional to U^2 and depends on the sea state. Therefore the calculation of the total hull resistance (R_T) is split in two parts [8]: the resistance in still water (R_{TS}) and the added resistance (R_{Add}) due to waves, wind, current and other external factors. R_T is then found by adding up both terms. Naturally, this section is split into two subsections; the still water resistance and the added resistance.

2.1.1 Still water resistance

The resistance in still water can be estimated by different methods for example: ITTC 1978, Holtrop and Mennen's Method, Hollenbach's method and CFD methods. The first three methods are empirical/experimental methods. In most papers where the propeller in waves or fuel consumption in waves is studied, CFD methods are not used. Therefore no further attention is given to the CFD based methods. Some examples of such papers are: [19], [20] and [21]. It must be said that when papers are focused on the resistance in waves CFD based methods are often used as in [22].

2.1.1.1 Bare hull resistance by ITTC 1978

This method [23] is used to calculate the resistance of a ship based on towing tank data. This data can be from a parent model in a data base or by carrying out a towing test with a model of the ship.

The resistance of a scale model can not be scaled straight forward, because the Reynolds similarity is not obeyed. The ITTC '78 method gives a suggestion on how this conversion can be done. In order to use this method the model and ship should have the same shape and fulfil the Froude similarity ($Fr = \frac{U}{\sqrt{gL_{PP}}}$).

Generally the ITTC'78 method is only used in the last phases of ship design because towing tests are expensive and time-costly, yet accurate. When performing a towing test the model can not be too big with respect to the towing tank otherwise the blockage effect disturbs the results [24]. In research it is often used to verify other resistance calculation methods e.g. in [25] where this method is compared to

a new proposed CFD method and full scale ship trial measurements. [3] also used it when comparing different methods to determine the still water resistance.

2.1.1.2 Holtrop and Mennen's method

This method is a statistical method based on data of 334 models and data of full ships. The model tests were mostly carried out at MARIN. Based on the gathered data regression analyses were carried out. The method is fully described in [26], [16] and [27]. The base formula is as follows:

$$R_{TS} = R_V + R_W + R_A + R_{APP} + R_B + R_T R + R_A \tag{2.1}$$

with

- R_V representing the viscous resistance
- R_W representing the wave resistance (wave-making + wave-breaking)
- R_{APP} representing the resistance of the appendages
- R_B representing the additional pressure resistance of bulbous bow
- R_{TR} representing the additional pressure resistance of transom stern
- R_A representing the model-ship correlation allowance

R_V is found by:

$$R_V = (1 + k_1) R_F \tag{2.2}$$

where R_F is the frictional resistance found by the ITTC 1957 line given in equation 2.3 and k_1 is the form factor for the bare hull, and is calculated using equation 2.4.

$$\begin{aligned} C_F &= \frac{0.075}{(\log Re - 2)^2} \\ Re &= \frac{V L_{PP}}{\nu} \end{aligned} \tag{2.3}$$

$$1 + k_1 = 0.93 + 0.4871 c_{14} \Big(\frac{B}{L_{WL}}\Big)^{1.0681} \Big(\frac{d}{L_{WL}}\Big)^{0.4611} \Big(\frac{L_{WL}}{L_R}\Big)^{0.1216} \Big(\frac{L_{WL}^3}{\Delta}\Big)^{0.3649} (1 - C_P)^{-0.6042} \tag{2.4}$$

In this formula c_{14} takes into account the shape of the stern, L is the length of the waterline, L_R is the length of run and C_P is the prismatic coefficient.

R_W, R_{APP},... are also calculated with empirical formulae, these can be found in the original papers mentioned earlier in this paragraph.

The advantage of this method, compared to the ITTC 78, is that there is no need to have towing tank data as only the main parameters of the ship are needed. This means that this method can be calculated without extra expenses and already in early design phases which is where it is commonly used. The method is only valid within certain boundaries of speeds and hull shapes, as this method is based on regression analyses.

This method is often used in papers such as [20] where the method is used to calculate the still water resistance of a ship in order to estimate the speed loss and CO_2 emissions caused by a sea way. As the still water resistance is not influenced by the sea, it was not necessary to have a more accurate

method. In [19] where the influence of engine control on the fuel consumption is studied, this method is also applied.

2.1.1.3 Hollenbach´s method

Just like the previous method, Hollenbach's method [28] is an empirical method aimed for the use in preliminary design. This method includes an estimation for the resistance of twin-screw ships while the one discussed above does not. The method is based on 433 model tests carried out in the Vienna ship model basin. 3 different formulae/curves are given by the method, namely a best fit curve and a lower envelope. The last one gives the minimum a designer might achieve after extensive optimisation of the ship lines. Next to that it gives an estimation for the maximal resistance based on the best fit curve. This could be of use for ships with several design constraints. Moreover, the method does not use a form factor and the total resistance is given by:

$$R_{TS} = R_F + R_R \tag{2.5}$$

R_R is the residual resistance which is calculated as follows:

$$R_R = C_R \frac{1}{2} \rho U^2 \frac{Bd}{10} \tag{2.6}$$

In formula 2.6 $\frac{Bd}{10}$ is used instead of the more often used wetted surface. This was done because in the preliminary phase the wetted surface is not known. This remark should also be taken into account for the calculation of R_F based C_F that is defined by the ITTC '57 line (equation 2.3). C_R is given by:

$$\begin{aligned} C_R =& C_{R,standard} C_{R,Fnkrit} k_L \Big(\frac{d}{B}\Big)^{b_1} \Big(\frac{B}{L_{PP}}\Big)^{b_2} \Big(\frac{L_{OS}}{L_{WL}}\Big)^{b_3} \Big(\frac{L_{OS}}{L_{PP}}\Big)^{b_4} \Big(1 + \frac{d_A - d_F}{L_{PP}}\Big)^{b_5} \\ & \Big(\frac{d}{d_A}\Big)^{b_6} (1 + N_{Rudd})^{b_7} (1 + N_{Brac})^{b_8} (1 + N_{Boss})^{b_9} (1 + N_{Thruster})^{b_{10}} \end{aligned} \tag{2.7}$$

In this formula L_{OS} is used next to L_{PP} and L_{WL}. L_{OS} is the length over surface and is defined as the length between aft end of the waterline (excluding the rudder) and the most forward point of the ship below the waterline. The formula N_i represents the number of 'i' on the ship. The other symbols are defined in the nomenclature or are defined by other formula or tables that are given in [28].

This method is the most modern empirical method. In [3] the method is compared to Holtrop and Mennen's method, and the calculations based on the potential flow with the results of the towing test. The paper used NavCad for the resistance calculations with the Holtrop en Mennen's method and use a self-made own code for the Hollenbach's method as it is claimed Hollenbach's is easy to code.

A comparison of the total resistance, residual resistance and wave making resistance is shown in figure 2.1. On the graph it can be seen that residual resistances, calculated according to the Holtrop and Mennen's Method and to Hollenbach's methods, are in close alignment with the residual resistance obtained from the model test. The Hollenbach's method gives the values, which are in better agreement, particularly at higher speeds. The biggest differences can be seen for the total resistance. When using Hollenbach's method for the maximum total resistance instead of the best fit, there is not such a big difference between the model test. In [3] it is suggested that the reason for this is that the tested hull was designed with several restrictions.

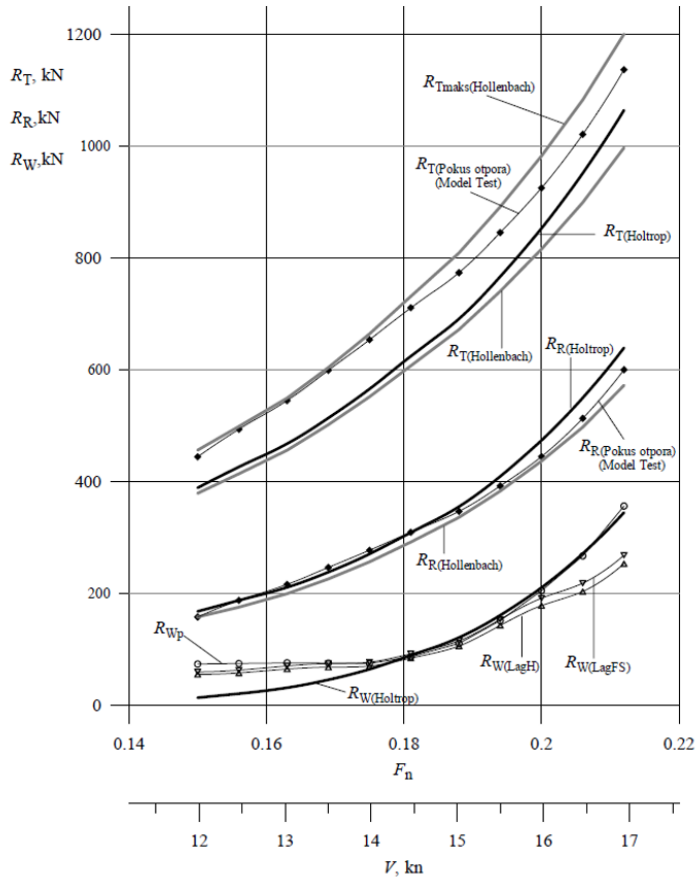

Figure 2.1: Ship resistance comparison for different methods for a ship of 169m [3]

2.1.2 Added resistance

Depending on which environment the ship is sailing, the ship will have more or less resistance compared to the still water resistance. In [19] is was concluded that the effect of the wind is negligible in comparison to the effect of waves on the resistance. Other factors that influence the resistance are current, depth and width of the waterway. The current causes a difference between the speed over ground and the speed in water of the ship. This will not be studied further because no current is assumed in this thesis. In confined water there is an increase of resistance because the water is limited in its movement around the ship. In this thesis the ship is assumed to be sailing at sea where the water is free to move and the deep water assumption is valid. Therefore, the confined waters effect will not be studied either.

The only added resistance that is significant at sea is the one caused by waves. From here on-wards when the added resistance is mentioned, this refers to the added resistance in waves. The added resistance of waves can be calculated by different methods. There are two main analytical methods that are widely used in literature: the far-field method and near-field method.

2.1.2.1 Far-field method

The far-field method is based on the conservation of momentum in the fluid around the ship and was introduced in [29]. The principle of the method is that the mean force acting on the ship should be equal to the momentum generated by the ship evaluated across a control surface far away from the ship. A simplified method, based on the radiated wave energy, was proposed in [30]. This method was then

extended in [31]. Later in [18], [30] was applied using the basic results of the STF. The strip theory is studied in section 2.2. This combination of STF and [30] gave quite satisfactory results in [4].

The far-field approach was applied in [32], using frequency domain and more advanced time domain potential codes for the solution of the sea-keeping problem.

The extended method was used in [11] in a study over the effect of waves on engine-propeller dynamics and propulsion performance of ships. In this paper the ship motion RAO's were computed using strip theory, potential theory and pressure integration, implemented in the *ShipX Veres* software.

In general these far-field methods are simple because the boundary value problem should be solved completely to find the body pressure which makes this method popular. The disadvantages of this method is that the it's not very intuitive and has limitations regarding the handling of a control surface. Furthermore, it also has some stability issues in following and quartering seas. It is also not suited for multi body problems (eg. catamaran, trimaran) because the mutual influence of the bodies is not properly taken into account.

2.1.2.2 Near-field method

The near-field method is based on a direct second order integration of the hydrodynamic pressure acting on the wetted surface of the hull. This method was introduced in [33], where only the pressure induced by the incident wave according to the Froude-Krylov approach is considered. This near-field method was extended in [34], where a more advanced formulation based on the full Bernoulli equation was proposed. However, the method does not include all the terms. Later on, in [35] and in [2] a 3D formulation that is exact to the second order for the zero-speed and forward speed cases was proposed. In [35] only long wave lengths (more than half of the ship length) were studied and the focus was put on floating structures. In [2] on the other hand a method for wavelengths shorter than half of the ship length was proposed and the paper focused on ships in particular. The behaviour of the ship in waves with a small wavelength is different as the ship has a more asymptotic behaviour. In those waves the ship behaves more as a wall in the water as there is almost no ship motion due to the waves. This method is only accurate for blunt shapes [4]. In [36] a semi-empirical formula for the case of short wavelengths was derived, this formula has the same drawbacks as the short wavelength method given in [2]. In [37] semi-empirical formula given is [36] was improved based on experimental data.

In [20], where the speed loss and added CO^2 emissions in a seaway are estimated, the method given in [2] is used to calculate the added resistance for small and big wavelength. The study focused on estimating the effect due to the propeller and engine in the sea state.

The advantage of these near-field methods is that they are more intuitive to understand the under-laying physical phenomenon than the far-field method. Furthermore, they are extendable to multi-body or non-linear problems. A disadvantage is that these method require more computer power which used to be problem in the past.

2.2 Ship motions

In order to calculate the added resistance not only the wave properties should be known but also the ship motions. There are multiple methods to estimate the ship motions, for example the frequency-domain strip method and the time-domain Rankine method.

2.2.1 Strip theory

The frequency-domain strip (STF) method was proposed in [17] and is still widely used because of its simplicity and good results. The strip theory considers a ship structure as a finite amount of 2D strips attached to each other. Each strip has the shape of a certain segment of the ship and is analysed in the frequency domain as an infinite long floating shape. Afterwards this information is combined to have the properties and behaviour of the complete ship. This reduces the problem from a 3D problem to a 2D problem which is easier to solve. This method also makes some simplifications which imposes the following limitations:

- The hull should be slender so the normal vector is in the 2D surface for each strip.
- Due to the 2D approximation, it is impossible to calculate the surge motions with this theory.
- Frequency of oscillation is high , however, this is not a big problem as the low frequency external forces are dominated by Froude-Krilov diffraction and restoring forces.
- Incident waves and motions are of small amplitude.
- The ship's forward speed is low as the forward speed effects are introduced in a simplistic way namely only by the angle of attack.
- The hull has vertical sides around the still waterline.

In general the method is good for estimating the vertical motions, for the horizontal motions some caution should be taken. Because the ship motions have a linear behaviour, superposition is possible to calculate the motion in irregular waves. A problem with the strip method might arise with following and quartering waves as the encounter frequency can become zero or negative.

2.2.2 Time-domain Rankine method

The Rankine method is a 3D method based on the potential theory. The method is well described in [4], where the method is compared with the strip method, the Cartesian grid method and experiments or the ship motions in waves. The comparison is shown in figures 2.2 and 2.3. Based on these results, it was concluded that the differences are small yet the peak of the strip theory is slightly moved towards a higher frequency and the Cartesian peak towards a lower frequency.

Furthermore the strip method and the Rankine method were combined with a far- and near-field method in that paper. This was done in order to compare the results for added resistance for different ship models at different speeds. Some of the results are shown in figures 2.4 and 2.5. Based on these graphs and the other data, the following conclusions were made:

- In the low speed case, the results of the different methods are similar and agree with the experimental data.
- In the high speed case, small discrepancies among the numerical results are shown. In particular, the peak value frequency of the strip method is slightly shifted to the short wave region. The reason for this is that the effect of the ship speed cannot be exactly accounted for.
- Generally the added resistances calculated by strip methods show reasonable correspondence with the experimental data expected for short waves. Some discrepancy is present when the ship speed is high, and the ship has a relatively blunt body. Therefore, the strip theory is a good practical tool when the bow shape is not too blunt, the ship speed is not very high and if it is combined with an appropriate approximation method for short wave range.

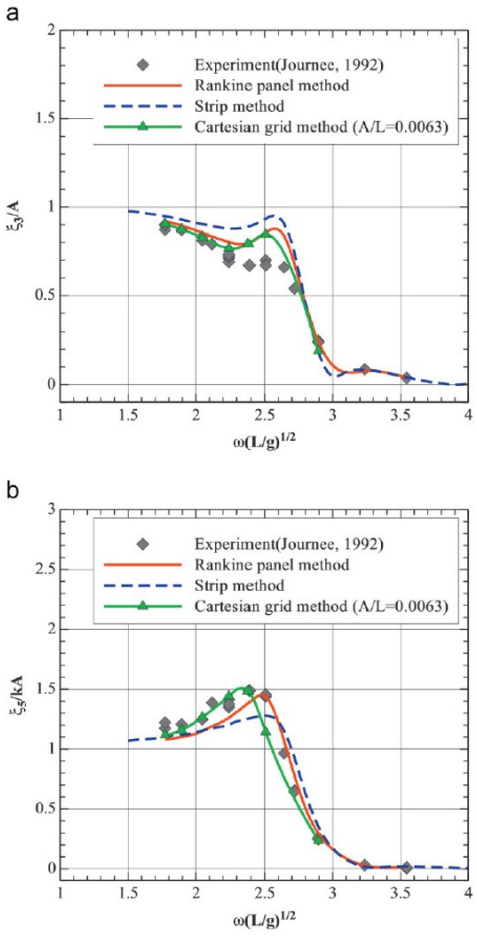

Figure 2.2: Comparison of vertical motions: Wigley III, $Fn = 0.2$, head waves (a) Heave motion RAO and (b) Pitch motion RAO [4]

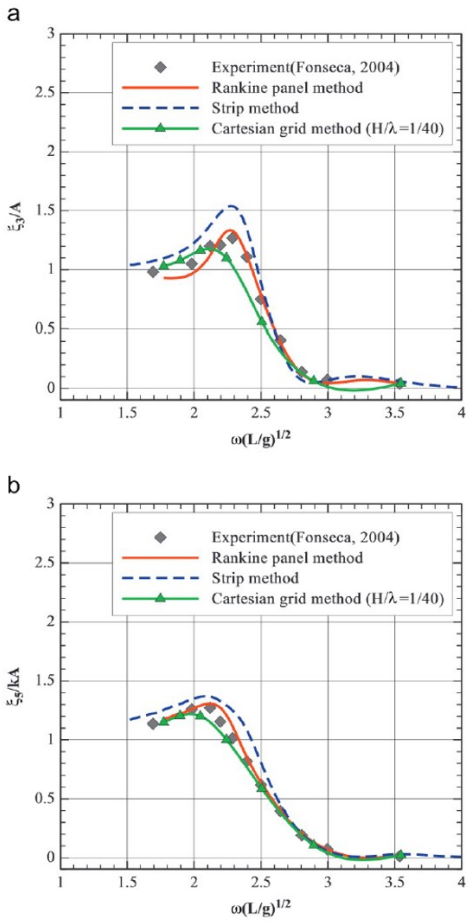

Figure 2.3: Comparison of vertical motions: S175 containership, $Fn = 0.25$, head waves (a) Heave motion RAO and (b) Pitch motion RAO [4]

In addition the strip method and Rankine method with the different methods for short waves were compared. Some of these results are shown in figures 2.6 and 2.7. Based on these graphs and the the other data, it was concluded that only the method given in [37] gave reasonable results for slender ships. For blunt ships the method described in [36], in [2] and in [37] all gave reasonable results.

2.3 Propeller

The propeller for the ship can be chosen in several ways. A specific propeller can be designed or a propeller can be selected from a standard series. If a specific propeller is designed, the design is often tested according to the ITTC 1978 recommendations [23] to verify the efficiencies. In the scope of this dissertation only the standard series are further studied.

There are multiple propeller setups possible on a ship: single screw, multiple screw, ducted propeller, azimuth thruster,... In this thesis the ship has a single open screw propeller because this is the most common on normal commercial vessels for transportation of goods. Furthermore this thesis assumes the vessel to be sailing at conventional speeds during a voyage, so it is reasonable to assume that the propeller is only operating in the first quadrant ($U_a > 0, T > 0$).

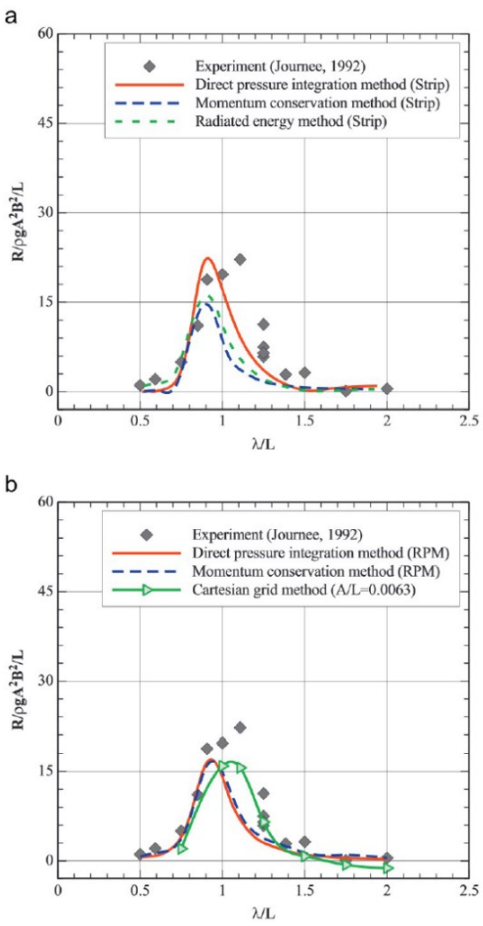

Figure 2.4: Comparison of added resistance on Wigley III model: $Fn = 0.2$, head waves (a) Strip method and (b) Rankine panel method and Cartesian grid method [4]

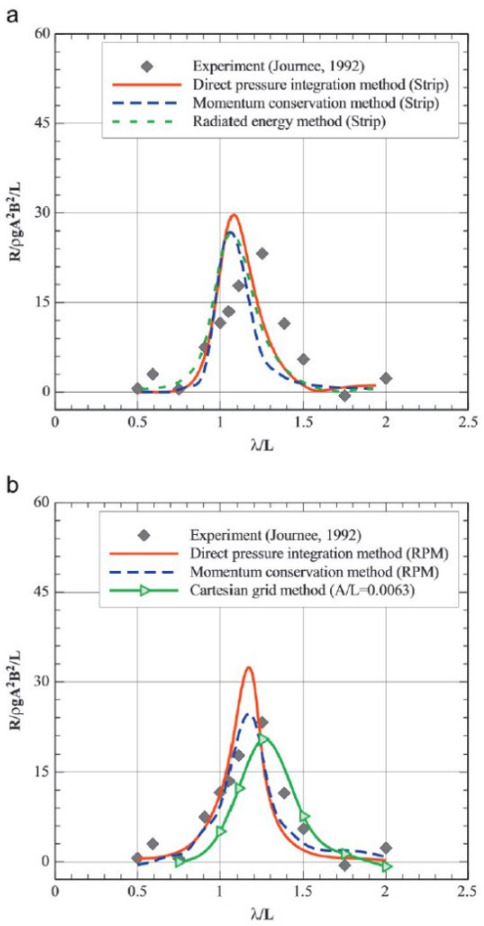

Figure 2.5: Comparison of added resistance on Wigley III model: $Fn = 0.3$, head waves (a) Strip method and (b) Rankine panel method and Cartesian grid method [4]

This section is split into three subsections:

- **B-series diagrams and still water propeller selection** in which the Wageningen diagrams are discussed and the way these diagrams are used to select a propeller in still water.
- **Cavitation** in which cavitation and different criteria are studied.
- **Propeller in waves** in which the behaviour of the propeller in waves and it's influence on the propeller efficiency is studied.

2.3.1 B-series diagrams and still water propeller selection

Depending on the ship a standard propeller is chosen. There are multiple standard series of which the Wageningen B-screw series is the most extensive and used series. This series was tested at MARIN (Maritime Research Institute Netherlands), the tests were presented in [38], [39] and [40] . There were some irregularities in this series mostly due do scaling factors, these were corrected in [41]. The series has three sub series: the A, B and C. The C series is for controllable pitch propellers and is not discussed further. The A-series consist of propellers with wing profile blade sections, narrow blades and with a high open water efficiency. These propellers are only suited for low thrust coefficient due to sensitivity to cavitation. The B-series has wider blades near the tip and circle segment shapes for $r > 0.8R$.

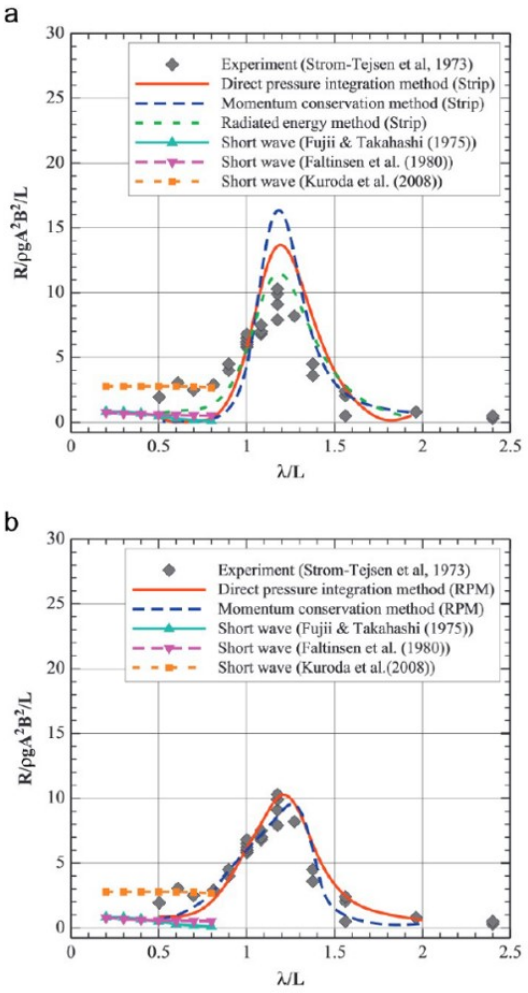

Figure 2.6: Comparison of added resistance on Series 60 $C_B = 0.7$ model: $Fn = 0.222$, head waves (a) Strip method and (b) Rankine panel method and Cartesian grid method [4]

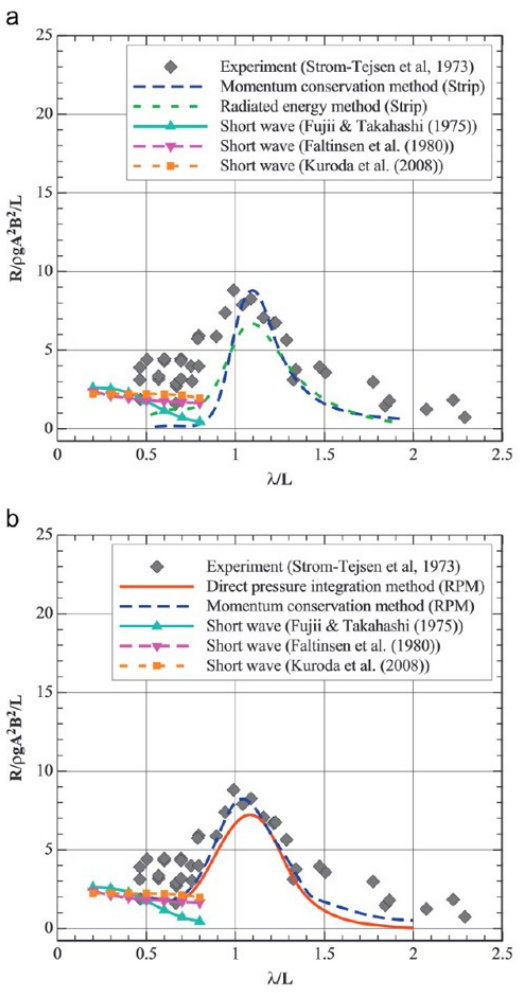

Figure 2.7: Comparison of added resistance on Series 60 $C_B = 0.8$ model: $Fn = 0.15$, head waves (a) Strip method and (b) Rankine panel method and Cartesian grid method [4]

This reduces the risk of cavitation and singing of the propeller. For this reason the B-series is further investigated. The propellers in this series are denoted as *X Z-00* in which X is A,B or C defining the subseries, Z the number of blades and 00 is equal to A_E/A_0 in percentage. In [41] polynomials are also given that fit the Wageningen B-screw series. Later in [7] another set of polynomials were proposed which are used nowadays [5]. These polynomials are often called the Oosterveld polynomials.

2.3.1.1 Classic Wageningen diagrams

The Wageningen B standard series originally provided three different open water graphs:

- K_T,K_Q and η_0 as ordinates with J as abscissa and P/D as parameter. P/D is the pitch ratio and J is the advance coefficient defined as:

$$J = \frac{U_a}{nD} \tag{2.8}$$

  The types are called $K_T - J$ or $K_Q - J$ diagrams, an example of such a graph is shown in figure

2.8. K_T and K_Q are defined as follow:

$$K_T = \frac{T}{\rho D^4 n^2}$$
$$K_Q = \frac{Q}{\rho D^5 n^2} \tag{2.9}$$

To avoid confusion in later parts of this section, we will use K_{T0} and K_{Q0} to refer to K_T and K_Q of the open water diagrams. As consequence the open water efficiency can also be found as follow:

$$\eta_0 = \frac{JK_{T0}}{2\pi K_{Q0}} \tag{2.10}$$

It can be seen that for fixed pitch open propellers the K_{T0} and K_{Q0} curve are similar, for example on fig. 2.8. In [42] is was showed that this is true by showing that for a given propeller, a change ΔK_{Q0} of K_{Q0} implies a proportional change ΔK_{T0} of K_{T0} by formula 2.11.

$$\Delta K_{T0} = c_t \Delta K_{Q0}$$
$$\implies K_{T0} = b_t + a_T K_{Q0} \tag{2.11}$$

Where a_t, b_t and c_t are constant for fixed pitch propellers. This was applied in [43], where full-scale experimental results are provided to show that this relationship is stable for a large range of propeller operating conditions, including varying advance ratios, in waves and for a propeller behind the ship.

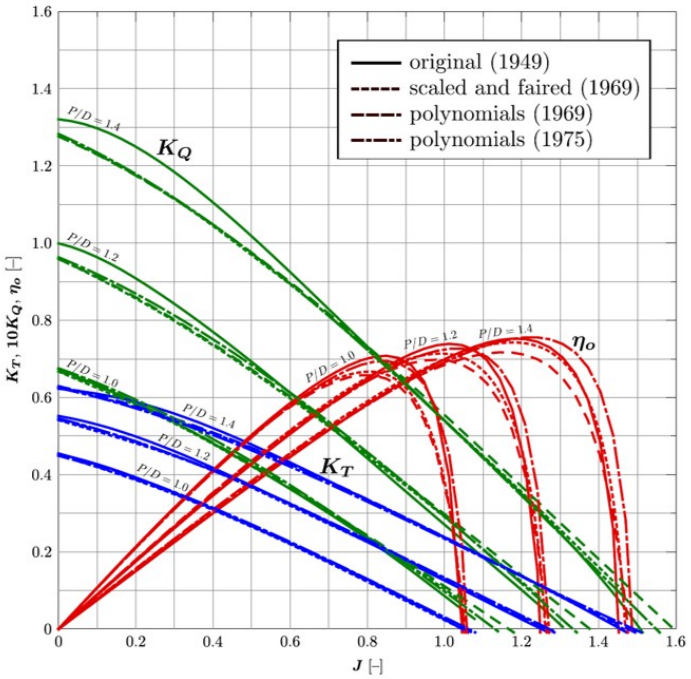

Figure 2.8: Open water diagram for propeller B4-70. The Reynolds number is $2.72\ 10^5$ for the original data, otherwise $2\ 10^6$ [5]

- P/D as ordinate, $K_{Q0}^{\frac{1}{4}} J^{\frac{-5}{4}}$ as abscissa and $1/J$ and η_0 as parameters.
- P/D as ordinate,$K_{Q0}^{\frac{1}{4}} J^{\frac{-3}{4}}$ as abscissa and $1/J$ and η_0 as parameters.

The last two graphs are commonly referred to as $B_P - \delta$ diagrams, an example is shown in figure 2.9. δ

is the inverse advance coefficient $(1/J)$. These diagrams can be used to select the best propeller for a ship. $K_{Q0}^{\frac{1}{4}} J^{\frac{-5}{4}}$ is used to find the optimal diameter if the propeller speed is fixed and known. When the propeller diameter is fixed, $K_{Q0}^{\frac{1}{4}} J^{\frac{-3}{4}}$ can be used to find the optimal propeller speed.

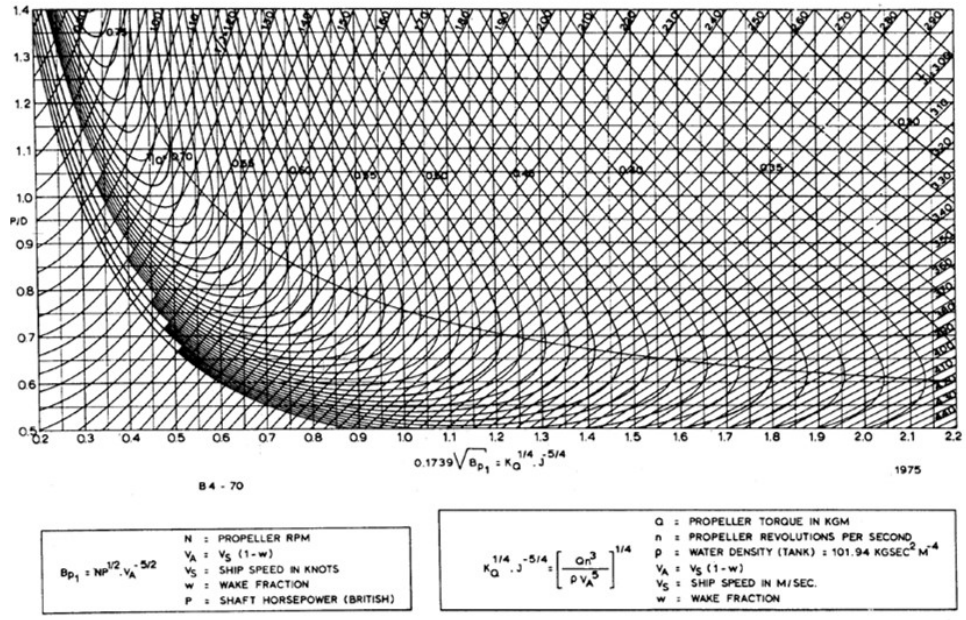

Figure 2.9: $B_P - \delta$ diagram for propeller B4-70 [6]

The best propeller to match the ship based on these graphs can be found by repeating the next procedures for a set of propellers with a different number of blades(Z) and A_E/A_0 ratio. The limits of Z and A_E/A_0 are defined vibration, noise and cavitation criteria. To find the best propeller for a given Z and A_E/A_0 the following procedure is often used:

- **Determination of optimal propeller diameter**:

  1. Define P_E by calculating R_T for the speed where the optimum should be found. In this point the characteristic is linearised as such that U is proportional to n.
  2. Calculated η_D. If it is the first estimation, a value between 0.7 and 0.75 is taken.
  3. Calculate P_D.
  4. If needed redefine the engine if the required maximal engine power is not close to the one of the engine.
  5. Calculate n with the propeller law:
  $$\frac{P_D}{n^3} = C \tag{2.12}$$
  6. Estimate the wake factor based on towing test of empirical.
  7. Calculate U_a.
  8. Determine $K_{Q0}^{\frac{1}{4}} J^{\frac{-5}{4}}$ by:
  $$K_{Q0}^{\frac{1}{4}} J^{\frac{-5}{4}} = \Big(\frac{P_D n^2}{2\pi\rho U_a^5}\Big)^{\frac{1}{4}} \tag{2.13}$$
  9. Use the graph to find η_0, P/D and $delta$.

10. Calculate D_0 based on δ by equation 2.8. In this calculation a uniform wake is assumed. A slightly smaller diameter can be chosen to compensate for this assumption[6]. The smaller diameter is found by taking a percentage of the diameter $(4 - 8\%)$ or taking a percentage of δ_0 before calculating the diameter.

11. Verify if D is within the limitations ($D < 0.65d$,cavitation criteria,...). If D is too big take the maximal D possible within the limits. From this calculate J and find $\eta_{0,max}$ and P/D from the diagram.

12. If the new η_D based on the found η_0 is far from the estimate η_D then iterate.

- **Determination of optimal propeller speed:** The working method is analogue for the determination of the optimal diameter but $K_{Q0}^{\frac{1}{4}} J^{\frac{-3}{4}}$ is used instead of $K_{Q0}^{\frac{1}{4}} J^{\frac{-5}{4}}$ because this is equal to:

$$K_{Q0}^{\frac{1}{4}} J^{\frac{-3}{4}} = \Big(\frac{P_D}{2\pi\rho D^2 U_a^5} \Big)^{\frac{1}{4}} \tag{2.14}$$

  n is then found by finding δ in the diagram.

2.3.1.2 Efficiency maps

Nowadays alternative representations of the $B_P - \delta$ diagrams are also used. These are called efficiency maps [5]. The first type of efficiency maps showed the T_D and T_{n0} curves in the $K_T - J$ ordinates and P_{D0} and P_{n0} curves in the $K_Q - J$ ordinates. Subscript n0 means T in still water for constant rotational speed. Similar D represents diameter. Later in [44] the P_{D0} and P_{n0} curves were put on the $K_T - J$ and vice versa. In these diagrams the η_0 and P/D curves are also shown. This makes it easier to select a propeller as all the needed information is shown in one graph. The use of these graphs is not complicated as is explained in detail in [5]. Furthermore, lines with the maximal open water efficiency for constant J, P/D and P_D & P_n or T_D & T_n are also plotted depending on the graph. Such types of diagrams are called Danckwardt, an example is shown in figure 2.10, a legend of the figure is shown in figure 2.11. The $K_Q - J$ is used if the thrust is known and $K_T - J$ is used if the power or torque is known. In order to avoid confusion with the original $K_T - J$ and $K_Q - J$ diagrams, the $K_T - J$ is called $P - J$ referring to the use when the power is known and $K_Q - J$ is called $T - J$ referring to the use when the torque is known.

In [5] it is was noticed that in these diagrams some $\eta_{0,max}$-lines curved back resulting in possibilities of finding multiple optimums or no optimum at all. This is not the case in the original Danckwardt curves. A physical explanation for the backwards curving could not be given however it was proposed that the use of polynomials is the reason. As the polynomials cause some mistakes because they are based on re-scaling of the original B-series data to the same Reynolds number.

Next to the advantages of having all the needed data in one diagram for selecting an optimal propeller, the Danckwardt diagrams also include the situation of bollard pull which is not included in the original $B_P - \delta$ diagrams. In the original $B_P - \delta$ diagrams δ is used instead of J, as a consequence bollard pull is at infinite.

2.3.2 Cavitation

2.3.2.1 The phenomenon

Cavitation normally occurs on light or heavy loaded propellers. In light loading conditions cavitation occurs in case of a negative inflow angle for some blade sections. This creates cavitation at the pressure

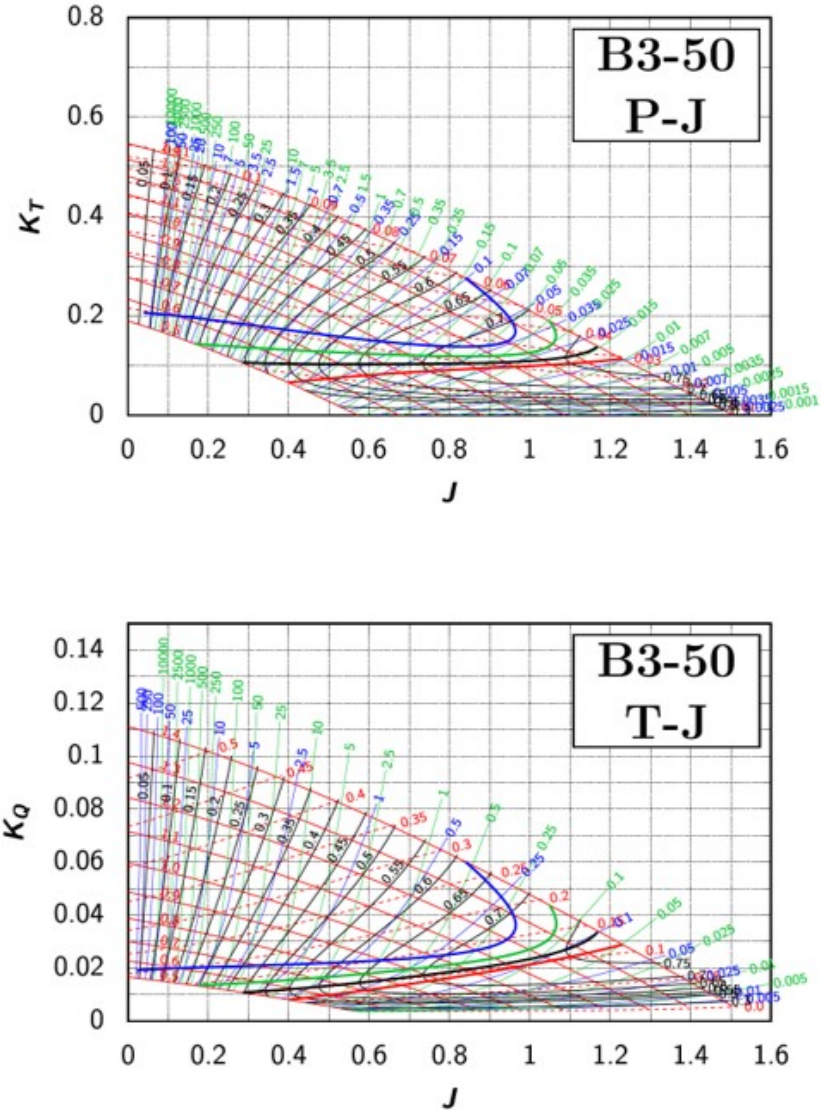

Figure 2.10: P-J and T-J efficiency maps of the B3-50 found in [5] based on the Oosterveld polynomials [7]

side close to the leading edge. It will disappear if the loading increases. In heavy loading conditions the cavitation is at the suction side near the blade tips which often leads to visible tip vortexes. If the loading increases the more the cavitation will extend over the suction side and implosions will happen near the trailing edge. The risk of cavitation is monitored by the cavitation number (σ) that gives an indication of the margin till cavitation.

$$\sigma = \frac{p_0 - p_v}{1/2\rho V_0^2} = \frac{p_0 - p_v}{q} \tag{2.15}$$

p_0 is the total static pressure, this is equal to the atmospheric pressure plus hydrostatic pressure. The hydrostatic pressure component fluctuates with the height of the water above the blade. This height depends on the position of the blade and the position of the propeller shaft in the waves. In most calculations this dynamic component is kept static and is defined in different ways depending on the criteria used[6]. V_0 is the relative inflow velocity. Just as p_0, V_0 is as well in multiple ways. q is called the stagnation pressure.

Cavitation will happen if the cavitation number is less than or equal to $-\frac{\delta p}{q}$. This is a basic application of

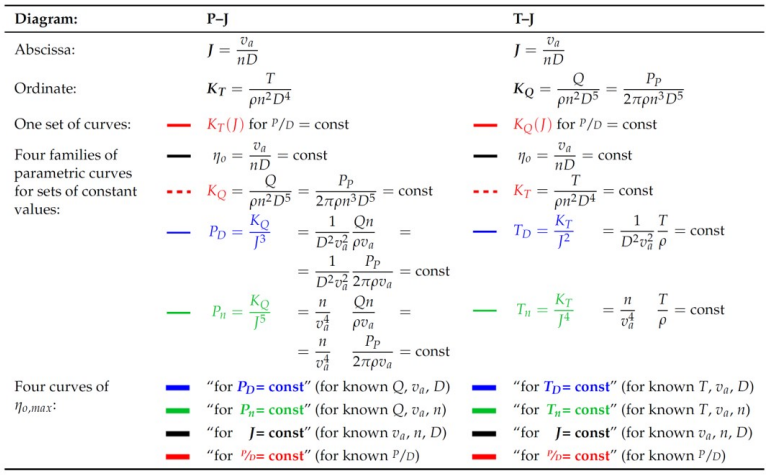

Figure 2.11: Legend regarding P-J and T-J efficiency maps (fig. 2.10) [5]

the Bernoulli law where:

$$\delta p = p_P - p_0 = \frac{1}{2}\rho\left(V_0^2 - V_P^2\right) \tag{2.16}$$

Here subscript P stands for the propeller, commonly taken at $0.7R$ which means that $\delta p/q$ is a function of the propeller profile and inflow angle. p_v is depending on the fluid, temperature, and size of the largest cores which makes it difficult to predict.

2.3.2.2 Criteria

In turbo machines [45] it is said that erosion due to cavitation is happening when $\sigma \leq 0.3$ and a performance drop is noticeable when $\sigma \leq 0.15$. This requires knowledge of the exact pressure distribution over the blade. In propellers this is not constant due to the wake and the dynamic behaviour of the static pressure. For this reason it is common to use general criteria in naval design.

The oldest criteria is the criteria of Barnaby[46]. This uses the principle of limiting the average thrust per unit of projected blade area to a critical value. Such a criteria is not accurate as the shape of the blade, pressure distribution, lift coefficient and other variables are not taken into account.

The criteria used nowadays are based on results of experiments, research on ships and calculations. Mostly the criteria can be represented in a diagram with as ordinate the cavitation number and the non-dimensional thrust per blade area. Most of the criteria accept a maximum of 5% cavitation as non critical cavitation.

A popular criterion nowadays is the criteria from Burrill [47]. A uniform flow around the propeller is assumed, this is not in line with the reality where the propeller is in the wake of the ship. This criteria uses σ_R as defined in equation 2.17.

$$\sigma_R = \frac{p_0 - p_v}{1/2\rho\left(U_A^2 + (0.7\pi nD)^2\right)} = \frac{p_0 - p_v}{1/2\rho U_{0.7R}^2} = \frac{p_0 - p_v}{q_{0.7R}} \tag{2.17}$$

With the total static pressure taken at the shaft, stagnation pressure with respect to the total velocity for $r = 0.7R$ and $p_0 - p_v$ is approximated as:

$$p_a + \rho g(d - E + \zeta_A) \tag{2.18}$$

With d the draft, E the height of the propeller shaft above the baseline and ζ_A the amplitude of the stern

wave in still water ($\approx 0.0075L$). The non-dimensional propeller (τ_C) load is represented by:

$$\tau_C = \frac{T}{A_P q_{0.7R}} \tag{2.19}$$

Lines of percentage of cavitation are presented graphically (fig 2.12) by defining the minimum expanded blade area (A_E) as:

$$\left(\frac{A_E}{A_0}\right)_{min} = \frac{T}{A_0\left(1.067 - 0.229\frac{P}{D}\right)\left(0.3\sigma_R^{0.5} - 0.03\right)q_{0.7R}} \approx \tau_C \tag{2.20}$$

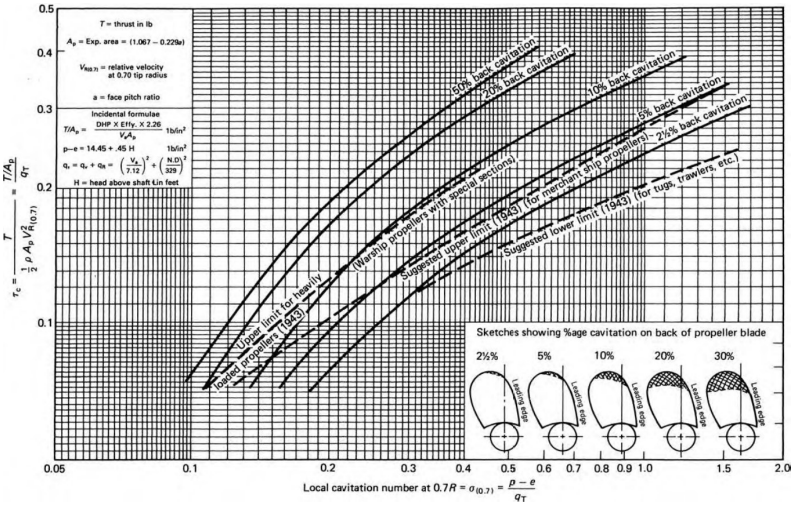

Figure 2.12: Burrill cavitation diagram for uniform flow found in [8]

Another criterion used these days it the criterion given in [48]. Just as Burrill a uniform flow is assumed. This criterion uses σ_0 (eq. 2.21) instead of σ_R. The non dimensional propeller load is represented by:

$$\sigma_0 = \frac{p_0 - p_v}{1/2\rho U_A^2} \tag{2.21}$$

$$\tau = \frac{T}{A_P(p_0 - p_v)} \tag{2.22}$$

The propeller load is then graphically presented in function of σ_0 by a line of 5% cavitation. The criterion can also be formulated as the minimum projected blade area:

$$A_{P,min}^2 = \frac{T^2}{3.65(p_0 - p_v)^{1.5}U_a} \tag{2.23}$$

An alternative for these graphs are the so called bucket diagrams (fig. 2.13). Bucket diagrams represent the cavitation behaviour of a wing, fin or propeller blade in a two dimensional sense. The diagram is then plotted as a function of section (hydrofoil) angle of attack versus section cavitation number (σ). The diagrams are not for the whole propeller but are used for analysing a section of a propeller. In [49] a numerical study on these diagrams for a hydrofoil was done.

These empirical criteria are used in the early design phase and in general for smaller vessels. For bigger ships CFD, especially RANS, is often used to understand the cavitation on the propeller[8].

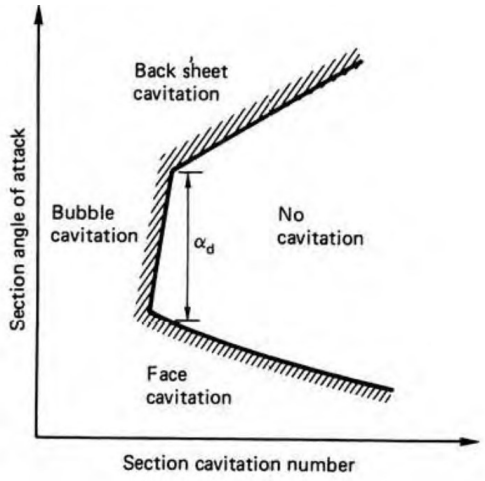

Figure 2.13: Example of a cavitation bucket diagram [8]

2.3.3 Propeller in waves

Waves have influence on environment in which the propeller is working. This change in environment has an effect on the performance of the propeller in multiple ways:

- **Dynamic loading:** the loading of the propeller changes continuously due to the constant changing resistance of the ship in waves and the two variations mentioned below.
- **Changing wake** behind the ship will influence the loading and water inflow of the propeller
- **Ventilation** due to a big decrease of water height above the propeller can significantly reduce the propeller performance.
- **Thrust deduction factor** is influenced by sea waves yet this influence is negligible in most cases [11].

As a result the thrust is not equal to the thrust in open water. In [9] this is taken into account by factor β_T. Similar to β_T, β_Q is defined too, yet in [2] it is concluded that β_T and β_Q are not equal due to the drag force of the propeller. In that paper it is posed that both β are linked by equation 2.24. This was based on model tests given in [50].

$$\beta_Q = \beta_T^m \tag{2.24}$$

Different loss effects influence each other, as a consequence the superposition principle is not valid in general[9].

2.3.3.1 Dynamic loading

In subsection 2.1.2, the added resistance due to waves was seen as an average added resistance over a wave. Yet in reality, it varies over time. This variation is also transferred to the loading of the propeller[9]. It is straight forward that a different loading of a propeller will influence the efficiency. As these variations happen with a finite speed, there will be a dynamic behaviour of the loading on the propeller. The dynamics can be split in three parts: shaft dynamics, motor dynamics and flow dynamics of which the first two are not further discussed because the engine and shaft are not modelled in this thesis.

The flow dynamics were first studied in [51] where a one-state model with lumped parameters for the shaft and flow dynamics was proposed. In this model the shaft friction is neglected. In [52] this model

was improved with the help of the momentum theory where the advance velocity is assumed to be zero. Later the water around the propeller was included as mass-damper system leading to a two-state model. This model was further extended in [53] to make it valid for $U_a \geq 0$. In [54] it is concluded that the flow dynamics for surface vessels have no significant influence as their transition is faster than the response of the vessel [9].

2.3.3.2 Changing wake

In [55] is was showed that in presence of waves and ship motions, wake velocities fluctuate. Moreover, the mean of these fluctuations is different from the calm water wake. Hence, in presence of waves, mean wake changes along with the fluctuations. Later in [10] it was demonstrated that fluctuating wake velocities are caused by the wave induced particle motion and surge motion of the ship. Next to the fluctuating motions, a mean propeller inflow increase was noticed in [55]. In [2] it is proposed that the increase in mean propeller inflow due to the pitching motion of the ship is caused by potential flow effects. Wake velocities due to the pitching motion of the ship can be calculated assuming the bottom of the ship to be a flat plate.

The combination of these models was compared this with data observed in CFD and measurements in [11] and it was observed the model followed the same trends as the measurements. In that paper the model is then used to take the wake variations into account in the study of engine-propeller dynamics.

2.3.3.3 Ventilation

Ventilation, or aeration, is the phenomenon that happens when air gets sucked into the propeller with a loss of thrust and torque as a consequence. This can happen when there is not enough water above the propeller or when the blades emerge out of the water. The submergence of the propeller hub is influenced by the waves and the movement of the ship, especially the heave and pitch movements. Note that the submergence has also a direct influence on the risk of cavitation.

Ventilation can be split into three phenomenon [9]:

- **Loss of propeller effective disk area** happens when a part of the blade emerges out of the water, the emerged part has no propulsive force. This can be seen as a reduction of the propeller disk area ([56] and [57]). The corresponding thrust loss factor β_{TA} can be found from a simple geometrical consideration, by assuming that the resulting thrust is proportional to the submerged propeller disc area. Later an alternative representation where the hub diameter is also taken into account was proposed in [58]. This loss model is assumed to be valid for any propeller loading. Based on the results in [2], another alternative representation which includes the air suction and hysteresis effect was proposed in [59].

  In [9] it is stated that the model given in [59] is convenient if the dynamic effects of ventilation can be neglected and only the average thrust values are needed. This model was used in [11] in a study regarding the effect of waves on the engine-propeller dynamics and on the performance of the propulsion.

- **Air suction (ventilation)** happens when the blades emerge or when the blades create of a low enough pressure on the suction side. When this low pressure is close to the water surface, it creates a funnel which sucks air into the propeller. From this moment a self-amplifying process starts and the propeller may lose as much as $70 - 80\%$ of its thrust and torque when it ends up being fully ventilated.

This phenomenon is usually split into three regimes: non-ventilated regime, partially ventilated regime and fully ventilated regime [9].

In the non ventilated regime the propeller is deeply submerged or fully submerged with a low propeller loading. In this case there is no air sucked in.

In the partially ventilated regime, the propeller is not stationary ventilated. The level and location of cavities is time dependent. This regime can only be stable for high advance ratios, for low advance ratios the regime is a transition between the two other regimes.

In the fully ventilated regime a single cavity covers each propeller blade. As a consequence the pressure on the suction side is atmospheric. This regime is rather stable.

- **Lift hysteresis effect** describes the slower thrust recovery to the nominal value than the thrust reduction due to the two points above. The thrust build up will only happen when the air supply stops. The three most common causes for the air supply to stop are a rise of the water column above the propeller, disturbances in the water and a decrease of the propeller loading. The first two causes mentioned above end the air supply relatively fast. When the air supply stops the thrust is not restored immediately. First the air cavities on the blades have to dissolve and then the lift of the blades has to build up. In [60] such a phenomenon is studied for a two-dimensional foil and noticed that when the cavities disappear a sudden increase of the lift from around 50% of the steady-state lift. This was called the Wagner effect and described with the Wagner function which gives the ratio of the instantaneous lift and the steady-state lift. Further in the paper is was noted that the foil must travel around 20 chord lengths to recover its full lift. A similar behaviour for propellers was suggested in [2]. In [58] it is stated that a typical propeller with a pitch ratio around one must travel about 4 revolutions at full submergence to regain its full thrust. This is often used as a general rule of thumb, for example in [9].

The thrust loss can be modelled as the superposition of the three phenomenon discussed above.

In [9] a different way to model the ventilation was used. Firstly the propellers of interest were tested in a cavitation tunnel to create a non-dimensional map, an example is shown in figure 2.14 on the left side. Subsequently this was parametrised to a model map as shown on the right side of figure 2.14. And later the lift hysteresis effect was also added to the model by restricting $\dot{\beta}_{VH}$.

This model was later also used in [20] as part of the estimations of the speed loss due to the sea state. In that paper the influence of the waves on the advance speed was not taken into account.

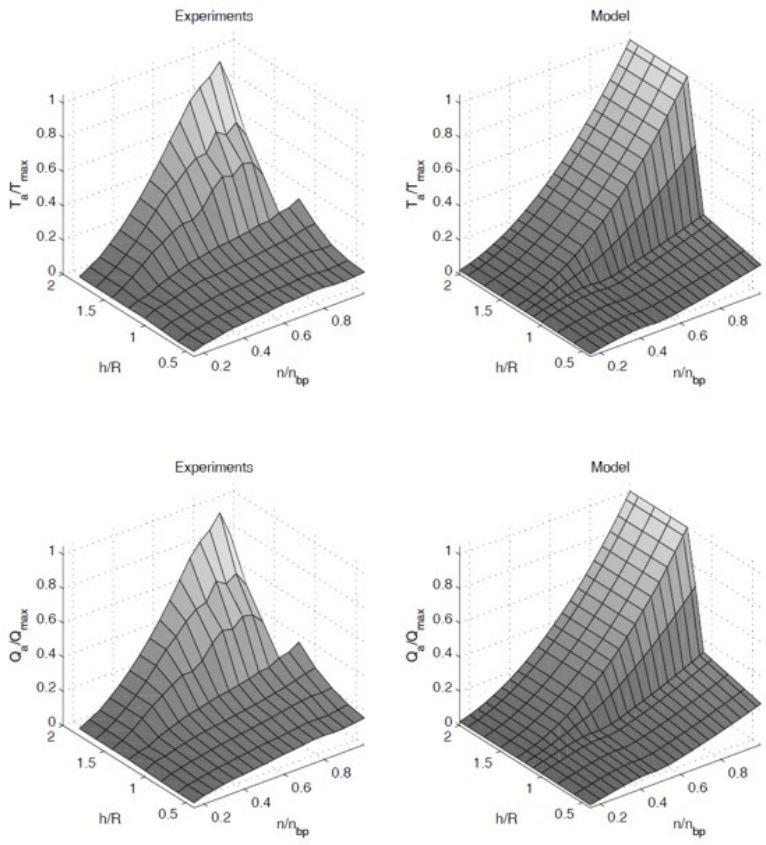

Figure 2.14: Comparison of the thrust and torque of an open propeller during ventilation [9]

Chapter 3

Methodology

In this chapter the methodology adopted for the selection of the most efficient propeller in waves for a single open propeller and its implementation is discussed. First a general overview of the propulsive power flow is given where some choices of the selection procedure are made. Afterwards the selection procedure and its implementation in Matlab are discussed. In appendix B, the flowcharts given in this chapter but with the names of the Matlab code can be found. A selection of the most important Matlab codes are given in appendix C.

3.1 Global power flow

The global power flow of a ship with a single open propeller is illustrated in figure 3.1. In this section the global power flow and losses are summarised in order to highlight the effects which have a significant influence on the efficiency and give some formulae.

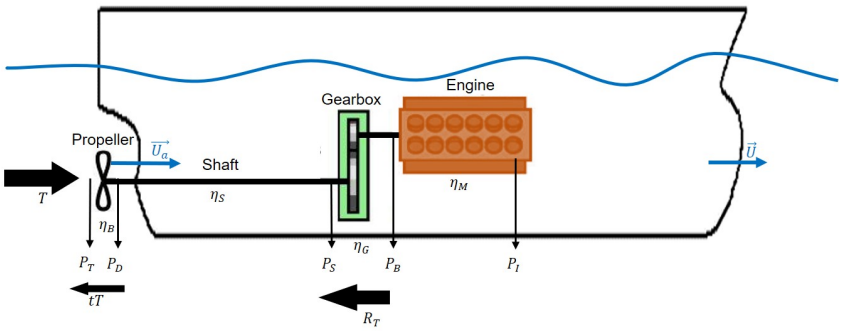

Figure 3.1: Schematic overview of the power, efficiency and forces in a propulsion system

Ideally there would be no losses in the system and the indicated power (P_I) of the engine would be equal to the effective power (P_E), which is the power needed to overcome the resistance of the ship (R_T) at a certain speed ($\vec{U}$). The resistance of a ship was studied in section 2.1 and is a key factor in the design of the propulsive system of the ship.

The first losses occur inside the engine. The engine gives the brake power (P_B) in form of rotation and torque to the shaft which is less than P_I. The efficiency of this conversion is the mechanical efficiency (η_M), defined as:

$$\eta_M = \frac{P_B}{P_I} \tag{3.1}$$

Although the engine is a key element in the efficiency of the propulsive system, it is not modelled, instead the engine is modelled to deliver constant rotational speed in this thesis. In [11] simulations of the ship in waves were done with and without the engine-propeller dynamics being modelled. The reference concluded that if relevant effects like wake variation, ship motions and propeller depth variation are included, the simulations without a diesel engine model will give conservative estimates of variation in propeller forces, torque and power. However, for accurate estimates of system response the coupled engine propeller model should be used. Therefore, the assumption of constant engine speed is justified for this purpose where the averages are of importance for the optimisation.

Depending on the engine, a gearing system is required to have the propeller shaft turning at a reasonable speed. A gearing system is not without losses either, yet these losses are small ($\eta_G \approx 0.94 - 0.98$)[61]. Therefore, the gearing system is not considered in the propeller selection procedure. Furthermore, the shaft itself also has some minor losses due to the bearings and the length of the shaft ($\eta_S \approx 0.97 - 0.98$)[6]. Thus, this is also not considered in the proposed propeller selection procedure. At the end of the shaft the propeller receives the delivered power, this is defined by equation 3.2.

$$P_D = NQ_{eff} \tag{3.2}$$

Where Q_{eff} is the effective torque at the end of the shaft and N the engine speed in rad/s.

The propeller converts this torque into a thrust that counteracts the ship resistance. This conversion was studied earlier in section 2.3. At the end, the total efficiency (η_T) of the propulsion configuration can be written as:

$$\eta_T = \frac{P_E}{P_I} = \eta_M \eta_G \eta_S \eta_D \tag{3.3}$$

η_D is the delivered efficiency and represents how good the propeller, in combination with the ship, can convert the torque into ship speed. Generally, the delivered efficiency in still water has a value between 0.7 and 0.75 [6]. This efficiency will be used to select the propeller in waves and is defined as follows:

$$\eta_D = \overline{\left(\frac{P_E}{P_D}\right)} = \overline{\left(\frac{R_T U}{NQ_{eff}}\right)} \tag{3.4}$$

3.2 Main principle of the selection procedure

A flowchart of the general selection code is shown in figure 3.2. The first step in this code is to define the environment (*'Setup'*), in this part a code developed at CENTEC is used to obtain ship in still water and ship in waves and characteristics.

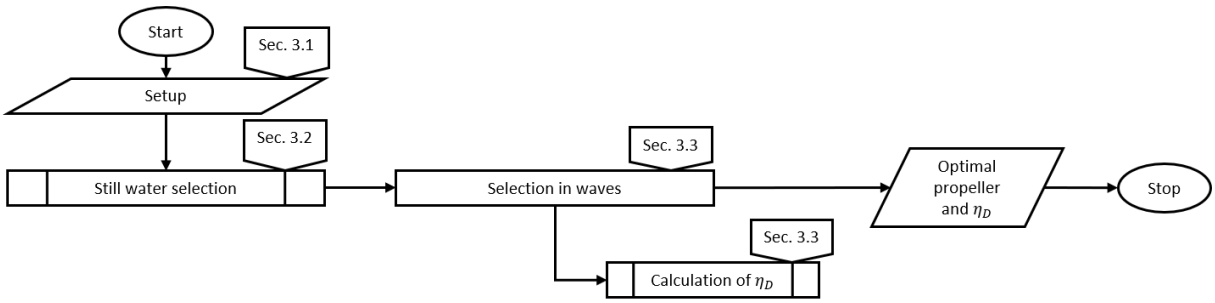

Figure 3.2: Flowchart of the propeller selection procedure in waves

After the *'Setup'*, two levels of propeller selection are performed: the basic still water propeller selection

and a more advanced propeller selection taking into account the effect of waves. Both levels of selection are executed by the Matlab built-in function *'fmincon'*. This function finds the minimum of constrained non-linear multi variable function. The first level is used as initial guess in the other approaches and serves as a benchmark.

The second level of selection selects the best propeller for a specific sea state or for a long-term considering a scatter diagram. This level uses the delivered efficiency (η_D) instead of the open water efficiency because it includes the effect of waves on the propeller. As the engine is not modelled, it would not be correct to use total efficiency. In case of propeller selection for a single sea state, formula 3.4 is used to calculated the delivered efficiency. To avoid confusion this is abbreviated by $\eta_{D,s}$ where the subscript s denotes the efficiency is for a sea state (delivered sea specific efficiency). When the selection has to be done for a scatter diagram, the delivered efficiency is calculated using formula 3.5. In this case the delivered efficiency is abbreviated by $\eta_{D,z}$ (delivered zone specific efficiency).

$$\eta_{D,z} = \frac{\sum_s p_s \eta_{D,s}}{\sum_s p_s} \tag{3.5}$$

Where p_s is the probability a sea state occurs.

In addition to this, the selection procedure can also be used to optimise a propeller for a certain route. Here $\eta_{D,r}$ (delivered route specific efficiency) is used as abbreviation and is computed using equation 3.6. However, such a propeller selection has limited applicability in real life. It is only useful for ships with a fixed route such as ferries. The propeller route specific efficiency will not be used in this thesis to optimise a propeller. It was implemented in the code in order to compare the performance of different propellers for a voyage of the ship. However, at the end it was decided to omit this comparison for several reasons, most importantly because the comparison is expected to add no value due to the small differences between the propellers (see chapter 5).

$$\eta_{D,r} = \frac{\sum_z t_z \eta_{D,z}}{\sum_z t_z} \tag{3.6}$$

Where t_z is the time that the ship sails in a certain zone in the route, it is computed using formula 3.7. In the calculation of $\eta_{D,r}$ each zone resembles a part of the route where the sea state has a certain probability distribution.

$$t_z = X_z \frac{\sum_s p_s}{\sum_s p_s \overline{U_s}} \tag{3.7}$$

Where X_z is the distance to sail in the given zone.

3.3 Setup: define ship and environment

Before the selection procedure can start, the ship and its environment for which the propeller has to be selected need to be defined. This is done in the *'Setup'*, which is split in three sections:

- **Ship characteristics** (sec.3.3.1)
- **Boundary conditions of propeller and initial guess** (sec. 3.3.2)
- **Sailing route** (sec. 3.3.3)

3.3.1 Ship characteristics

First the ship characteristics that are independent of the propeller are defined. These are the ship hydrostatic, ship still water and ship in waves characteristics. The ship hydrodstatic characteristics are manually defined. Based on these manual characteristics, the other parameters, except for the surge, are calculated by a code developed at CENTEC. The code and the acquisition of the surge, are further discussed in section 3.3.4.

Next to the ship characteristics, the general environmental parameters such as the density of water, atmospheric pressure and gravitational acceleration are also specified.

3.3.2 Boundary conditions of propeller and initial guess

The propellers considered are the Wageningen B-screw series modelled by the Oosterveld polynomials. These are defined by the number of blades, pitch ratio, expanded blade ratio and the diameter of which the number of blades is fixed in the selection procedure. The other parameters are limited by eleven boundary conditions:

- **Six linear inequalities**, namely each parameter is limited by an upper and a lower value based on the original measurements of the B-series.
- **Five non-linear inequalities** of which two boundary inequalities verify if the propeller can deliver the required thrust to maintain the service speed in still water within the limits of the engine speed (lower and upper limit). The propeller speed is calculated by the K_T/J^2 polynomial. The procedure is as follows, first the required K_T/J^2 is computed using formula 3.8. Then, J is calculated by associating the required K_T/J^2 with the K_T/J^2 from Oosterveld polynomials. This is illustrated in figure 3.3. A vertical line is drawn from the crossing of the K_T/J^2 polynomial and the required K_T/J^2. This gives J, using equation 2.8 the engine speed is computed, which should lie within the speed limits of the engine.

  $$\left(\frac{K_T}{J^2}\right)_{required} = \frac{T}{\rho D^2 U_a^2} \tag{3.8}$$

  Two other inequalities verify if the delivered power for the ship in still water at service speed is within defined power limits. In the calculation of the delivered power, the torque is found from the K_Q-polynomial and the engine speed is equal to the one calculated above.

  The fifth non-linear inequality verifies if the propeller fulfils the cavitation criterion of Burrill (see section 2.3.2.2). This is verified for the thrust and engine speed required to propel the ship at service speed.

Next to the boundary conditions of the propeller, an initial propeller has to be defined. This serves as an initial guess that is required by the *'fmincon'* function. It is not required that the initial estimate respects the boundary conditions.

3.3.3 Sailing route

The third type of parameters define the environment for which an optimal propeller has to be selected. This environment can either represent regular waves or an irregular sea state(s). Whether the waves are regular or not, the heading, distance to be sailed and probability of occurrence need to be defined. The heading angle is defined such that 0 degrees indicates stern wave and 180 degrees head waves, this is illustrated in figure 3.4.

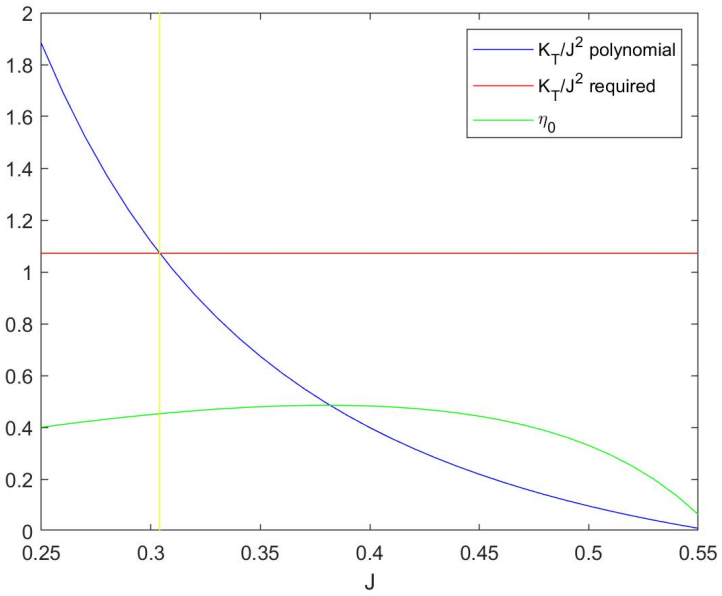

Figure 3.3: Example of how η_0 and J found for B4-43.2 with a pitch ratio of 0.47 with the Oosterveld polynomials

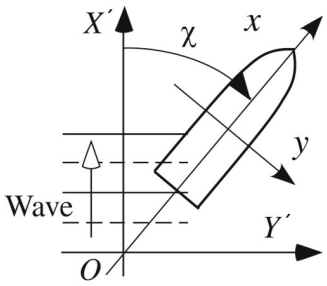

Figure 3.4: Coordinate system (OX´Y´, Earth fixed coordinate system; oxy, ship fixed coordinate system; χ, wave encounter angle/heading [10]

Additional parameters for irregular sea states are the peak period (T_p) and the specific wave height (H_s).

Although in the real world regular waves never occur, the regular wave option is programmed. The reason is that in literature regular waves are more often studied as they are easier to understand and to compare. As a consequence this option makes it possible to verify the simulation part of the code based on literature. In the case of regular waves the dimensionless wavelength (λ/L_{PP}) and the wave amplitude (A_w) are required next to the general sailing route parameters.

3.3.4 Discussion of the ship characteristic calculation

As mentioned earlier, most of the ship characteristics are computed by the code developed at CENTEC. This code calculates three types of characteristics:

- **Still water resistance** according to the method of Holtrop and Mennen [16] (see section 2.1.1.2). Additionally the code gives the still water wake factor and thrust reduction factor.
- **Ship motions in the frequency domain** according to the strip theory as formulated in [17]. A shortcoming of this theory is its inability to calculate any motion related to surge. The surge

amplitude is in fact required in later calculations in the simulation. This shortcoming was solved by estimating the RAO of the KVLCC2 based on the graph shown in [11]. Therefore, in the following chapter the KVLCC2 is used for the validation of the simulation code. Alongside the fundamental RAOs of ship motion, the RAO of the relative vertical motion of the propeller hub is computed. This is calculated using formula 3.9.

$$RAO_{RM,P} = RAO_{VM,P} - wave_c \tag{3.9}$$

Where $RAO_{VM,P}$ is the RAO of vertical motion at the propeller hub defined in formula 3.10 and $wave_c$ is the complex wave elevation given in formula 3.11.

$$RAO_{VM,P} = RAO_3 - x_P * RAO_5 + y_P * RAO_4 \tag{3.10}$$

$$wave_c = -\cos(k\cos(\chi)x_P) - i\sin(k\sin(\chi)y_P) \tag{3.11}$$

Where k is the wave number and x_P, y_P are the x and y coordinates of the the propeller hub.

- **Added resistance in head and bow waves** according to the far-field theory as formulated in [18] (see section 2.1.2.1). In stern quartering seas, the added resistance is forced to zero due to the inconsistency of the far-field method for such conditions. Therefore, the selection code is not valid for stern-quartering waves. This problem may be overcome by using another code to obtain the added resistance or defining the added resistance to be constant and equal to a certain percentage of the still water resistance. Moreover, as discussed in the literature study, the accuracy of this far-field theory in short waves is limited. For that reason the added resistance in the high frequency range is put equal to the added resistance of the highest frequency calculated. A preferred solution would be to complement the computations with a valid method specific for short waves for example [2]. Sometimes some numerical errors appeared in the low and medium frequency range, these are replaced by the average of the neighbouring frequencies was taken.

  The validation of the added resistance computations by the code can be found in [15] where the results of the added resistance is compared to a near field method. It is highlighted that the far-field method is more accurate for slender hulls, while hulls with high block coefficients can be subjected to larger errors. The influence of motion calculation method on the added resistance calculation is studied in [14] for difference added resistance calculations.

In the validation the KVLCC2 ship model is mainly used. This ship has a blunt hull shape, for such a shape the used methods are not so accurate, therefore some inaccuracies can be expected. The reason this ship is still used, is because it is also used in [11] to which the simulation code is compared in chapter 4. Furthermore the surge amplitude could be estimated based on that paper.

3.4 Still water propeller selection

The optimal Wageningen B-series propeller in still water is selected with two purposes. The first purpose is to compare the propeller with the optimal propeller found in waves. The the second purpose is to serve as the initial guess for the propeller selection in waves.

The still water optimisation is done by the built-in Matlab function *'fmincon'*. This requires an initial guess and boundary constraints as discussed in section 3.3.2. The still water efficiency for a given propeller ($Z, A_e/A_0, P/D$ and D) sailing at service speed is computed by the use of the K_T/J^2-

polynomials. The procedure is illustrated in figure 3.3. A vertical line is drawn from the crossing of the K_T/J^2 polynomial and the required K_T/J^2. The open water efficiency is equal to the point where the η_0-polynomial intersects with the vertical line. This procedure is written in a Matlab function (*'calc_sol_still_eff_0.m'*, see appendix C). *'Fmincon'* finds the minimum instead of the maximum, therefore the inverse of *'calc_sol_still_eff_0'* is given to *'fmincon'* as function to minimise.

3.5 Propeller selection in waves

The selection of the propeller in waves is done by calculating the maximum of delivered efficiency by the *'fmincon'* function. Similar to the selection of the propeller in still water, the inverse of the function is used. The difference with the still water selection is the function to maximise. Here, the function calculates η_D which depends on on the waves instead of η_0.

Figure 3.5 shows a flowchart of how η_D is calculated. The required inputs for this calculation are the propeller parameters ($Ae/A0$, P/D and D) and everything defined in the *'Setup'* (sec. 3.3) except the boundary conditions.

In the most simple case when a propeller is selected for a single sea state, only the black part of the flowchart is applicable. The flowchart consists then of four calculation blocks. The first two blocks calculate the input parameters for the third part. In the third part, the ship is simulated in the sea state for a certain amount of time. This part is discussed in section 3.6. Lastly, the averages and $\eta_{D,s}$ are computed.

When a propeller has to be selection based on a scatter diagram, a loop over all sea states is added (green part on figure 3.5). For each sea state $\eta_{D,s}$ is calculated. When the loop has ran over all sea states, $\eta_{D,z}$ is calculated according to equation 3.5.

If the delivered route specific efficiency has to be computed, another loop over the previous loop is added (blue part on figure 3.5). This loop covers all zones of the route and calculates the average speed and t_z in addition to $\eta_{D,z}$. These extra values are calculated according to equation 3.7 and 3.6 respectively.

3.5.1 Wave related input

In the first block, wave related input is calculated. In the case of irregular waves the wave spectrum is computed according to the ISSC spectrum (eq. 3.12, [62]). In this spectrum the heading is assumed to be constant.

$$S(\omega) = \frac{0.313 H_s^2 \omega_p^4}{\omega^5} e^{-1.25(\frac{\omega_p}{\omega})^4} \tag{3.12}$$

When the ship in regular waves is considered, the wave frequency and period are calculated based on λ/L_{PP}.

3.5.2 Average speed estimation

When the sea state is defined, the attainable speed based on the added resistance is calculated. This is used as the initial speed in the simulation to have a quicker convergence to the regime speed in the sea state. The faster the regime speed is reached, the shorter the time domain simulation can be with little or no decrease in accuracy of the averages. It is important to have a good estimate because the simulation is the bottleneck of the selection code.

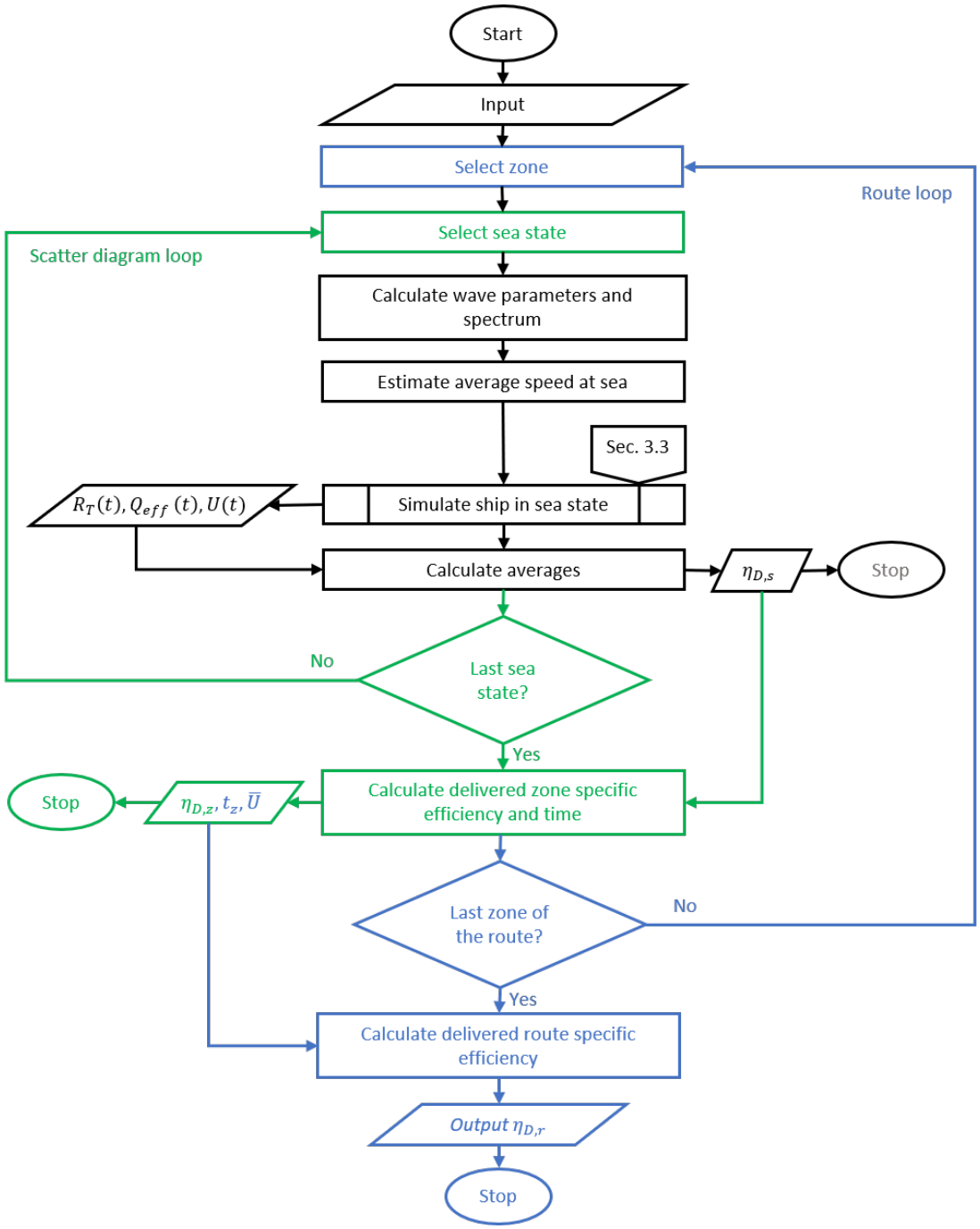

Figure 3.5: Flowchart of the function that calculates the delivered efficiency

This procedure is done in an iterative process because the resistance of the ship depends on the vessel's speed. After each iteration, the ship's speed is estimated by the average of the old ship speed and the calculated speed. The iteration stops when the relative change of speed is less than ϵ or when more than 2000 iterations have occurred. ϵ is the allowable error and it is defined in the *'Setup'*. The ship's speed in each iteration is calculated using equation 3.13.

$$U_a = (1 - w_s)U \tag{3.13}$$

Where w_s is the still water wake fraction and U_a the advance speed is found in the $K_T - J$ diagram

based on the required thrust which is calculated using equation 3.14.

$$R_T = (1-t)T \tag{3.14}$$

Where R_T is the total resistance that is calculated by summing up the still water resistance and the average added resistance. The average added resistance for the sea state is found using formula 3.15 for an irregular sea state and using formula 3.16 for regular waves.

$$\overline{R_{add}}(U) = 2\sum_{\omega} \Phi_{AW}(\omega, U) S_w(\omega) \Delta\omega \tag{3.15}$$

$$\overline{R_{add}}(U) = A_w^2 \Phi_{AW}(\omega, U) \tag{3.16}$$

Where Φ_{AW} is the dimensioned added resistance coefficient is calculated as follows:

$$\Phi_{AW} = \sigma_{AW}(\omega) \rho g B^2 L_{PP}^{-1} \tag{3.17}$$

σ_{AW} is the added resistance coefficient calculated in the *'Setup'*.

3.5.3 Processing simulation output

When the simulation is completed, the averages are calculated from the start onwards. When there is a transition time, for certain ships and sea states, an elimination of the first several minutes may be required. This transition will be present when the initial speed given is not close to the regime speed, for example due to ventilation. This is further elaborated in section 4.7. When the averages are calculated, the delivered sea specific efficiency is obtained using formula 3.4.

3.6 Simulation of the ship in a sea state

The simulation of the ship with propeller in a sea state is based on [11]. However, in the reference the engine-propeller dynamics were modelled while this is not done here for the reasons given in section 3.1.

The simulation is done in the time and space domain because some factors that influence the performance have a non-linear behaviour and cannot be consistently treated in the frequency domain. For instance, the ventilation loss factor (sec. 2.3.3.3) is described by a non-linear model, with values between 0 and 1, which makes superposition of waves with different frequencies not valid.

Furthermore, the simulation does not consider the behaviour of the ship master. For example, the voluntary slowing down of the vessel to avoid slamming in a severe sea state. The working principle of the simulation code is illustrated by the flowchart given in figure 3.6. The simulation code is split into two parts:

- **Initialisation** in which the input data is received and the starting parameters are set up (section 3.6.1).
- **The simulation** itself which consists of a double loop (section 3.6.2). The outer loop runs over the time of the simulation and stops two peak periods before the end of the simulation time. The early stopping criteria is because the next zero up-crossing should be within the initialised simulation time. The inner loop runs until the speed at the time step has converged. The initial speed given

to the ship at the first iteration of each time step is the final speed found at the previous time step. At the first time step, this initial speed is the average speed that was calculated in section 3.5.2. After each time step the X-position of the ship is updated by the formula shown in the flowchart. This X-axis is stationary and in line with the ships centreline.

3.6.1 Initialisation

Prior to launching the simulation, the starting values used in the first iteration are defined. One of these values is the starting time which is not equal to zero but twice the peak period. The reason for this is that the passed zero up-crossing must have a positive time due to the way the code is implemented. The passed zero up-crossing is required in several calculations later on in the simulation. For similar reasons, the simulation code stops two peak periods before the end of the simulation time.

3.6.2 Simulation

The calculations within the loop can be split into four zones as indicated with the dashed lines on figure 3.6. The zones are divided based on the type of parameter calculated:

- **zone 1**: wave parameters (sec. 3.6.2.1)
- **zone 2**: ship motion parameters (sec. 3.6.2.2)
- **zone 3**: thrust influencing parameters (sec. 3.6.2.3)
- **zone 4**: ship working point (sec. 3.6.2.4)

As can be seen on the flowchart most of these calculations happen within the inner loop. The parameters calculated within the inner loop are directly or indirectly dependent on the speed of the ship.

3.6.2.1 Wave parameters

In the case of irregular waves the 'quasi' regular wave properties are calculated first. This 'quasi' regular wave simplifies the irregular waves as if the ship is sailing in regular waves. The 'quasi' regular wave profile is defined by the wave period and amplitude just as a normal regular wave. The period is equal to the time between the previous and the upcoming zero up-crossing at the centre of the ship. The wave amplitude of the 'quasi' regular wave is equal to the average of the lowest trough and the highest crest within that period. Both parameters change in an irregular sea so the 'quasi' regular wave changes as well during the simulation. The 'quasi' regular wave profile is used for the calculation of the added resistance and the wake velocity. In the case of the added resistance, this method is used to make the added resistance vary between different waves. This method was proposed in [2] and used in [20]. The 'quasi' regular wave approach is implemented in the wake calculations because the used model does not work with superposition of different wave frequencies and phases (more specific due to the α-factor and exponential with wave number. These will be discussed in section 3.6.2.3). In order to calculate the 'quasi' regular wave properties, the wave elevation at midship is calculated using formula 3.18.

$$H_w(t) = \sum_{\omega} \sqrt{2S_w(\omega)\Delta\omega}\cos(\omega t - \phi(\omega) - kX\cos(\chi)) \tag{3.18}$$

Where k is the wave number, X the position of the ship in the stationary reference frame and $\phi(\omega)$ the phase of the waves at different frequencies. This phase is created with a built-in random generator function of Matlab. To ease the comparison between simulations of different propellers, $\phi(\omega)$ is fixed in the *'Setup'*(section 3.3).

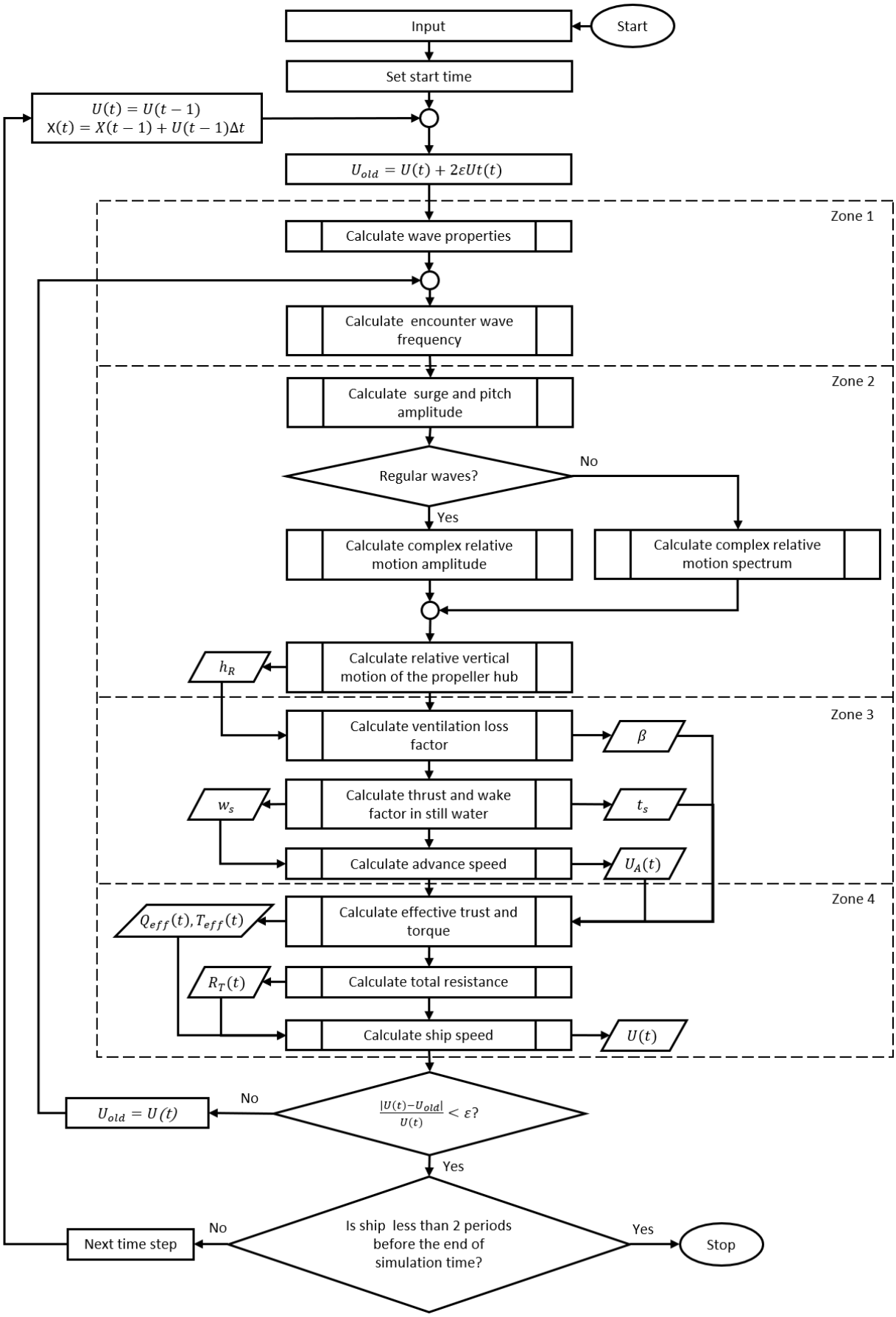

Figure 3.6: Flowchart of the simulation of the ship and propeller

Furthermore the encounter frequency is calculated using equation 3.19.

$$\omega_e = \omega - \omega^2 U \cos(\chi)/g \tag{3.19}$$

3.6.2.2 Ship motion parameters

The main objective of this section is to calculate the the complex surge amplitude, the complex pitch amplitude and the submergence of the propeller's hub. The first two of these parameters are calculated for the 'quasi' regular wave because their amplitude and not instantaneous motion is necessary in the calculation of the wake later on.

The complex surge and pitch amplitudes are calculated according to the following formula:

$$z_i = A_w RAO_i(\omega, U) \tag{3.20}$$

Where A_w is the ('quasi') regular wave amplitude and ω the ('quasi') regular wave frequency. Subscript i represents a ship motion.

The submergence of propeller hub is computed using formula 3.21 for regular waves and using 3.22 for irregular waves.

$$h_{prop}(t) = |z_{RM,prop}| \cos(\omega t - \varphi - kX\cos(\chi)) - z_P \tag{3.21}$$

$z_{RM,prop}$ is the complex amplitude of relative motion of the propeller hub and φ is the angle of $z_{RM,prop}$, which is calculated using equation 3.20. The z-coordinate of the propeller hub is subtracted to find the hub submergence. Subtraction is used because the z-axis is defined as such that the positive is pointing upwards and the zero point is located on the waterline.

$$h_{prop}(t) = \sum_{\omega} \sqrt{2|S_{RM,prop}(\omega)|\Delta\omega}\cos(\omega t - \varphi(\omega) - \phi(\omega) - kX\cos(\chi)) - z_P \tag{3.22}$$

$S_{RM,prop}$ is the spectrum of the complex relative motion at the propeller hub and is calculated using formula 3.23.

$$S_{RM,prop}(\omega) = RAO_{VM,P}(\omega, U)^2 S_w(\omega) \tag{3.23}$$

3.6.2.3 Thrust influencing parameters

In section 2.3.3 different factors that influence the working of propeller in waves were discussed. There were three factors: ventilation, wake and dynamic loading. The latter is not modelled in the simulation because the dynamic loading for surface vessels has no significant influence as their transition is faster than the response of the vessel [9].

The ventilation loss model given in [59] is chosen because this model is said to be convenient when only the averages are of interest [9]. Moreover, the formula takes the both important ventilation phenomena (loss of effective disk area and air suction) into consideration (sec. 2.3.3.3). In addition the model makes it possible to compare the results of regular waves with [11]. The model is given below:

$$\beta_{TA} = \begin{cases} 0 & h_{prop}/R \leq -0.48 \\ 1 - 0.675(1 - 0.769 h_{prop}/R)^{1.258} & -0.48 \leq h_{prop}/R \leq 1.3 \\ 1 & 1.3 \leq h_{prop}/R \end{cases} \tag{3.24}$$

The advance speed is modelled according to equation 3.25 as mentioned earlier this is done by the 'quasi' regular wave approach. The calculation of the advance speed requires the wake factor in still

water (w_s). This is calculated together with the thrust reduction (t_s) factor by interpolation in function of the speed. The wake factor and thrust deduction factor for certain speeds were calculated in the the *'Setup'* of the ship characteristics (sec. 3.3.1).

$$U_{A,total} = U_{A,fluctuating}\frac{U_{A,mean}}{U} \tag{3.25}$$

Where $U_{A,fluctuating}$ is the fluctuating part of the advance speed calculated by equation 3.26 as proposed in [10]. $U_{A,mean}$ is the mean increase of propeller inflow velocity calculated by equation 3.28 as given in [2].

$$U_{A,fluctuating} = (1-w_s)(U-\omega_e|z_1|\sin(\omega_e t-\zeta_1)) + \alpha\omega A_w \exp(-kz_P)\cos\chi\cos(\omega_e t - kx_P\cos\chi) \tag{3.26}$$

Where $|z_1|$ is the surge amplitude, ζ_1 the surge phase and α is a coefficient representing the effect of wave amplitude decrease at the stern given as follows:

$$\alpha = \begin{cases} 0.2\frac{\lambda}{L_{PP}|\cos\chi|} + 0.5 & \frac{\lambda}{L_{PP}|\cos\chi|} \leq 2.5 \\ 1 & \frac{\lambda}{L_{PP}|\cos X\chi|} > 2.5 \end{cases} \tag{3.27}$$

$$U_{A,mean} = U\sqrt{1-\frac{\Delta\bar{p}}{0.5\rho U^2}} \tag{3.28}$$

Where $\Delta\bar{p}$ is the mean pressure increase due to pitching of the ship, this is estimated by equation 3.29 as proposed in [2].

$$\Delta\bar{p} \sim -\frac{\rho}{4}\omega_e^2|z_5|^2x_P^2 \tag{3.29}$$

Where $|z_5|$ is the pitch amplitude.

3.6.2.4 Ship working point

In the last zone the ship´s speed is estimated which is done in two steps, first a new speed is computed based on Newton's first law (eq. 3.30). Afterwards, the ship's speed is estimated by average of the newly calculated ship's speed and the old ship's speed (U_{old} in figure 3.6).

$$M\frac{\mathrm{d}U}{\mathrm{d}t} = T_{eff} - R_T \tag{3.30}$$

Where M is the sum of the mass of the ship (m) and the hydrodynamic added mass of surge (m_{11}). This cannot be calculated by the 2-D strip theory. Instead, the empirical formula 3.31 is used [63].

$$m_{11} = \frac{m}{\pi\sqrt{\rho L_{pp}^3/m} - 14} \tag{3.31}$$

The effective thrust (T_{eff}) is calculated using formula 3.32.

$$T_{eff} = \min\left[\max\left(\beta_T K_T, 0\right), K_{T,max}\right](1-t_s)\rho n^2 D^4 \tag{3.32}$$

K_T is obtained for the $K_T - J$ polynomial with the advance speed as in waves. T_{eff} is assumed to be positive and less than or equal to the thrust linked to $K_{T,max}$ which is the thrust coefficient when the advance coefficient is zero. These assumptions are used because the polynomials are only valid if the propeller is working in the first quadrant ($U_a > 0$ and $n > 0$). Furthermore t_s, the thrust deduction factor is assumed to be the same as for the ship sailing in still water, thus neglecting it varies in presence of

waves [64] as this variation is negligible in most cases [65].

The total resistance is computed by adding the still water resistance and the added resistance together. The still water resistance for the given speed is found by interpolation of the the still water resistances calculated in the *'Setup'*(sec. 3.3). The added resistance calculation uses the 'quasi' regular wave properties and is thus calculated using equation 3.16. This method is used to take into account the resistance increase when the ship encounters a bigger wave train.

Furthermore, the effective torque (Q_{eff}) is calculated using equation 3.33 as this is required for the calculation of the delivered efficiency.

$$Q_{eff} = \min\left[\max\left(\beta_T^m K_Q, K_{Q,min}\right), K_{Q,max}\right] \rho n^2 D^5 \tag{3.33}$$

The factor m takes into account that there is less torque loss than thrust loss as stated in [2]. m is set at 0.83 because this is in the median of the range given in that paper. Similar to K_T, K_Q is calculated from the $K_Q - J$ polynomial and has a maximum value equal to $K_{Q,max}$. The minimum value of $K_Q (= K_{Q,min})$ is the residual torque coefficient equal to the torque coefficient for which the thrust coefficient is zero.

Chapter 4

Validation of the simulation code

The simulation code implemented in the previous chapter is a key element of the propeller selection in waves. Thus, it is fundamental to verify its accuracy before further employment. As previously mentioned, the simulation code is based on [11]. It is therefore logical that simulation is mainly compared to that work. Nevertheless, it must be noted that not all the results presented in [11] could be used. To obtain obtain all the results, a more complex engine model would have to be implemented as consequence only four results are compared: RAO of pitch, RAO of relative propeller hub motion and effect of waves on the wake and on the torque. In [11] information about still water resistance is not reported. Moreover, a modified geometry of the KVLCC2 propeller is used, which is not a Wageningen B-series propeller. Thus, the validation of these inputs has been done by comparison to other literature. The Wageningen B-series is validated using [5], the still water resistance using [12] and the added resistance using [66]. In the last section of this chapter some simulation results in irregular sea states are discussed.

The main characteristics of the KVLCC2, used for the validation, are given in table 4.1. This vessel was chosen to make the comparison of some simulation results given in the main reference paper possible. The propeller used in this chapter is the $B4-432$ with $P/D=0.47$ and $D=9.86$. The only difference between this propeller and the propeller used in the main reference is that the latter has a skew of $21.15°$.

$L_{PP}\ [m]$	$L_{WL}\ [m]$	$B\ [m]$	$d\ [m]$	$\Delta\ [ton]$	C_B	$U_S\ [kn]$	$x_P\ [m]$	$z_P\ [m]$
320	325.5	58	20.8	312622	0.8098	15.5	$-0.49L_{PP}$	$-0.045L_{PP}$

Table 4.1: Ship particulars of the KVLCC2

4.1 Verification of the Oosterveld polynomials

The polynomials are verified to guarantee that there are no fundamental mistakes in the evaluation of the propeller's (open water) performance. The results of the polynomials generated by the code coincide with those found in the literature as shown in figure 4.1 for the particular case of the B4-70 propeller.

4.2 Verification of the RAO

According to the adopted models, surge and pitch motions have an influence on wake velocity and, consequently, on the performance of the propeller. Moreover, the relative motion of the propeller hub

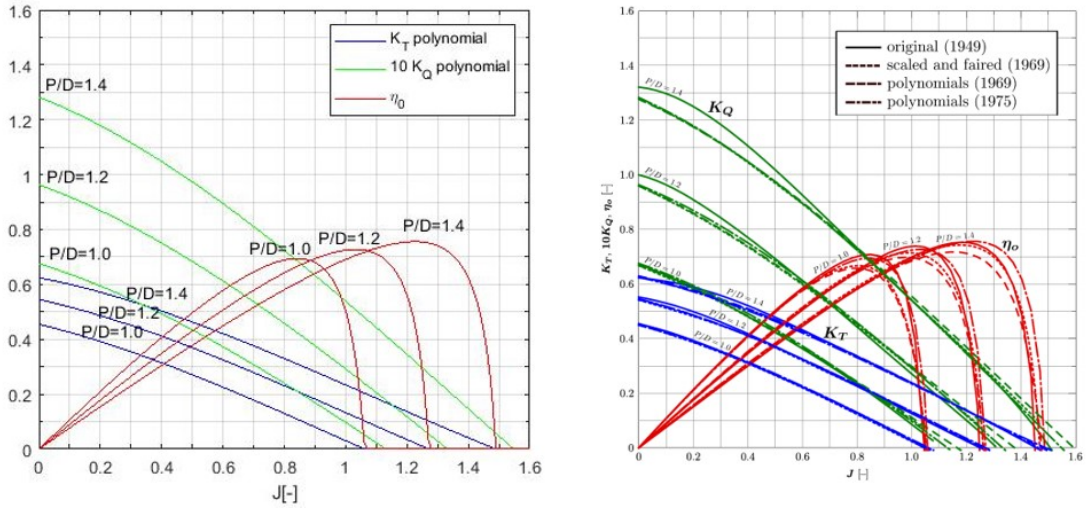

Figure 4.1: Comparison between by code generated polynomials (left) and polynomials shown in [5](right) for the Wageningen B4-70

influences ventilation. The RAO of surge could not be calculated by the strip theory that is used in the code developed at CENTEC. Therefore, the RAO of surge is directly based on the inputs of [11], thus it will not cause mismatch in the following steps. As a preliminary step to allow a correct comparison of the wake and torque later on, the RAOs related to pitch and relative motion are compared with those used in [11]. In the reference the RAOs of the ship motion are calculated using linear strip theory, as implemented in the ShipX Veres software. The RAO in the simulations is calculated by the code developed by CENTEC that is also based on the strip theory as formulated in [17].

In figure 4.2 the RAOs of the pitch motion for different wave directions are compared. Although some minor differences can be identified, these are within acceptable limits.

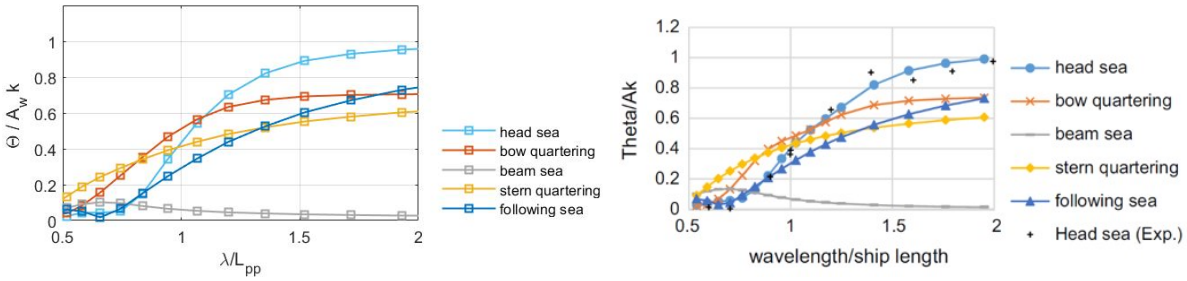

Figure 4.2: Comparison of the RAO of pitch amplitude used in the simulation (left) and used in [11](right)

The RAO of the relative motion of the propeller hub is shown in figure 4.3 and its phase in figure 4.4. The amplitude matches well, yet the phase does not match. This can be explained by the fact that in the sea-keeping code, developed at CENTEC, the regular waves are assumed to have a through on the position of the centre of gravity. This results in phase of the motions to have a 180° shift with respect to the usual convention.

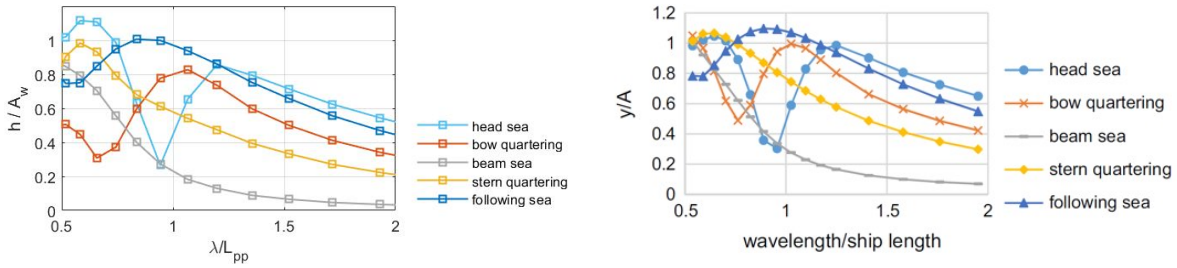

Figure 4.3: Comparison of the RAO of relative motion amplitude used in the simulation (left) and used in [11](right)

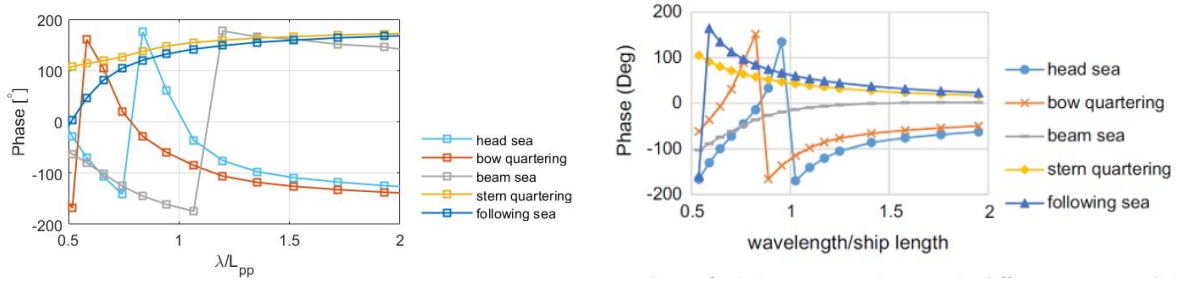

Figure 4.4: Comparison of the RAO of relative motion phase angle used in the simulation (left) and used in [11](right)

4.3 Verification of the wake variation

In section 3.6.2.3 the procedure adopted for the calculation of the propeller inflow velocity was presented. In [67] wake measurements were made in regular waves for three wavelengths with an amplitude of 3 meters. In [11] simulations were done for the same waves. These simulations are repeated with simulation code. The comparison is shown in figure 4.5. These measurements and simulations were done with the ship sailing at constant design speed, not taking into account the balance between propeller thrust and ship resistance, thus the wake varies only due to the ship motions. In the figure the still water wake factor is also plotted. The still water wake factor calculated according to [26] gave a values of around 0.1 lower than in the measurements, therefore it is forced to the value of the measurements made in [67] to allow fair comparisons to be made. Table 4.2 gives the mean propeller inflow increase due to pitch calculated by both references and by the simulation code. The increase is given in percentage compared to still water wake velocity. Both the table and figure show a good correlation between the simulation and the references. It can be concluded that the simulation of the wake velocity is consistent.

λ/L_{PP}	A_w	**% increase in mean wake velocities**		
		Simulation code	Simulations in [11]	Experimental data [67]
0.6	3	0.00%	0.03%	0%
1.1	3	2.50%	2.70%	5.0%
1.6	3	2.14%	2.66%	2.2%

Table 4.2: Comparison of increase in mean propeller inflow due to pitch in head waves using formula and experiments

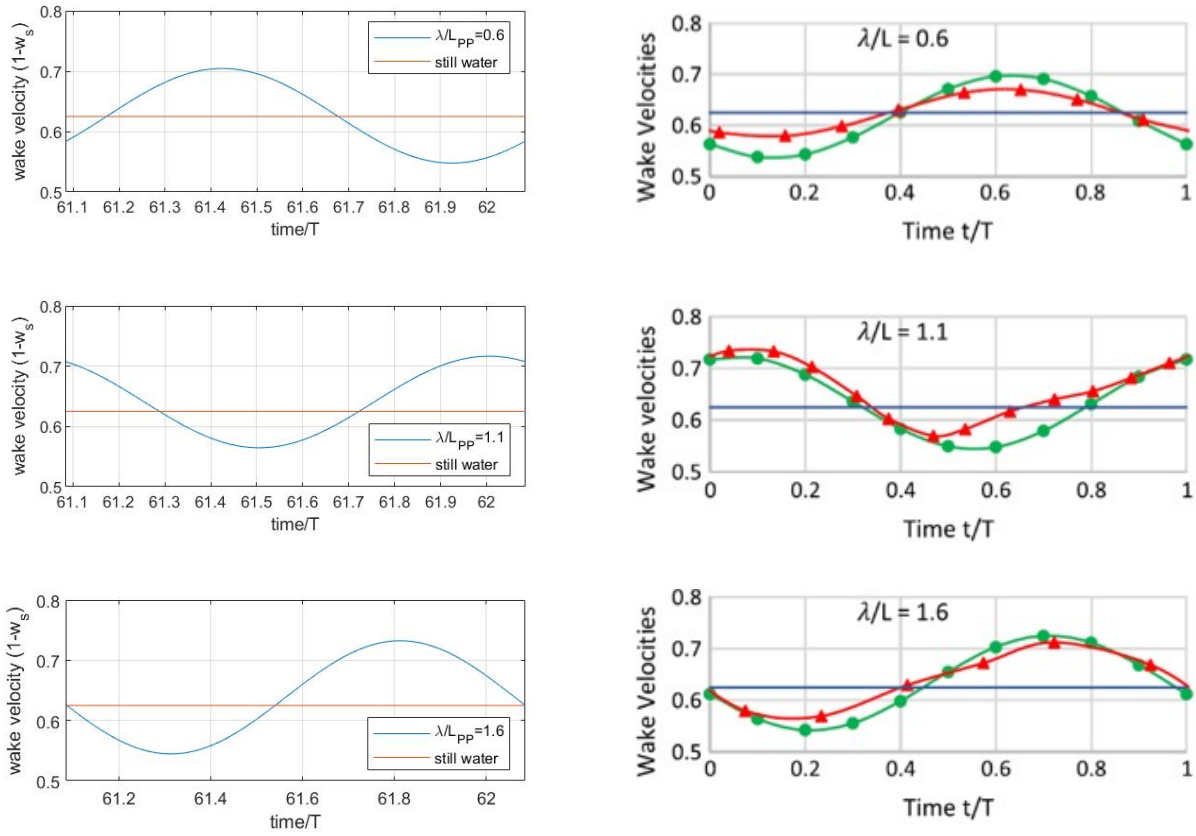

(a) Simulation

(b) Green: simulations of [11] Red: measurements [67], Blue: still water

Figure 4.5: Simulations of the fluctuating wake in regular waves with an amplitude of 3 meters

4.4 Verification of the still water resistance

The added resistance in the simulation is calculated by Holtrop and Mennen's method which was studied in detail in section 2.1.1.2. In [12] calculations by this method are compared to model tests of the KVLCC2. The comparison for the effective brake horse power (EHP) is shown in figure 4.6. For a Froude number between 0.055 and 0.085 the difference is more than 10%. This represents the speed range between 6 and 9.25 knots. This speed range is only reached when a speed drop of more than 40% occurs compared to the service speed. The ship propeller is normally not optimised for this speed range, nor will sail at such a speed in the simulation code. Therefore, the used method for the still water resistance is considered sufficiently accurate for the sake of these simulations.

4.5 Verification of the added resistance in regular waves

In [66] the added resistance of the KVLCC2 for different wave heights was obtained from towing tank measurements with a KVLCC2. This added resistance is compared to the ones calculated by the code developed at CENTEC in table 4.3. It can be seen that the calculated value by the code is always lower than the one of the measurements. Thus, it can be expected that the speed loss in the simulation will be less than the actual loss. The differences between the calculations and the measurements may due to the limitations of the far-field method for blunt ships and the estimation of the diffraction component of the added resistance in short waves. Another peculiarity is that with increasing speed the added

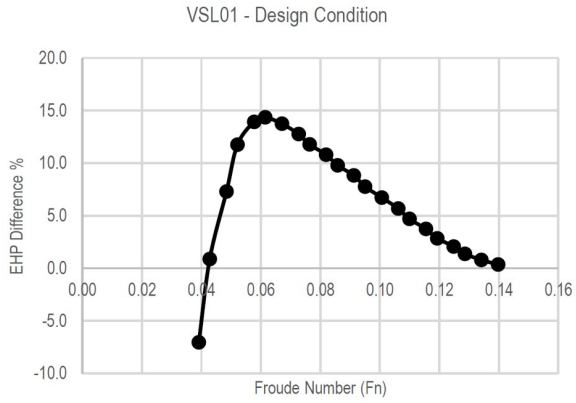

Figure 4.6: Distribution of the EHP difference (%) over different speeds at design load [12]

resistance does not always increase in the calculations. This can be due to some small humps in the curves of the calculated dimensionless added resistance coefficient that are more pronounced for lower speed.

A_w/λ	$R_{AWS,calc}[kN]$	$R_{AWS,Lee}[kN]$
Speed 15.5		
0.007	65	146
0.017	381	726
0.023	698	1241
0.033	1437	2621
Speed 15kn		
0.007	74	126
0.017	434	710
Speed 14.5kn		
0.007	82	110
0.017	486	696
Speed 14kn		
0.007	60	95
0.017	355	683

Table 4.3: Comparison of the added resistance for $\lambda/L_{PP} = 0.6$

4.6 Verification of the torque

In [11] simulations of the torque in regular waves with the same wavelengths as for the wake variation were done but with a wave amplitude of 5 meters. This high amplitude was taken to demonstrate the effect of ventilation. The ship's speed was kept constant and equal to 14.7 knots which is the attainable speed in still water with the given propeller at $95rpm$. The comparison between those simulations and the simulation code in this thesis is shown in figure 4.7, 4.8 and 4.9. The torque amplitudes are not matching the reference exactly but they are with acceptable limits. The average of the torque is higher than in the simulations of the reference this might be partly explained by the skew.

In figure 4.9 the effect of the ventilation can be seen in the reference simulation while this is not present in my simulation. This could not be explained until now and an email was send to the author of the

reference who, on the moment of writing could not explain why there is ventilation in fig. 4.9 and not in fig. 4.8 while the RAO of the relative motion is the more or less the same for both wavelengths.

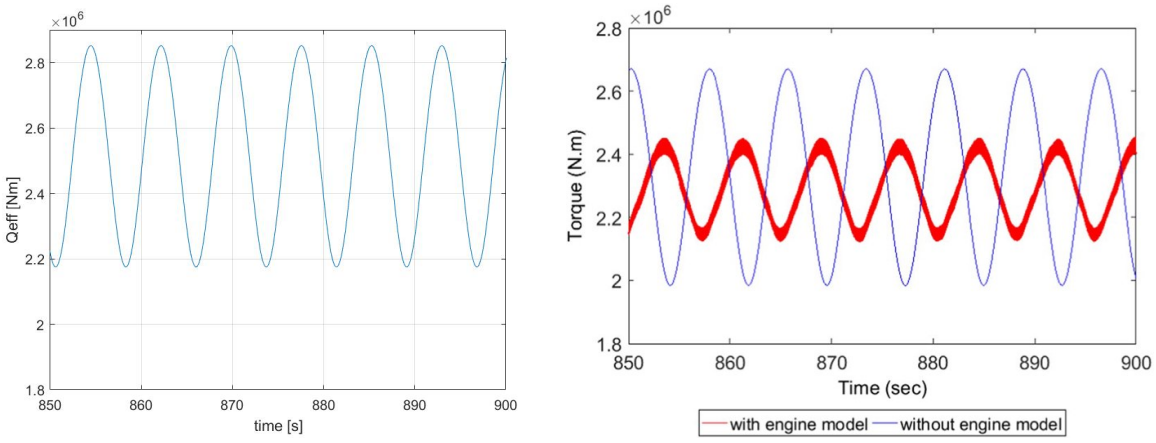

Figure 4.7: Comparison of the torque by the simulation code (left) and torque of the reference simulation (right) [11] for $\lambda/L_{PP} = 0.6$

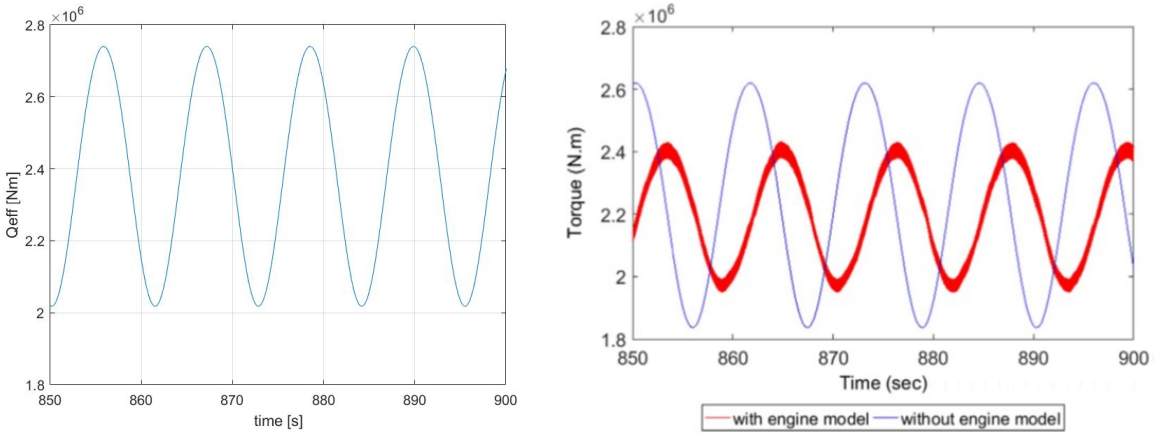

Figure 4.8: Comparison of the torque by the simulation code (left) and torque of the reference simulation (right) [11] for $\lambda/L_{PP} = 1.1$

4.7 Simulations in irregular sea

The KVLCC2 in combination with the same propeller and engine speed as above was simulated in five sea states based on the scatter diagram from DNV in the North Atlantic:

- **SS1**: the most probable sea state ($H_s = 1.5m$ and $T_p = 7.5s$)
- **SS2**: the average sea state ($H_s = 3.4m$ and $T_p = 8.9s$)
- **SS3**: a rough sea state that the ship might try avoid with a probability of 2.37%. ($H_s = 5.5m$ and $T_p = 9.5s$)
- **SS4**: a severe sea state that the ship would normally avoid with a probability of 0.70%. ($H_s = 7.5m$ and $T_p = 10.5s$)

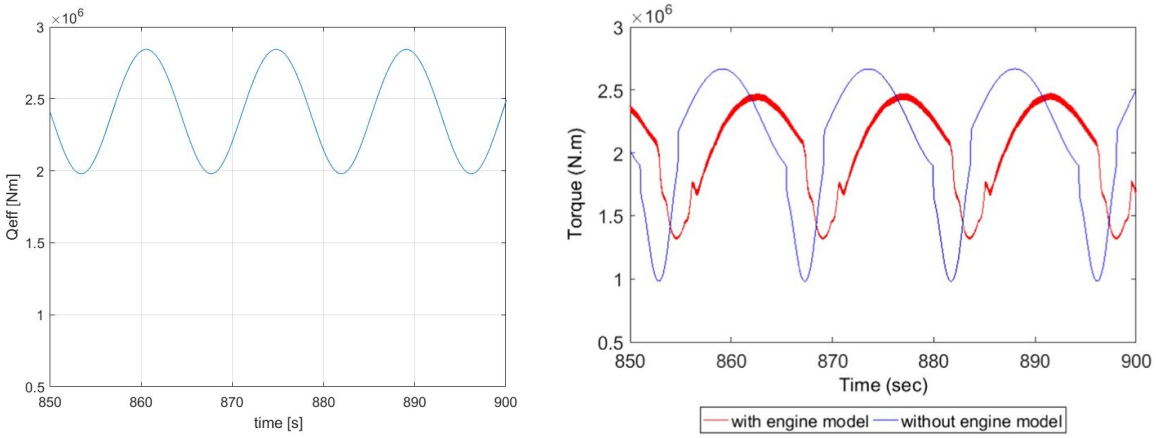

Figure 4.9: Comparison of the torque by the simulation code (left) and torque of the reference simulation (right) [11] for $\lambda/L_{PP} = 1.6$

- **SS5**: a very severe sea state that the ship would normally never be in a probability of 0.01%. ($H_s = 12.5m$ and $T_p = 12.5s$)

For all these sea states, five simulations of 120 minutes have been performed. In all five simulations, the wave frequencies have another phase (ϕ) with respect to each other. As consequence each wave profile different and thus also the simulation. The simulations serve to verify the consistency of the results and to verify if the speed loss is realistic. Next to this the simulations are also used to find a simulation time that gives good accuracy while not requiring excessive computation time. The different speed plots are shown in figure 4.10. The numerical averages and differences of several parameters are summarised in table 4.4, these parameters are:

- Average speed taken over the 5 runs ($\overline{U}$)
- Difference in average speed ($\Delta\overline{U}$) between the 5 runs
- Average delivered efficiency ($\overline{\eta_{D,s}}$) taken over the 5 runs
- Difference in delivered efficiency ($\Delta\overline{\eta_{D,s}}$) between the 5 runs
- Speed loss compared to still water

The speed loss is given for the average speed of the 120 minute simulation. The other parameters are given for three different simulation periods. Namely for 120 minutes, 45 minutes and 20 minutes.

4.7.1 Ventilation in irregular seas

In the severe sea states simulations (SS4 and SS5), ventilation is expected to occur. Therefore the ventilation loss factor is plotted for those simulations in figure 4.11. As expected ventilation occurs, however the effect is only present in SS5. The practically non-existent ventilation loss is due to the fact that the propeller hub is positioned around 14.4 meter below the still water line and the RAO of the relative motion is never much higher than one.

A close-up of the speed, ventilation loss factor, ship resistance and effective thrust of a simulation in SS5 is shown in 4.12 and a deeper close-up is shown in figure 4.13. In the close-ups the added resistance has blocked shape due to the 'quasi' regular wave approach. In fact, as long as the same 'quasi' regular wave is at midships, the added resistance is taken as for the regular wave with the corresponding

	SS1	SS2	SS3	SS4	SS5
$\overline{U}$ $[kn]$ (120min)	14.81	14.78	14.67	14.31	7.53
$\overline{U}$ $[kn]$ (45min)	14.81	14.78	14.67	14.27	7.45
$\overline{U}$ $[kn]$ (30min)	14.81	14.78	14.67	14.26	7.36
$\Delta\overline{U}$ $[kn]$ (120min)	0.00	0.00	0.00	0.03	1.68
$\Delta\overline{U}$ $[kn]$ (45min)	0.00	0.00	0.00	0.01	1.70
$\Delta\overline{U}$ $[kn]$ (30min)	0.00	0.00	0.01	0.05	7.36
$\overline{\eta_P}$ (120min)	0.555	0.554	0.552	0.543	0.319
$\overline{\eta_P}$ (45min)	0.555	0.555	0.552	0.541	0.312
$\overline{\eta_P}$ (30min)	0.555	0.555	0.552	0.539	0.328
$\Delta\eta_P$ (120min)	0.000	0.000	0.000	0.001	0.060
$\Delta\eta_P$ (45min)	0.000	0.000	0.000	0.003	0.036
$\Delta\eta_P$ (30min)	0.000	0.000	0.002	0.008	0.009
speed loss	0.0%	0.2%	0.9%	3.4%	49.1%

Table 4.4: Comparison between the several simulation runs and simulation periods

amplitude and length. Thus is nearly constant during this time. The slightly tilted horizontal lines in the resistance are only due to the variation in the vessel speed. The blocked shape could be reduced by taking the average 'quasi' regular wave over a certain length of the ship. This is not done in the simulation code because this would have a big negative influence on the calculating speed. The calculation of the regular wave properties already takes 73% of the simulation time, more details are given in the profile summary in appendix A.1 (function name is *calc_0upcrossing*). The blocked shape of the resistance is the cause of the sharp corners in the close-up of the speed. When looking at the close-up of the effective thrust, there is a drop when ventilation happens. In addition, the effective thrust shows several other jumps, these are caused by the 'quasi' regular wave approach used in the calculation of the wake velocity. Similar as for the resistance, this approach causes a sudden jump. At the moment of the ventilation, a reduced steepness in the vessel speed increase can be noticed. This effect is very limited due to the dampening effect of the big inertia of the ship and the short time of thrust reduction. It can be concluded that the code of ventilation loss factor works yet the effect of ventilation is minimal and might be underestimated as there was no ventilation in the regular waves while the reference paper had ventilation for regular waves (section 4.6).

4.7.2 Discussion of ship's speed and delivered efficiency

When looking at the speed plots of it seems that for some sea states it takes around 15 to 20 minutes for the ship speed to fluctuate around a fixed average. The reason might be the small difference between the estimated speed for the average added resistance of irregular waves and the varying added resistance calculated for the 'quasi' regular wave. As to verify if it is required to exclude an initial transition from the statistical analysis of the results, a moving average over 20 minutes was taken for the simulations. The plot of the moving average of SS1 and SS3 is shown in figure 4.14. No significant variations can be noticed to justify the elimination of the initial results, neither when different averaging windows are considered.

Thus it is justified to compute the averages from the beginning of the simulation, this reduces the simulation period and, therefore, the computation time. The fact that the initial speed is close to the speed of the ship proves that added resistance calculated by the 'quasi regular wave properties gives a good representation of the average added resistance of the wave spectrum.

In simulations in more severe the sea states, the differences between the runs is bigger. This is expected because the bigger wave amplitude makes the effect of different ϕ more pronounced. It is also intuitive

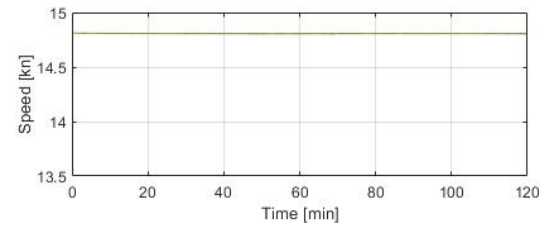

(a) SS1

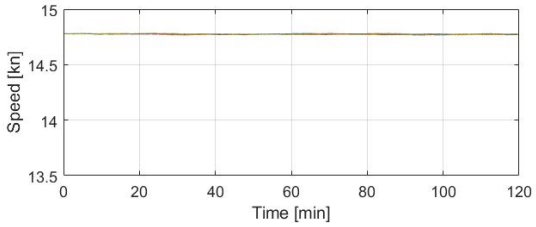

(b) SS2

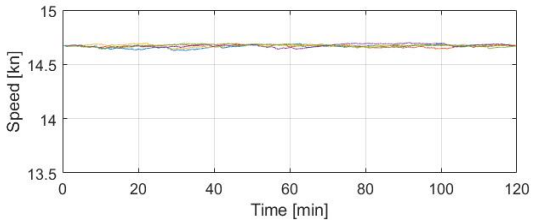

(c) SS3

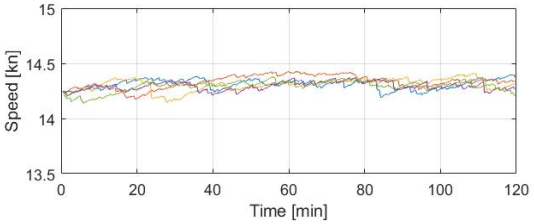

(d) SS4

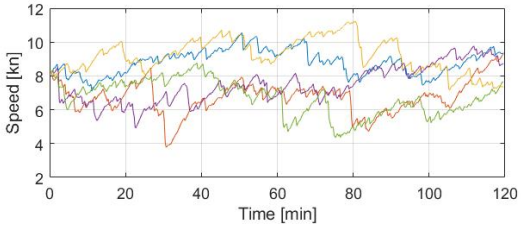

(e) SS5, note that a different scale on the y-axis than in the other simulations is used

Figure 4.10: Five runs in several sea states for an engine speed of $100rpm$ and the a $B4-432$ with $P/D=0.47$ and $D=9.86$ propeller during 120 minutes

to understand when thinking about such a situation in real life. It can happen that while two ships are sailing within sight of each other one ship hits a heavy wave train and loses speed while the other ship might just hit a calmer wave train and gain speed. This visible trend is also confirmed by $\Delta\overline{U}$ in table 4.4. However, it must be noted that in the very severe sea state the Shipmaster will slow down the ship and that not all non-linearities of the real world are modelled. These two factors cause the simulations to be less representative of the more complex reality in severe sea states.

The table also shows a comparison of different simulation times, this is used in combination with the moving average to determine the simulation time to be used in the propeller selection. The simulation of 120 minutes is used as reference and is assumed to be free of statistical inaccuracies. This simulation time is not practical for the optimisation because it takes around 15 minutes to simulate one run (see

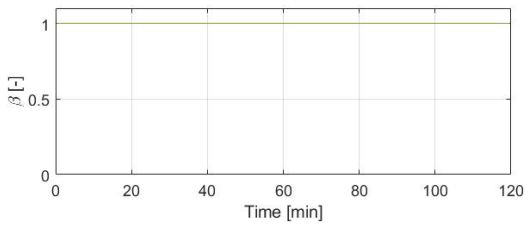

(a) SS4

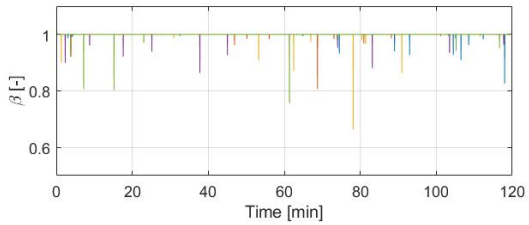

(b) SS5

Figure 4.11: Ventilation loss factor in SS4 and SS5 for an engine speed of $100rpm$ and the a $B4-432$ with $P/D=0.47$ and $D=9.86$ propeller during 120 minutes

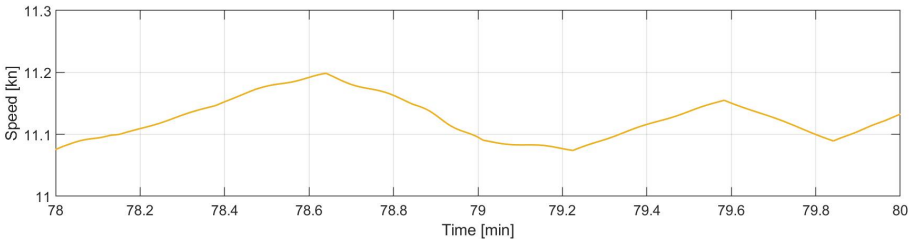

(a) Vessel speed

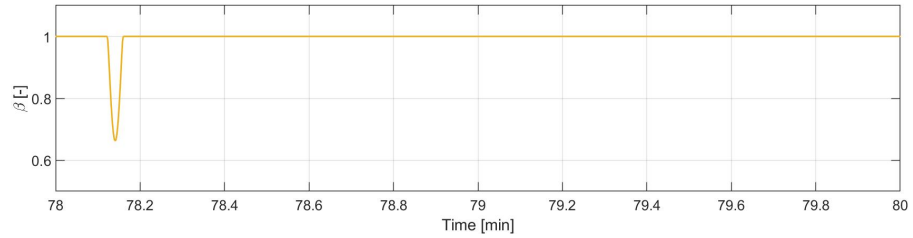

(b) Ventilation loss factor

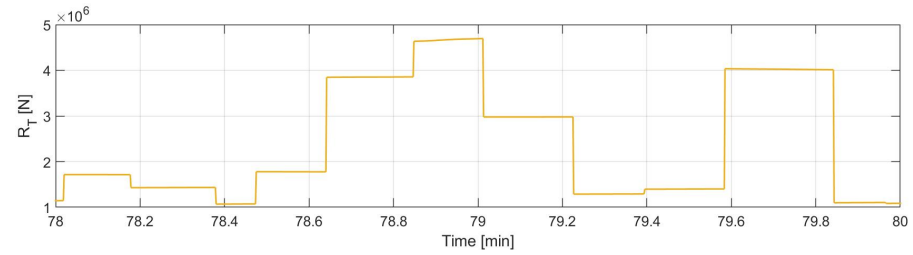

(c) Total ship resistance

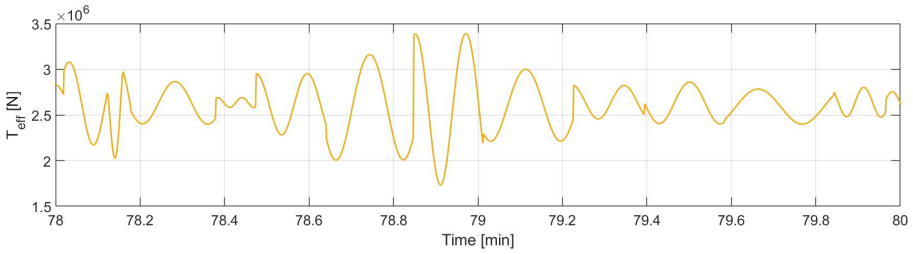

(d) Effective thrust

Figure 4.12: Close-up of the orange run in SS5 of figure 4.11($H_s = 12.5m$ and $T_p = 12.5s$)

profile summary in appendix A.1). Except for SS5, the differences between the simulation times are very small. The average speed and delivered efficiency do barely change and the spreading of the averages is not significant, so the 20 minutes simulation gives good results while having a shorter computation time.

When looking at the results in the table for SS5, differences between the simulation periods are present. In such a sea state the short simulations times are not accurate because the variance between the waves is amplified. On longer runs this variance is levelled out as all simulations will have heavy wave trains and calm wave trains. SS5 and even SS4 are not considered in the propeller optimisation because the Shipmaster will avoid these sea states in real life. Therefore, it can be concluded that a 20 minute simulation is adequate, this is further justified by the plots of the moving average (fig. 4.14). This conclusion might not be valid for smaller vessels as they are more sensitive to waves, therefore similar simulations should be executed before starting a propeller selection in waves for smaller ships.

Another interesting parameter is the speed loss, which increases with a more severe sea state. This is as expected because the added resistance increases. As mentioned section 4.5 the added resistance

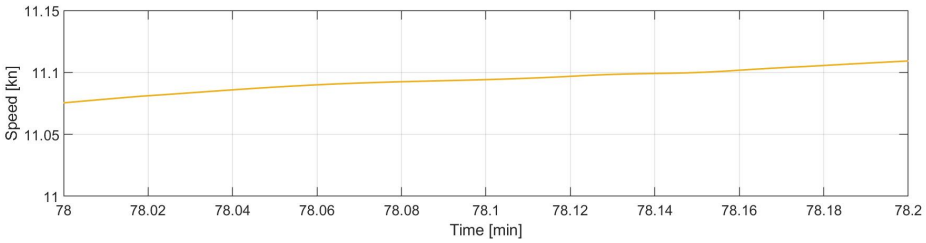

(a) Vessel speed

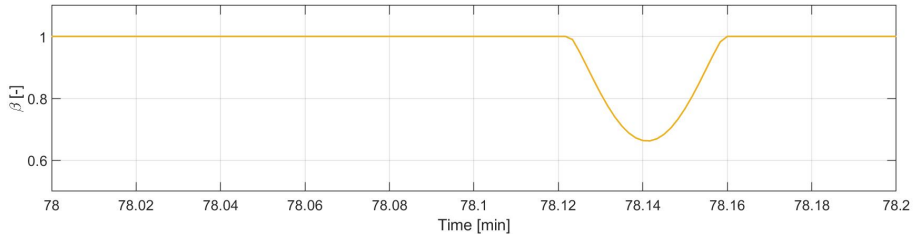

(b) Ventilation loss factor

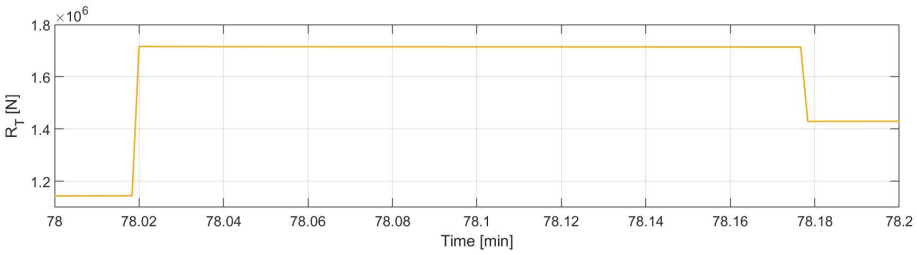

(c) Total ship resistance

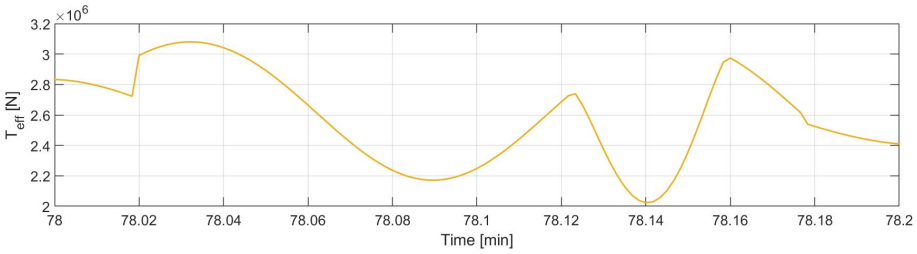

(d) Effective thrust

Figure 4.13: Very deep close-up of the orange run in SS5 of figure 4.11($H_s = 12.5m$ and $T_p = 12.5s$)

is underestimated and therefore the speed loss will be underestimated too.

The delivered efficiency can be compared to the values given in the literature for still water. They lay usually between 0.7 and 0.75 which is higher than the delivered efficiency in the simulation [6]. This was expected because the propeller used in these simulations is not an optimised propeller and is used in waves. Furthermore, the ship´s shape is not efficient either.

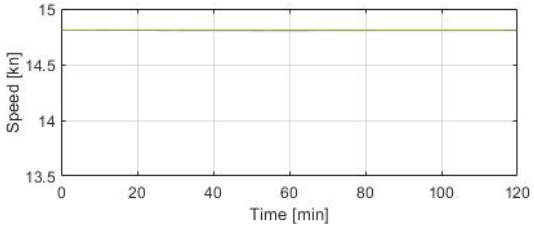

(a) SS1

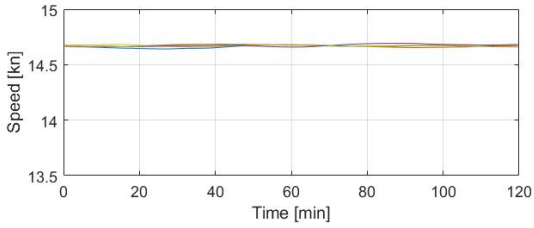

(b) SS3

Figure 4.14: 20 minute moving averages of the ship's speed

Chapter 5

Propeller selection

In what follows, the propeller selection procedure is applied to select propellers for the KVLCC2 tanker and the S175 containership. Based on the validation done in the previous chapter, it is clear that the simulation code presented has some limitations, but still provides a reasonable representation of the propeller operations in waves. Consequently, the results presented in this chapter can be considered as indications and can show the tendencies in the selection of the propeller of real weather conditions, although a certain level of inaccuracy is expected.

5.1 Propeller selection for the KVLLC2

In this section a propeller for the KVLCC2 sailing in head waves is selected for four different conditions, including still water and three different waves conditions. The selection for still water operations is firstly discussed, recalling that the resulting propeller is used as an initial guess in the other selections. The main parameters of this ship were given earlier in table 4.1.

To start the selection, the boundary conditions and an initial guess of the propeller are required. All the boundary conditions except for the cavitation criteria are defined as listed below:

$$\begin{aligned} &0.5 \leq P/D \leq 1.4 \\ &0.4 \leq A_e/A_0 \leq 1.00 \\ &0.3d \leq D \leq 2/3d \\ &76rpm \leq n \leq 110rpm \\ &0.6MCR \leq P_D \leq 0.9MCR \end{aligned} \tag{5.1}$$

The KVLCC2 has no dedicated engine assigned, therefore it is assumed to use a slow running diesel engine without a gearing system. As a consequence the boundaries of the rotation speed are limited by average speed limits of such an engine as found in [68]. Furthermore, the power is limited to 60% till 90% of the maximum continuous rate (MCR) of the engine power, assimilating the common recommendations of the engine manufacturers for long continuous operations (above 2 hours). The MCR is estimated to be equal to $P_E/0.5$ which is approximately $3.5\ 10^4 kW$. This estimation is based on the calculation of the delivered power of the optimal propeller selected in still water at service speed without power boundary conditions. P_E is computed for the ship operating in still water at service speed.

5.1.1 Still water selection for the KVLCC2

In the propeller selection in still water, the propeller previously adopted in the simulations in irregular waves ($B4-43.2$ with $P/D = 0.47$ and $D = 9.86$) is considered as the initial guess. The still water selection procedure required 7 iterations to find the maximal efficiency as shown in figure 5.1a. This figure does show $1/\eta_0$ on the Y-axis and therefore these values are bigger than one. The still water selection itself took 0.291 seconds and the total time that the code ran was 5.978s. This time includes the reading of the values defined in the *'Setup'*, therefore the use a better initial guess of the propeller is not required as it would not result in a significant faster calculation time.

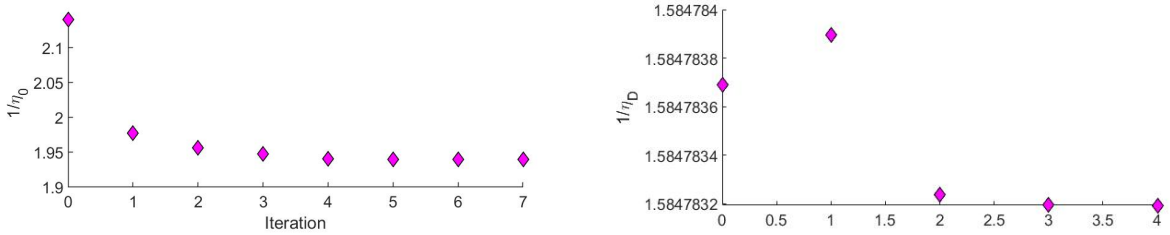

(a) (b)

Figure 5.1: Function value for each iteration for the propeller selection for the KVLCC2 in still water(a) and in SS2 (b)

Next to the still water selection done by the *'fmincon'* non-linear optimisation function, a simpler code was implemented to validate the selection. This simple code selects the best propeller from a given set of A_e/A_0, P/D and D limited by the boundary conditions (sec. 5.1). The step size in this set was put on 0.01 for all three variables. For all the combinations in the set, the still water efficiency in the code is computed by the use of the K_T/J^2-polynomials, in the same way as it is calculated within the *'fmincon'* function. Given the finite step size, this code has limited accuracy. The selected propellers given by the simple code and by *'fmincon'* are summarised in table 5.1. While these propellers are not the same, the difference is small and the simple code gives a lower efficiency while the computation time was over 30 minutes. Thus, the *'fmincon'* function is providing satisfying results and is significantly faster.

	A_e/A_0	P/D	$D\ [m]$	η_0	$n\ [rpm]$
fmincon	0.479	0.644	10.252	0.5153	76.0
simple code	0.480	0.640	10.270	0.5151	76.1

Table 5.1: Comparison of the propeller selected by the 'fmincon'-function and by a simple Matlab code

5.1.2 Propeller selection of the KVLCC2 for specific sea states

A simulation period of 20 minutes is used in the selections as this gives good ratio between accuracy and computation time (see section 4.7.2). Furthermore, ϕ is kept constant during each selection procedure to have exactly the same wave profile in all of the simulations. The engine speed is kept constant during the simulation of a propeller, however it varies between different propellers in such way that it is equal to the rotation speed required by that propeller to propel the ship at service speed in still water.

Three different propellers are selected. Each one is selected to be optimal for a distinct sea state, namely SS1, SS2 and SS3 as defined in section 4.7, thus excluding the most extreme conditions. The results of these selection procedures are summarised and compared to the propeller selected for still water in table 5.2. Besides the propeller properties, the total computation time (t_c) and the number of

iterations (N_{it}) are also given in the table. The number of iterations is not the same as the amount of simulations executed; in fact for each iteration *'fmincon'* does several simulations to identify in which 'direction' the minimum is located. The amount of simulations executed in each iteration is not fixed, therefore it may happen that while the number of iterations is the same, the total computation time is different. In addition, the computation time of a simulation is also depended of the sea state, propeller and ship.

	Still water	**SS1**	**SS2**	**SS3**
Acronym propeller	$KVLCC2.0P$	$KVLCC2.1P$	$KVLCC2.2P$	$KVLCC2.3P$
A_e/A_0	0.4788	0.4786	0.4792	0.4788
P/D	0.6447	0.6445	0.6451	0.6447
$D\ [m]$	10.246	10.247	10.244	10.246
$n\ [rpm]$	76	76	76	76
$t_c\ [min]$	0.1	59	69	771
N_{it}	7	4	4	14
$\eta_{D,s,optimised}$		0.6308772	0.6310011	0.6283390
$\eta_{D,s,KVLCC2.0P}$		0.6308772	0.6310009	0.6283389
$\eta_{D,still}$	0.6309	0.6309	0.6309	0.6309
η_0	0.5155	0.5155	0.5155	0.5155
$\overline{U}_{optiwave}\ [kn]$	15.50	15.50	15.47	15.39
$\overline{U}_{optistill}\ [kn]$		15.50	15.47	15.39

Table 5.2: Propellers selected for the KVLCC2 with still water resistance boundary conditions

The evolution of the function values for the optimisation in average sea (SS2) is shown in figure 5.1b. This evolution is similar to the one shown for the still water selection (fig. 5.1a).

The characteristics of the propellers selected based on certain sea-state are only minimally altered with respect to the propeller selected for still water operation. These minor changes resulted in a negligible increase of delivered efficiency in the given sea-state and additionally the selection in waves took a lot longer. To explain the reason of such negligible differences, it must be considered that the propeller is deeply submerged ($14.4m$) and the KVLCC2 is a very large ship, thus its motions are not significantly amplified by the frequency ranges of the wave spectra found with higher probabilities. Furthermore, the propeller characteristics are not used in the inflow velocity model thus the changes are 'quasi' independent of the propeller. Another factor that could have contributed, is the underestimation of the added resistance as this lowers the difference between still water and the sea-states. Thus, it can be concluded that the operation of the propellers of such large ships is not significantly influenced by the presence of waves. So, the proposed selection procedure in waves is not practical for such type of ship.

5.2 Propeller selection for the S175

The propellers selected for the KVLCC2 in waves only had minor changes compared to the propeller selected in still water. It was proposed that this might be caused by the size of the ship, therefore the same procedure is applied for a smaller container-ship, the S175. The main parameters of this ship are given in table 5.3.

$L_{PP}\ [m]$	$B\ [m]$	$d\ [m]$	$\bigtriangledown\ [ton]$	C_B	$U_S\ [kn]$	$x_P\ [m]$	$z_P\ [m]$
175	25.4	9	24252.55	0.57	19	$-0.49L_{PP}$	-6

Table 5.3: Ship particulars of the S175

The ship motion and resistance characteristics are computed by the code developed by CENTEC. This code has been validated for the S175 in [14] and [15]. However, as already previously mentioned, the RAO of surge can not be calculated by that code. Therefore, the surge is assumed to dependent on λ/L_{PP} and less influenced by the shape of the ship. In other words, the non-dimensional curve used for the KVLCC2 is assumed to be valid for the S175. Furthermore, the boundary conditions are adapted to suit the S175 and are as follows:

$$\begin{aligned} &0.5 \leq P/D \leq 1.65 \\ &0.45 \leq A_e/A_0 \leq 1.05 \\ &0.3d \leq D \leq 2/3d \\ &76rpm \leq n \leq 110rpm \\ &0.6MCR \leq P_D \leq 0.9MCR \end{aligned} \tag{5.2}$$

The same reasoning as for the KVLCC2 is used for the calculation of the engine speed and the maximal continuous rate. This gives the same engine speed limits and MCR equal to $1.24\ 10^4 kW$. The selections are executed for a five-bladed propeller, as is commonly found in container ships.

5.2.1 Still water selection for the S175

The initial guess for the still water propeller selection is based on the initial guess for KVLCC2, but with a reduced diameter and five blades ($B5-43.2$ with $P/D = 0.47$ and $D = 5.86m$). This propeller does not satisfy the boundary conditions, but *'fmincon'* does not require this. In this case, *'fmincon'* changed the values to meet the boundary conditions. The properties of the selected propeller in still water are given in table 5.5.

5.2.2 Propeller selection of the S175 for specific sea states

In section 4.7.2 the KVLCC2 was simulated sailing for 120 minutes in different sea-states. It was noted that similar simulations should be executed before starting a propeller selection in waves for other ships. Therefore, the S175 with propeller selected for still water is simulated in SS2 and SS3. For both sea-states five simulations of 120 minutes were carried out, the speed plots are shown in figure 5.2. As expected the speed loss in SS3 is larger than in SS2 just as it was for the KVLCC2.

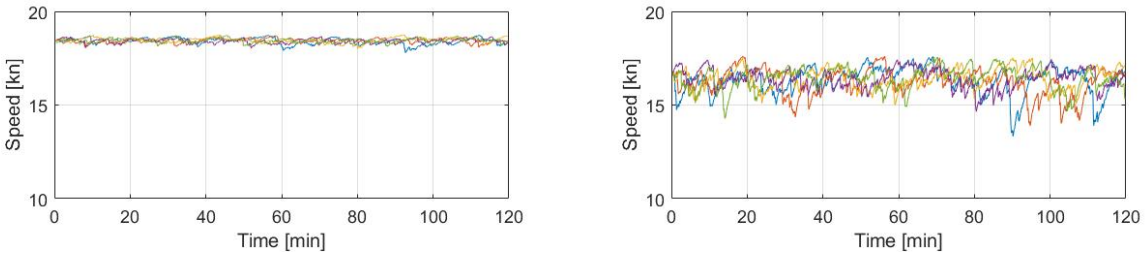

(a) SS2 (b) SS3

Figure 5.2: Speed of the S175 and the $B5-69.1$ propeller with $P/D = 0.981$ and $D = 6m$ during 120 minutes in SS2 and SS3

When these speed plots are compared to those of the KVLCC2 (fig 4.10), the speed fluctuations are more evident. In fact, this can be expected considering as the ship is smaller, subjected to larger motions and the probability of propeller emergence is higher. Therefore, longer simulations might be required

to ensure time independent statistical averages for the propeller selection. In order to determine an adequate simulation time, moving averages over 20, 30 and 40 minutes are taken. These are shown in figure 5.3 for the simulation in SS3. In those figures a vertical black line was drawn at the midpoint of the first averaging window. For example, a black line is drawn at 10 minutes for a 20 minute moving average. The figures demonstrate clearly that a longer time of the moving average flattens the lines, nevertheless it never completely flattens. Furthermore, the difference between the 30 and 40 minute moving average is minimal, while the difference with a 20 minute moving average is more pronounced. Therefore, 30 minute simulations are used for the propeller selection procedure of the S175.

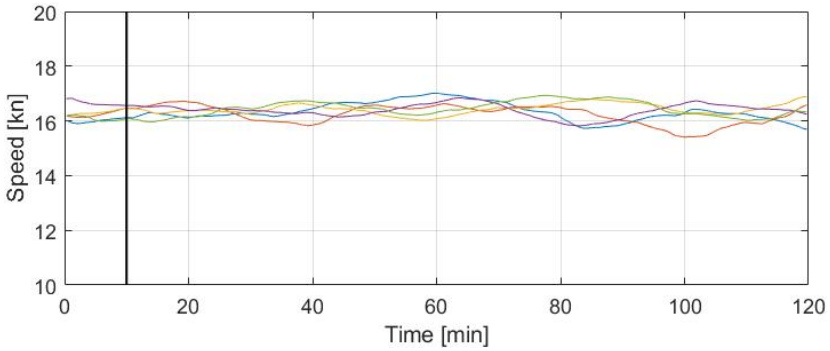

(a) 20 minute moving average

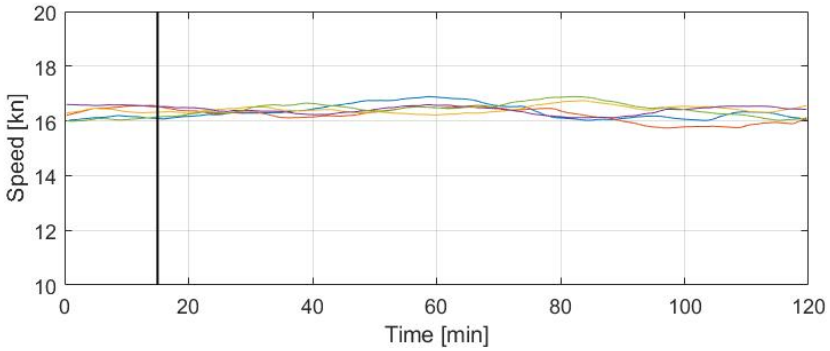

(b) 30 minute moving average

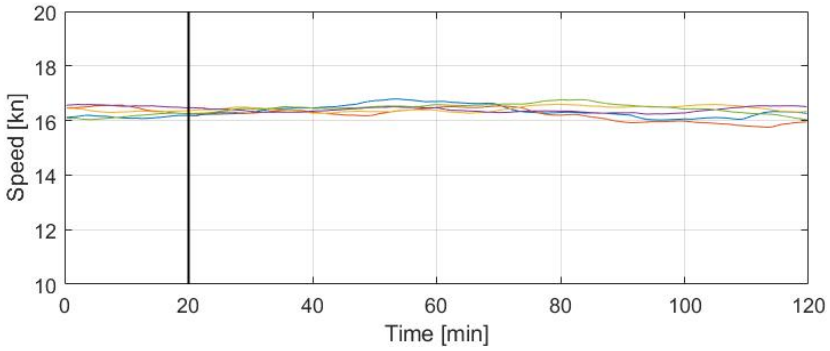

(c) 40 minute moving average

Figure 5.3: Moving averages of the ship's speed in SS3

In addition to a propeller selected for still water, SS1, SS2 and SS3, a propeller is also selected based on a reduced scatter diagram based. This reduced scatter diagram includes the sea states with a probability of occurrence higher than 5% given the DNV North Atlantic scatter diagram. Not the whole DNV North Atlantic scatter diagram is used because taking all sea states into consideration would lead to an unreasonably long computation time. Moreover, sea states with lower probability would have a minor

effect on the selection, and the Shipmaster will avoid the heaviest wave conditions, thus the reduction is not critical. This limitation reduced the scatter diagram to six sea states that are summarised in table 5.4. The formula used to calculate the delivered efficiency for a scatter uses a weighted average (eq. 3.5), therefore it is not necessary to normalise the probabilities of these six sea-states.

T_P	7.5	7.5	8.5	8.5	8.5	9.5
H_s	1.5	2.5	1.5	2.5	3.5	3.5
p_s	7.7%	6.2%	5.6%	7.4%	5.7%	5.1%

Table 5.4: Sea states of the DNV North Atlantic scatter diagram with a probability of occurrence higher than 5%

The results of the propeller selections are summarised in table 5.5. The propeller selected based on SS1 did not result in any visible increase of efficiency because SS1 represents a relatively calm sea state. The delivered efficiency and ship's speed obtained in the scatter diagram selection, lay between the values of SS1 and SS2 because its average sea lays between those sea states.

	Still water	**SS1**	**SS2**	**SS3**	**Scatter**
Acronym propeller	SWP	SS1.0P	SS2.0P	SS3.0P	SC.0P
A_e/A_0	0.643	0.642	0.638	0.626	0.649
P/D	1.117	1.115	1.107	1.082	1.098
$D\ [m]$	6	6	6	6	6
$n\ [rpm]$	99	99	99	101	100
$t_c\ [min]$	0.12	47	85	73	2147 ($\approx 36h$)
N_{it}	6	3	5	6	6
$\eta_{D,s,optimised}$		0.7037	0.6974	0.6489	0.6988
$\eta_{D,s,SWP}$		0.7037	0.6971	0.6475	0.6986
$\eta_{D,still}$	0.7045	0.7045	0.7045	0.7041	0.7044
η_0	0.6643	0.6643	0.6643	0.6640	0.6642
$\overline{U}_{s,optimised}\ [kn]$	19	18.97	18.44	16.28	18.71
$\overline{U}_{s,SWP}\ [kn]$		18.97	18.44	16.27	18.71

Table 5.5: Propellers selected for the S175 with still water resistance boundary conditions

Furthermore, a general trend over all the propellers is visible: pitch ratio decreases when a propeller is selected for a more severe sea state while the required engine speed increases. The diameter did not change but remains at the maximal diameter as defined by the boundary conditions as lower diameter would require a higher engine speed to deliver sufficient thrust. However, a higher engine speed lowers the advance coefficient which tends to reduce the open water efficiency.

With some simplifications, the lower pitch ratio and higher engine speed can be explained as follows: when the ship is sailing in waves the speed decreases which lowers the advance coefficient; besides this, the required thrust increases due to the added resistance. When a propeller has to be selected for a lower advance coefficient, a lower pitch ratio has a better open water efficiency. However, a lower pitch ratio moves all the open water curves to the left and slightly downwards which lowers the K_T-curve, therefore the engine speed has to increase to compensate the decrease of thrust in order to be able to sail at service speed in still water. This is illustrated in figure 5.4 where the propeller selected for still water (SWP) and a propeller with lower pitch (LP) are compared. This lower pitch propeller has a pitch ratio and propeller speed equal to SS3.0P but an expanded blade area equal to SWP. In the figure the average advance coefficient is plotted for both propellers to mark their working point in still water at service speed and in SS3. Furthermore the required K_T/J^2 in still water and K_T/J^2-curve are plotted, this parameter is plotted instead of the more often used K_T because the required K_T/J^2 in still water

is the same for both propellers as it is independent of the engine speed. At the working point of SS3, K_T/J^2 is slightly higher for LP which explains the higher average speed. In addition, the open water efficiency is also higher, therefore the LP delivers more thrust at a higher open water efficiency when the ship is sailing in SS3.

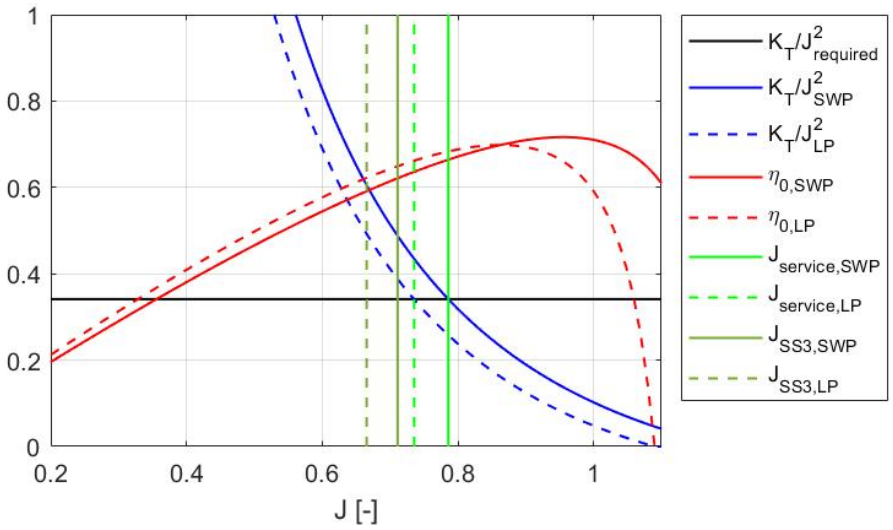

Figure 5.4: Illustration of the effect by a lower pitch for the S175

The expanded blade area ratio does show a trend between the single sea state selections. The cause of this is that for a lower pitch ratio, the minimal expanded blade area ration given by Burill's cavitation criterion is lower. However, the effect of A_e/A_0 is negligible on the open water curves as shown in figure 5.5. Moreover, the propeller selected for the scatter diagram does not follow this trend. This might be because that selection procedure stopped because the minimum step size was reached, whereas the selection procedures for the single sea states stopped because a maximum was found. The minimal step size could be lowered however, the effect of the expanded blade area ration is minimal and the selection procedure took already a day and a half.

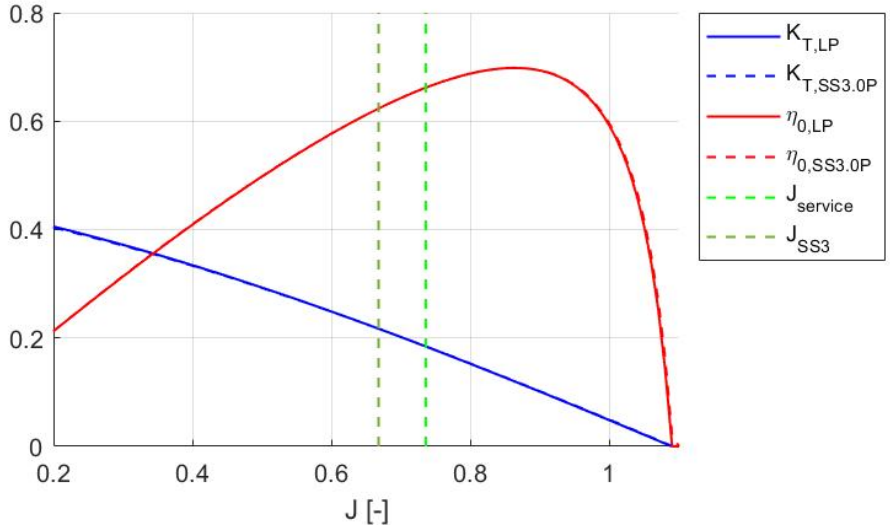

Figure 5.5: Illustration of the effect by a lower expanded blade ratio for the S175

Although, these changes have a positive effect on the delivered efficiency in the specific sea state,

they have an adverse effect on the efficiency in still water. In the case of SS3 sea state, the delivered efficiency was increased by 0.0014 or 0.22% relative to the delivered efficiency of the propeller selected for still water. On the other hand, the delivered efficiency of the propeller in still water decreased by 0.0004 or 0.06% relative to the delivered efficiency of the propeller selected for still water. When the propeller is selected for SS2, which is the average sea state of the scatter diagram and thus a more realistic scenario, the delivered efficiency in that sea state only increase by 0.0003 or 0.04% while the efficiency in still water decreases with 0.00003 or 0.004%. Therefore, the effect can be considered to be negligible and it should be questioned if it will result in a noticeable effect on the fuel consumption and performance of the propeller.

Hence, the reasoning above was mainly based on the speed loss and propeller speed, it is doubtful whether the changes are solely due to the added resistance or if fluctuations due to waves had an influence too. Furthermore, the speed loss in SS1 and SS2 may be counteracted by the Shipmaster who increases the power to maintain the service speed.

In an attempt to see the effect of the fluctuations, a propeller is selected taking in account the still water resistance and the average added resistance in SS2 at service speed (ADP) and other propellers were selected based on the proposed selection method but with the boundary conditions adapted for the increased thrust requirements in still water. Due to the fact that the increased resistance is already included, the upper limit of the power boundary condition is increased to 100% MCR. Furthermore, the engine speed in the simulations has been altered in such a way that the propeller delivers the thrust required to propel the ship at service speed with the increased resistance. The selection procedure in waves has been executed twice for the same sea state (SS2) but with a different wave profile (different ϕ) in order to verify the repeatability of the procedure. These results are summarised in table 5.6. This selection procedure is not repeated for SS3 because SS3 is a rough sea state where ventilation occurs for the S175. As consequence the Shipmaster would slow down the ship instead of increasing the power to maintain service speed. Moreover, the probability of this sea state is low, thus it does not make sense to select a propeller based on this sea state.

	Added resistance	**Including waves 1**	**Including waves 2**	
Acronym propeller	ADP	SS2.1P	SS2.2P	SS2.3P
A_e/A_0	0.690	0.692	0.692	0.0.690
P/D	1.063	1.067	1.068	1.064
$D\ [m]$	6	6	6	6
$n\ [rpm]$	106.2	105.9	105.8	106.1
$\eta_{D,s,optimised}$		0.6887	0.6888	0.6878
$\eta_{D,s,ADP}$		0.6887	0.6888	0.6878
$\eta_{D,still}$	0.6875	0.6875	0.6875	0.6875
η_0	0.6483	0.6483	0.6483	0.6483
$\overline{U}_{s,optimised}\ [kn]$	19	19.06	19.10	18.97
$\overline{U}_{s,ADP}\ [kn]$		19.06	19.10	18.97

Table 5.6: Characteristics of the propeller selected for still water taking into account the average added resistance in SS2 (ADP) and propellers selected for SS2 with boundary condition including the average added resistance (SS2.1P and SS2.2P)

The selected propeller based on the average resistance without taking into account the fluctuations and motions due to waves (ADP), has a higher expanded blade area, lower pitch and higher engine speed compared to the original selected propeller in still water conditions (SWP). This is explained by the fact that the required thrust is higher which is achieved by increasing the engine speed and thus lowers the advance coefficient. At the lowered advance coefficient, a lower pitch ratio has a higher the open water

efficiency. The expanded blade area is increased in order to meet the modified cavitation criterion, that now has to be met for the thrust required to cope with the still water resistance plus the added resistance. This criterion is not satisfied for the SWP and the SS2.0P. Although these propellers do not meet this criterion, they are also simulated in SS2 with the same wave profile for which SS2.2P was selected. In the simulation with SWP and SS2.0, the engine speed was increased compared to the one given in table 5.5, so that service speed could be maintained with the increase of added resistance. The simulations resulted in a theoretical delivered efficiency in that sea state of 0.6865 and 0.6866 for SWP and SS2.0P respectively. These efficiencies are lower than achieved by the ADP and SS2.2P. Moreover, this number is higher than in reality because cavitation will reduce the efficiency. How much the efficiency would be reduced cannot be estimated by the developed procedure and would require a more complete cavitation model to be included in the simulation code.

Furthermore, SS2.1P and SS2.2P are not exactly the same propeller. This is due to the different wave profile and the short simulation period. A longer simulation period could eliminate this inconsistency, however both propellers have a higher pitch ratio, expanded blade area and lower engine speed.

These changes can be explained by the increase of the advance coefficient and thus explains why both SS2.1P and SS2.2P have a higher pitch ratio. The higher pitch ratio implies that the engine speed has to slightly decrease to balance the higher thrust delivered by these propellers. The open water curves of SS2.1P and are compared to ADP in figure 5.6 where the increase of advance coefficient is illustrated. This is increase is caused by a raise of the mean advance speed which has two roots: raise due to pitching of the ship (eq. 3.28) and the higher ship´s speed. The higher ship´s speed appears to contradict the lower thrust coefficient for the working point with the higher advance coefficient. However, due to the 'quasi' regular wave approach used for calculation of the added resistance, the average total resistance in the simulation was around 2% lower than the estimated one used to define the propeller speed. In addition to the elevated pitch ratio, the expanded blade area ratio increased in order to satisfy the cavitation boundary condition.

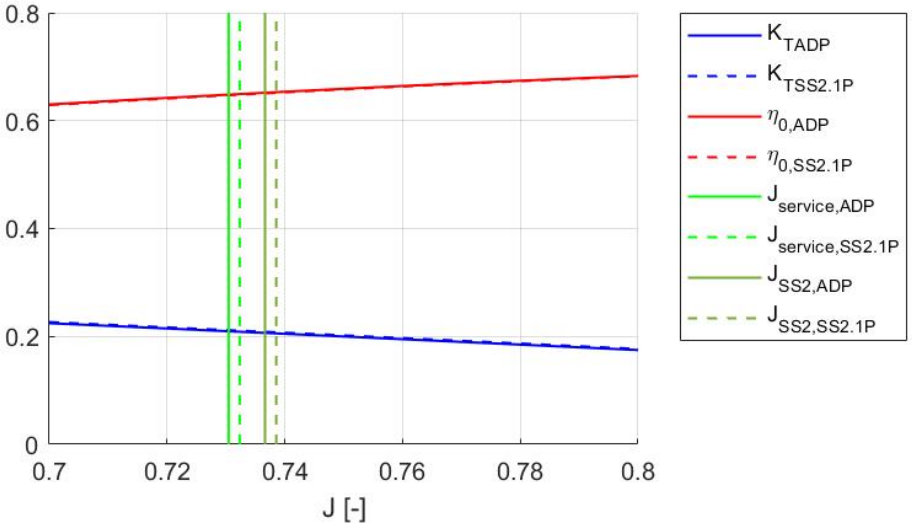

Figure 5.6: Open water curves for ADP and SS2.1P and their average advance coefficients

In order to have a better view on the effect of the waves, the same propeller selection is repeated but the average added resistance in the simulation is calculated by the wave spectrum instead of the 'quasi' regular wave approach. This was done for SS2 with the same wave profile of where SS2.1P was selected. The propeller selected with this procedure (SS2.3P) had a slightly higher pitch ratio than

ADP (1.064 instead of 1.063), slightly higher expanded blade area ratio (0.6902 instead of 0.6900) and a lower engine speed (106.1 rpm instead of 106.2 rpm). Just as earlier, the lower engine speed is a consequence of the higher pitch ratio. However, in this simulation the average ship's speed was 18.97 knots which is lower than the service speed (and simulation with 'quasi' regular wave approach). This is explained by the increase of average advance speed due to pitching of the ship (eq. 3.28) that causes the advance coefficient to increase as shown in figure 5.7. Just as it was the case for the selections with the 'quasi' regular wave approach, this increase of advance coefficient causes a propeller with higher pitch ratio to be more efficient. However, unlike in those simulations, here the lower thrust is not compensated by the lower added resistance and thus the ship slowed down.

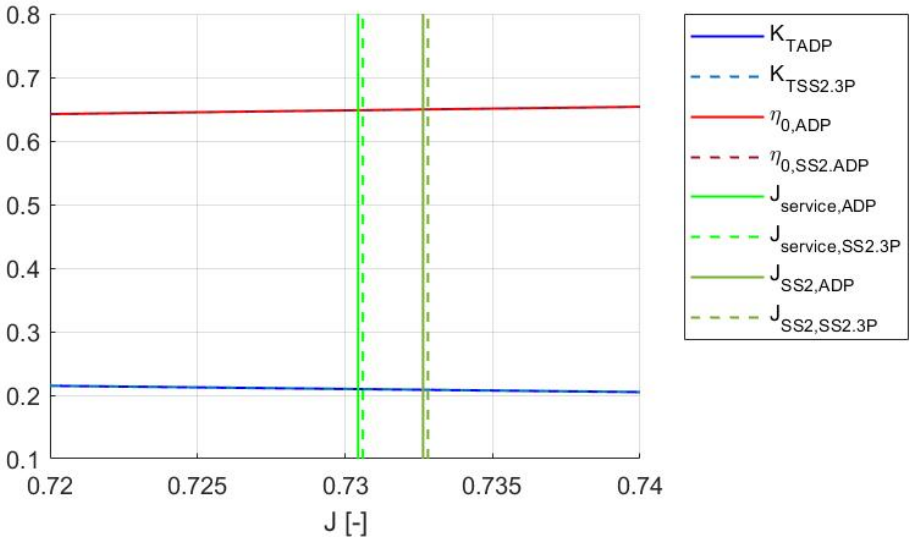

Figure 5.7: Open water curves for ADP and SS2.3P and their average advance coefficients

Regardless of this trend, the differences between the propellers including the effects of waves and the ADP propeller are minimal and the increase of delivered efficiency in waves negligible. Thus, it can be concluded that the differences are small and will not have a significant effect on the fuel consumption. However, it is recommended to select a propeller taking into account the added resistance of the expected average sea state the ship will sail in for example the average sea state of the DNV North Atlantic scatter diagram if the ship is expected to sail mostly in the North Atlantic. Including this added resistance in the propeller selection will reduce the risk of cavitation when the resistance increases in presence of waves and improve the real life efficiency.

Furthermore, it would be interesting to repeat the same selection procedure with a more advanced cavitation model embedded in the simulation code to see the effect on the propeller performance. However, this will increase the calculation time and should be tested on a single propeller simulation first to see if it has a noticeable effect on performance.

In addition to the simple cavitation criterion, the engine speed was kept constant and there was no power or torque limitation in the simulation. Incorporating these limitations or a more realistic engine model might as well alter the results and provide deeper insight. However, in [11] it was noted that the averages with and without engine model are comparable. On the other hand, adding a more complex engine model could lead to a more precise analysis and allow comparison of the fuel consumption rather than efficiencies.

Chapter 6

Conclusion

In this work, a selection procedure of the Wageningen B-series propeller for realistic wave conditions was proposed and compared to the optimal propeller selected in still water. Therefore, the effect of waves on the performance of the propeller and ship was studied first. This study was split into different key elements of the power flow: ship resistance, ship motions and propeller performance.

Based on this study, the selection procedure for the propeller was proposed. The delivered efficiency is used as a performance indicator of the propeller-ship combination in a given sea state. This efficiency is found by simulating the ship with propeller in the time and space domain. These simulations take into account ventilation, the varying added resistance and the fluctuating wake factor. The latter two were calculated using the 'quasi' regular wave approach rather than directly for the irregular sea state because the models used could not be adapted for an irregular sea state. In this approach the irregular sea is treated as series of regular waves of different amplitudes and frequencies as suggested in [2]. This selection procedure and simulation methodology were then implemented in a Matlab code.

The implementation of the simulation code in Matlab was then validated for the KVLCC2. The validation was done for by running different simulations in regular waves and comparing them with results in the literature. Furthermore, various simulations in irregular waves were performed and analysed. It was concluded that the code tends to give similar results to the literature, except for the ventilation and the added resistance due to different inputs considered. The latter is underestimated due to the blunt shape of the KVLCC2.

Considering that the code showed some inaccuracies, the best propeller for the KVLCC2 in several sea states was selected. The differences between the propeller selected in a given sea state and the one selected in still water conditions were negligible. This was explained by the fact that the propeller is deeply submerged and the ship is large, so the waves have no significant effect. Therefore, the propeller selection procedure is found not useful for large and slow ships.

In order to see if the proposed propeller selection procedure would be useful for smaller ships, it was applied to the S175. Some tendencies have been noticed on the propeller selected for sea state of increased severity. In particular the propellers selected for a given sea state had a lower pitch ratio and a higher engine speed compared to the one selected for still water. These changes were more pronounced for more severe sea states. The reason for these changes was that due to the added resistance, the required thrust increased and therefore the speed decreased. As a result the average advance coefficient decreased and hence shifted the working point in the open water curves to where a propeller with lower pitch has a better open water efficiency. In this case, as well as for the KVLCC2,

the propeller speed was set equal to the propeller speed required to sail at service speed in still water, therefore it was proposed that it might be more realistic to change the propeller speed to the one required to sail the ship at service speed in still water including the average resistance for a given sea state. This modified procedure was performed three times for the average sea state of the DNV North Atlantic scatter diagram (SS2). One time, only the average resistance in the sea state was only taken into account and two times all the effects of waves were included. The two selected propellers including the effect of waves were not identical due to minor differences in the averages of the simulations caused by the difference in the wave profile. Although both propellers are different, they changed in a similar way compared to the selected propeller without considering the effect of waves. Furthermore, these changes could be explained by the increase of advance coefficient and the cavitation criterion of Burill [47]. This increase of advance coefficient had two causes: increase of main advance speed due to pitching of the ship and increase of the ship´s speed due the lower average added resistance by the 'quasi' regular wave approach (maximal 2% lower than calculated by the wave spectrum). In order to have a better view on the effect of the waves, the same propeller selection including the added resistance was repeated but with the average added resistance in the simulation instead of the 'quasi' regular wave approach. This resulted in a slightly lower ship's speed than the service speed but still a higher pith ratio due to the mean increase of advance speed.

However, the differences between those propellers including the fluctuations due to waves and the one selected in still water including the average resistance for a given sea state were small and the increase of efficiency negligible. Therefore, it is concluded that the proposed selection procedure is not worth considering in the selection of a propeller. However, it is recommended to include the added resistance of the expected average sea state in which the ship will sail in the commonly used selection procedure to reduce the risk of cavitation. This sea still depends on where the ship is expected to sail for example if the ship is expected to sail mostly in the North Atlantic, the average sea state of the DNV North Atlantic scatter diagram can be used. Furthermore both ships are still big ships and ventilation was not present in SS1 and SS2. Repeating the selection procedure for an even smaller ship such as a fishing vessel might result in bigger improvements.

It was further noted that the inclusion of a more comprehensive cavitation model embedded in the simulation code itself, might influence the results in such a way that the differences with the still water optimal propeller are bigger. However, it should first be verified for a single simulation whether such a model has a noticeable effect on performance.

Furthermore, the propeller was given a constant rotational speed which is not a realistic model. This model was chosen because the averages with and without an engine model are comparable [11]. However, this affects the torque fluctuations and implementing a more complex engine model would be more accurate and lead to a better analysis. Furthermore, a better engine model would allow to compare fuel consumption rather than efficiency.

On a final note it must be said that all the propellers were selected for the ship in loaded condition while this does not reflects the reality. Therefore, it can be interesting to adapt the code as such that it includes ballast and loaded condition. I could be expected that this will change the results because the propeller will be more prone to cavitation and ventilation in ballast condition. However, the trends noticed for the S175 will remain because they are mostly based on reasoning of the advance coefficient.

Bibliography

[1] IMO, "Greenhouse Gas Emissions." http://www.imo.org/en/OurWork/Environment/PollutionPrevention/AirPollution/Pages/GHG-Emissions.aspx, 2020. Accessed on: May 8, 2020.

[2] O. Faltinsen, K. Minsaas, N. Liapis, and S. Skjordal, "Prediction of resistance and propulsion of a ship in a seaway," *Thirteenth Symposium on Naval Hydrodynamics*, pp. 505–529, 1980.

[3] D. Matulja and R. Dejhalla, "A comparison of a ship hull resistance," *Eng. Rev*, vol. 27, pp. 13–24, 2007.

[4] M. G. Seo, D. M. Park, K. K. Yang, and Y. Kim, "Comparative study on computation of ship added resistance in waves," *Ocean Engineering*, vol. 73, pp. 1–15, 2013.

[5] S. Helma, "Surprising behaviour of the Wageningen B-screw Series polynomials." prepint, not peer reviewed, dec 2019.

[6] G. Delefortrie, M. Candries, and M. Vantorre, "Course: Hydrostatics and Propulsion Chapter III and IV – Ship Propulsion." may 2019.

[7] M. W. Oosterveld and P. van Oossanen, "Further Computer-Analyzed Dat of the Wageningen B-Screw Series.," *International Shipbuilding Progress*, vol. 22, no. 251, pp. 251–262, 1975.

[8] J. Carlton, *Marine propeller and propulsion*. Elsevier, 2nd ed., 2007.

[9] O. N. Smogeli, *Control of marine propellers: from normal to extreme conditions*. PhD thesis, NTNU, 2006.

[10] M. Ueno, Y. Tsukada, and K. Tanizawa, "Estimation and prediction of effective inflow velocity to propeller in waves," *Journal of Marine Science and Technology (Japan)*, vol. 18, pp. 339–348, sep 2013.

[11] B. Taskar, K. K. Yum, S. Steen, and E. Pedersen, "The effect of waves on engine-propeller dynamics and propulsion performance of ships," *Ocean Engineering*, vol. 122, pp. 262–277, 2016.

[12] L. Nikolopoulos and E. Boulougouris, "A Study on the Statistical Calibration of the Holtrop and Mennen Approximate Power Prediction Method for Full Hull Form, Low Froude Number Vessels," *Journal of Ship Production and Design*, vol. 35, pp. 41–68, feb 2019.

[13] "Earth overshoot day." https://www.overshootday.org/, 2020. Accessed on: May 8, 2020.

[14] N. Vitali, J. Prpić-Oršić, and C. Guades Soares, "Uncertainties related to the estimation of added resistance of a ship in waves," in *Maritime Technology and Engineering III*, vol. 1, pp. 391–399, CRC Press, jun 2016.

[15] N. Vitali, J. Prpić-Oršić, and C. Guedes Soares, “Methods for Added Resistance Estimation in Head and Oblique Seas,” *Book of Abstract of the 22nd Symposium on Theory and Practice of Shipbuilding, In Memoriam prof. Leopold Sorta*, p. 17, 2016.

[16] J. Holtrop and G. Mennen, “An approximate power prediction method,” *Internation Shipbuilding progress*, vol. 29, no. 335, pp. 166–170, 1982.

[17] N. Salvesen, E. Tuck, and O. Faltinsen, “Ship Motions and Sea Loads,” *Transactions of the Society of Naval Architects and Marine Engineers*, vol. 78, pp. 250–287, 1970.

[18] N. Salvesen, “Added Resistance of Ships in Waves,” *Journal of Hydronautics*, vol. 12, pp. 24–34, jan 1978.

[19] R. Vettor, J. Prpić-Oršić, and C. Guedes Soares, “Impact of wind loads on long-term fuel consumption and emissions in Trans-Oceanic shippping,” *Brodogradnja*, vol. 69, no. 4, pp. 15–28, 2018.

[20] J. Prpić-Oršić and O. M. Faltinsen, “Estimation of ship speed loss and associated CO^2 emissions in a seaway,” *Ocean Engineering*, vol. 44, pp. 1–10, 2012.

[21] J. Prpić-Oršić, R. Vettor, O. M. Faltinsen, and C. Guedes Soares, “The influence of route choice and operating conditions on fuel consumption and CO2 emission of ships,” *Journal of Marine Science and Technology (Japan)*, vol. 21, no. 3, pp. 434–457, 2016.

[22] R. Skejić and S. Steen, “On Total Resistance of Ships in a Seaway,” *Practical Design of Ships and Other Floating Structures (Japan)*, pp. 1–23, 2019.

[23] ITTC, “1978 ITTC Performance Prediction Method - 7.5 – 02-03 – 01.4,” *ITTC Propulsion Commettee of the 28th ITTC*, no. 04, 2017.

[24] C.-y. Guo, P. Xu, C. Wang, and Z. Kan, “Numerical and Experimental Study of Blockage Effect Correction Method in Towing Tank,” *China Ocean Engineering*, vol. 33, no. 5, pp. 522–536, 2019.

[25] H. Mikkelsen, M. Lund Steffensen, C. Ciortan, and J. Honore Walther, “Full scale validation of CFD model of self-propelled ship,” *VIII International Conference on Computational Methods in Marine Engineering*, 2019.

[26] J. Holtrop and G. Mennen, “A statistical power prediction method,” *Internation Shipbuilding progress*, vol. 24, no. 270, pp. 253–256, 1978.

[27] J. Holtrop, “A statistical re-analysis of resistance and propulsion data,” *Internation Shipbuilding progress*, vol. 31, no. 363, pp. 272–276, 1984.

[28] K. U. Hollenbach, “Estimating resistance and propulsion for single-screw and twin-screw ships,” *Ship Technology Research*, vol. 45, no. 2, pp. 72–76, 1998.

[29] H. Maruo, “Resistance in waves. Research on Seakeeping Qualities of Ships in Japan,” *The Society of Naval Architects of Japan*, vol. 8, pp. 67–102, 1963.

[30] J. Gerritsma and W. Beukelman, “Analysis of the resistance increase in waves of a fast cargo ship,” *Internation Shipbuilding progress1*, vol. 19, pp. 285–293, 1972.

[31] T. Loukakis and P. Sclavounos, “Some extensions of the classical approach to strip theory of ship motions, including the calculation of mean added forces and moments,” *Journal of Ship Research*, vol. 22, pp. 1–19, 1978.

[32] S. Liu, A. Papanikolaou, and G. Zaraphonitis, “Prediction of added resistance of ships in waves,” *Ocean Engineering*, vol. 38, no. 4, pp. 641–650, 2011.

[33] T. Havelock, “The Resistance of a Ship among Waves,” *Proceedings of The Royal Society of London. Series A, Mathematical and Physical Sciences (1934-1990)*, vol. 161, pp. 299–308, 1937.

[34] P. Boese, “Eine einfache Methode zur Berechnung der Widerstandserhöhung eines Schiffes im Seegang,” *Shiffstechnik*, vol. 17, 1970.

[35] J. Pinkster, “Mean and low frequency wave drifting forces on floating structures,” *Ocean Engineering*, vol. 6, no. 593-615, 1979.

[36] H. Fujii and T. Takahashi, “Experimental Study on the Resistance Increase of a Large Full Ship in Regular Oblique Waves,” *Journal of the Society of Naval Architects of Japan*, vol. 1975, no. 137, pp. 132–137, 1975.

[37] M. Kuroda, M. Tsujimoto, T. Fujiwara, S. Ohmatsu, and K. Takagi, “Investigation on Components of Added Resistance in Short Waves,” *Journal of the Japan Society of Naval Architects and Ocean Engineers*, vol. 8, pp. 171–176, 2008.

[38] L. Troost, “Open water test series with modern propeller forms.,” *Trans. NECIES*, vol. 54, 1938.

[39] L. Troost, “Open water test series with modern propeller forms. II. Three bladed propellers,” *Trans. NECIES*, 1940.

[40] L. Troost, “Open water test series with modern propeller forms. III. Two bladed and five bladed propellers – extension of the three and four bladed B-series.,” *Trans. NECIES*, vol. 67, 1951.

[41] W. Lammeren, J. Manen, and M. Oosterveld, “The Wageningen B-screw series,” *Trans. SNAME*, vol. 77, pp. 269–317, 1969.

[42] H. W. Lerbs, “On the effect of scale and roughness on free runing propellers,” *Journal of the American Society for Naval Engineers*, vol. 63, pp. 58–94, mar 2009.

[43] V. Zhinkin, “Determination of the Screw Propeller Thrust when the Torque or Shaft Power is Known,” *Fourth Int. Symp. on Practical Design of Ships and Mobile Units*, 1989.

[44] E. Danckwardt, “Berechnungsdiagramme für Schiffsschrauben.},” *Schiffbautechnik*, vol. 2, pp. 22–30, 1956.

[45] J. Degroote, “Course: Turbomachines: Chapter 8 pumps.” sep 2018.

[46] S. Barnaby, “Cavitation of screw propellers,” *Proc. Inst Civil Engi.*, pp. 299–308, 1905.

[47] L. Burrill and A. Emerson, “Propeller cavitation: Further tests on 16in. propeller models in the King’s College cavitation tunnel1,” *International Shipbuilding Progress*, vol. 10, pp. 119–131, apr 1963.

[48] J. Auf’m Keller, “Enige Aspecten bij het Ontwerpen van Scheepsschroeven.,” *Schip en werf*, vol. 33, no. 24, pp. 658–663, 1966.

[49] S. Bal, “Numerical Investigation Cavitation Buckets for Hydrofoil Parametrically,” *Türk Denizcilik ve Deniz Bilimleri Dergisi*, vol. 1, no. 2, pp. 89–101, 2015.

[50] F. Gutsche, “Untersuchung von Schiffsschrauben in schräger Anströmung,” *Schiffbauforschung*, no. 3/4, pp. 97–122, 1964.

[51] D. Yoerger, J. Cooke, and J.-J. Slotine, “The Influence of Thruster Dynamics on Underwater Vehicle Behavior and Their Incorporation Into Control System Design,” *IEEE Journal of Oceanic Engineering*, vol. 15, pp. 167–178, 1990.

[52] A. Healey, S. Rock, D. Cody, S. and Miles, and J. Brown, "Towards an improved understanding of thruster dynamics forunderwater vehicles," *IEEE Journal of Oceanic Engineering*, vol. 20, pp. 340–352, 1994.

[53] M. Blanke, K.-p. Lindegaard, and T. Fossen, "Dynamic Model for Thrust Generation of Marine Propellers," *IFAC Proceedings Volumes*, vol. 33, 2000.

[54] M. R. Azimi-Sadjadi, J. Wilbur, and G. J. Dobeck, "Isolation of resonance in acoustic backscatter from elastic targets using adaptive estimation schemes," *IEEE Journal of Oceanic Engineering*, vol. 20, pp. 346–353, oct 1995.

[55] S. Nakamura and S. Naito, "Propulsive performance of a container ship in waves," *Soc. Nav. Archit. Jpn. Nav. Arch. Ocean Eng.*, 1977.

[56] F. Gutsche, "Einfluss der Tauchung auf Schub undWirknungsgrad von Schiffpropellern.," *Schiffbauforchung*, vol. 6, no. 5/6, pp. 256–277, 1967.

[57] K. P. Fleischer, "Untersuchungen über Das Zusammenwirken Von Schiff und Propeller Bei Teilgetauchten Propellern.," *Forschungszentrum des Deutschen Schiffbaus*, no. 35, 1973.

[58] K. Koushan, "Environmental and Interaction Effects on Propulsion Systems used in Dynamic Positioning, an Overview.," in *Proc. 9th Int. Symp. Practical Design of Ships and Other Floating Structures (PRADS'04). Lübeck-Travemünde, Germany*, pp. 1013–1020, 2004.

[59] K. Minsaas, O. Faltinsen, and B. Persson, "On the importance of added resistance, propeller immersion and propeller ventilation for large ships in a seaway," *Proceedings of the 2nd international symposium on practical design in shipbuilding. Tokyo & Seoul, Japan*, 1983.

[60] H. Wagner, "Über die Entstehung des dynamischen Auftriebes von Tragflügeln," *ZAMM - Zeitschrift für Angewandte Mathematik und Mechanik*, vol. 5, no. 1, pp. 17–35, 1925.

[61] "Comparison of Gear Efficiencies - Spur, Helical, Bevel, Worm, Hypoid, Cycloid." `http://www.meadinfo.org/2008/11/gear-efficiency-spur-helical-bevel-worm.html`, 2008. Accessed on: April 4, 2020.

[62] R. Vettor, S. Wang, and C. Guedes Soares, "Course: Ship dynamics and hydrodynamics," 2019.

[63] H. Søding, "Program PDSTRIP: Public Domain Strip Method (manual)," 2006.

[64] D. Moor and D. Murdey, "Motions and propulsion of single screw models in head seas-2," *Roy Inst Nav Architects Quart Trans*, vol. 112, no. 2, pp. 121–164, 1970.

[65] B. Taskar, *The Effect of Waves on Marine Propellers and Propulsion*. Phd thesis, NTNU, may 2017.

[66] C. M. Lee, J. H. Seo, J. W. Yu, J. E. Choi, and I. Lee, "Comparative study of prediction methods of power increase and propulsive performances in regular head short waves of KVLCC2 using CFD," *International Journal of Naval Architecture and Ocean Engineering*, vol. 11, no. 2, pp. 883–898, 2019.

[67] H. Sadat-Hosseini, P.-c. Wu, P. M. Carrica, H. Kim, Y. Toda, and F. Stern, "CFD verification and validation of added resistance and motions of KVLCC2 with fixed and free surge in short and long head waves," *Ocean Engineering*, vol. 59, pp. 240–273, feb 2013.

[68] MAN Diesel, "MAN B & W 70-60 ME-GI / -C-GI-TII Type Engines Engine Selection Guide Electronically Controlled Two stroke Engines," *MAN Diesel*, vol. 1, jun 2010.

Appendix A

Profile summary

Profile Summary (Total time: 883.989 s)

Generated 17-May-2020 00:00:59 using performance time.

Function Name	Calls	Total Time (s)	Self Time* (s)	Total Time Plot (dark band = self time)
simulate	1	880.918	7.205	
calc_0upcrossing	71647	645.405	28.270	
calc_wave_irr	5896801	610.646	610.646	
interp1	859822	122.439	82.622	
calc_T_andQ	71647	82.903	3.110	
fzero	71647	71.617	32.269	
calc_RAO_U	214941	34.817	2.599	
calc_T_andQ>@(x)calc_KT_poly(x,PD,AeA0,z)	1647881	31.702	5.957	
calc_KT_poly	1791177	29.128	29.128	
interp1>parseinputs	859822	26.174	18.801	
calc_Radd_instant_e	71647	25.184	2.223	
calc_S_prop	71647	19.293	3.841	
calc_mot_instant	71647	14.145	10.640	

Figure A.1: Profile summary of the most time consuming functions during a 120 minute simulation in average sea state

Appendix B

Flowcharts with names of the Matlab code

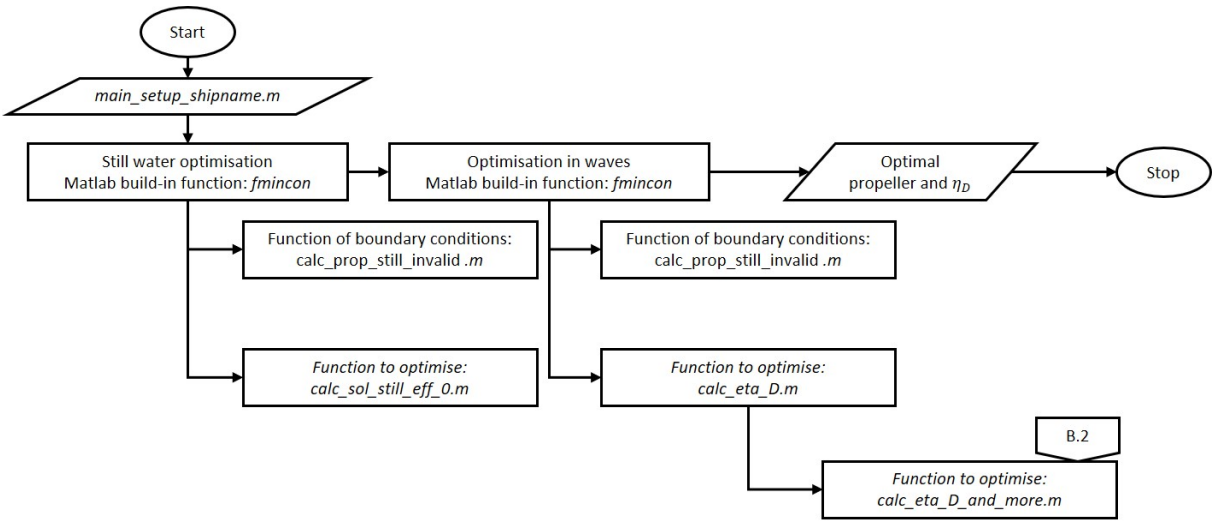

Figure B.1: Flowchart corresponding to figure 3.2 and representing matlab code: *'main_prop_select_waves.m'*

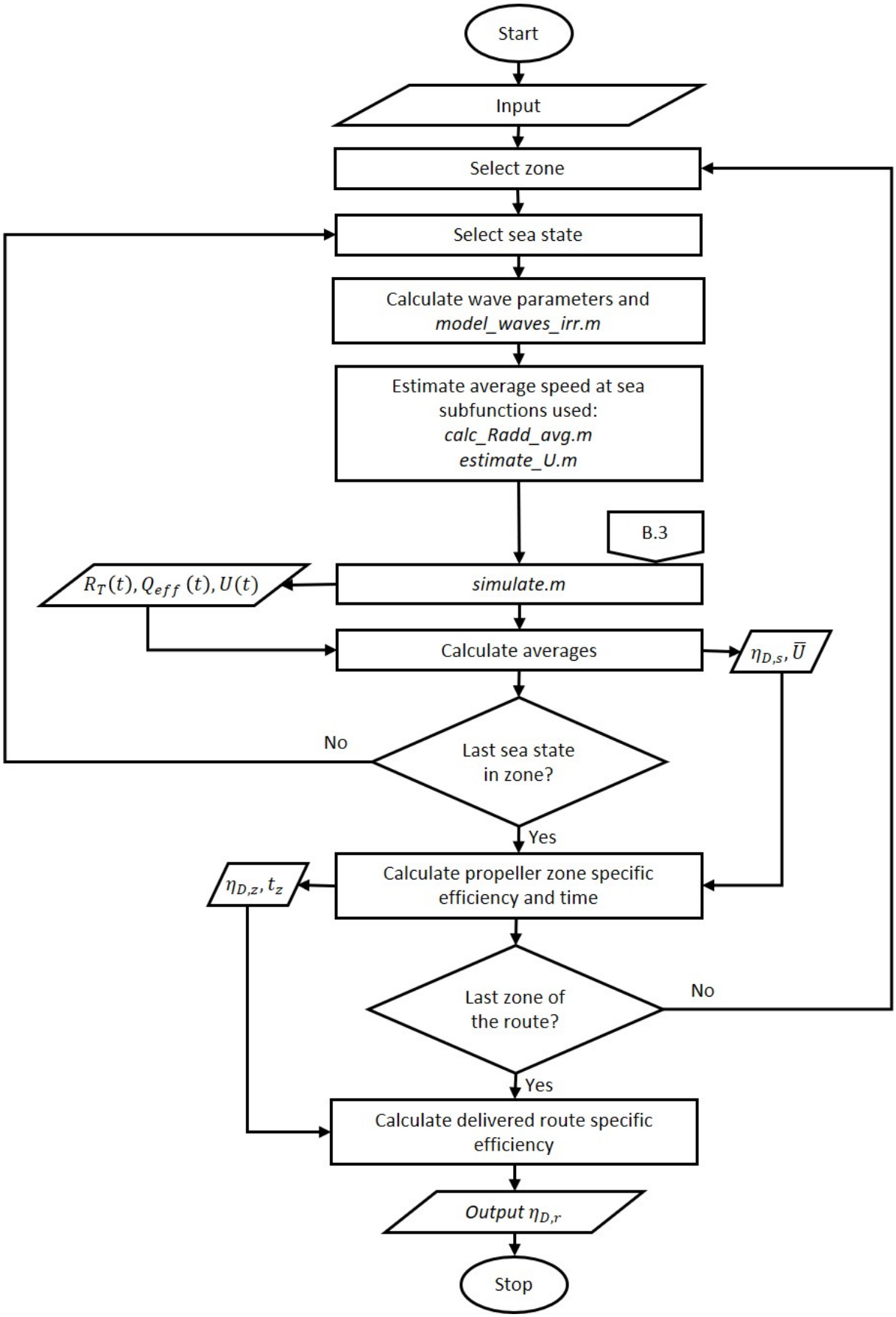

Figure B.2: Flowchart corresponding to figure 3.5 and representing matlab code: *'calc_eta_D_and_more.m'*

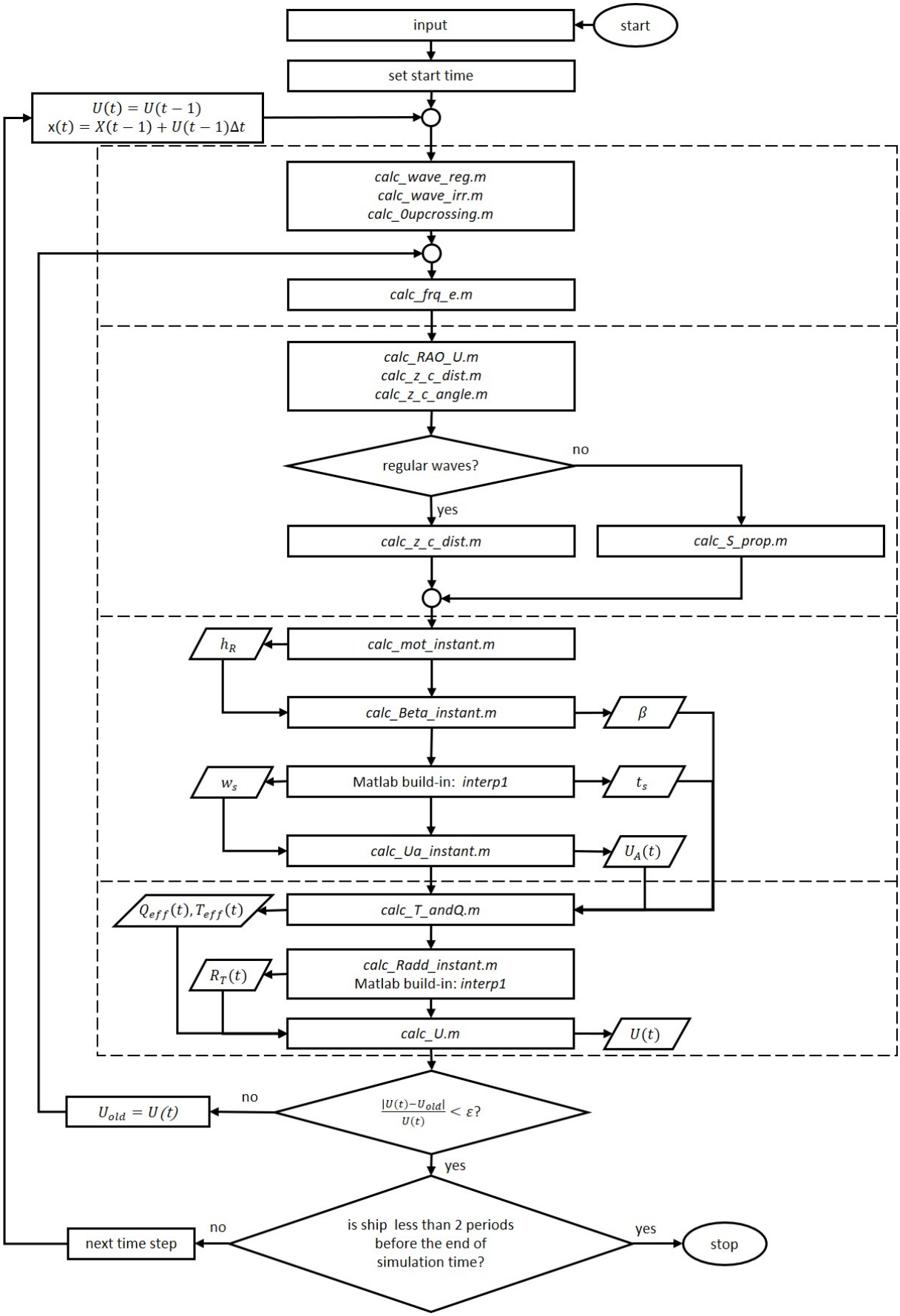

Figure B.3: Flowchart corresponding to figure 3.6 and representing matlab code: *'simulate.m'*

Appendix C

Most important Matlab codes

```
function [t_0up,frq_0up,Hw] = calc_0upcrossing(time,t_inst,x,stepf,frq_wave,k_wave,↙
phi_wave,S_w,heading)
%Calculates the properties of the quasi regular wave of a given wave profile in time↙
domain.
%   The properties returned are:
%       - Start time of a the zero upcrossing
%       - Frequency of the quasi regular wave between two zero upcrossings
%       - Encounter frequency of the quasi regular wave between two zero upcrossings
%       - Amplitude of the quasi regular wave between two zero upcrossings
%       - Time in the middle between two zero upcrossings
wave=zeros(size(time));
% 2 points to know where the ship with respect to the past and upcomming
% zero-upcrossing
wave(t_inst)=calc_wave_irr(time(t_inst),x,stepf,frq_wave,k_wave,phi_wave,S_w,↙
heading);
wave(t_inst+1)=calc_wave_irr(time(t_inst+1),x,stepf,frq_wave,k_wave,phi_wave,S_w,↙
heading);
t_start=t_inst;
t_end=t_inst;
count=0;
%loop to find the past and next upcrossing
if wave(t_inst)>0
    while t_start>1 && wave(t_start)>0
        t_start=t_start-1;
        wave(t_start)=calc_wave_irr(time(t_start),x,stepf,frq_wave,k_wave,phi_wave,↙
S_w,heading);
    end
    t_0up=interp1(wave(t_start:t_start+1),time(t_start:t_start+1),0,'spline');
    while t_end<length(time) && count<2
        t_end=t_end+1;
        wave(t_end)=calc_wave_irr(time(t_end),x,stepf,frq_wave,k_wave,phi_wave,S_w,↙
heading);
        if wave(t_end)<0
            count=1;
        elseif wave(t_end)>0 && count==1
            count=2;
        end
    end
    t_0up_end=interp1(wave(t_end-1:t_end),time(t_end-1:t_end),0,'spline');
    T_0up=t_0up_end-t_0up;
    Hw=(max(wave(t_start:t_end))+abs(min(wave(t_start:t_end))))/2;
elseif wave(t_inst)<0
    while t_start>1 && count<2
        t_start=t_start-1;
        wave(t_start)=calc_wave_irr(time(t_start),x,stepf,frq_wave,k_wave,phi_wave,↙
S_w,heading);
        if wave(t_start)>0
            count=1;
        elseif wave(t_start)<0 && count==1
            count=2;
        end
    end
    t_0up=interp1(wave(t_start:t_start+1),time(t_start:t_start+1),0,'spline');
    while t_end<length(time) && wave(t_end)<0
```

```
        t_end=t_end+1;
        wave(t_end)=calc_wave_irr(time(t_end),x,stepf,frq_wave,k_wave,phi_wave,S_w,↙
heading);
    end
    t_0up_end=interp1(wave(t_end-1:t_end),time(t_end-1:t_end),0,'spline');
    T_0up=t_0up_end-t_0up;
    Hw=(max(wave(t_start:t_end))+abs(min(wave(t_start:t_end))))/2;
elseif wave(t_inst)==0 && wave(t_inst+1)>0
    t_0up=time(t_inst);
    while t_end<length(time) && count<2
        t_end=t_end+1;
        wave(t_end)=calc_wave_irr(time(t_end),x,stepf,frq_wave,k_wave,phi_wave,S_w,↙
heading);
        if wave(t_end)<0
            count=1;
        elseif wave(t_end)>0 && count==1
            count=2;
        end
    end
    t_0up_end=interp1(wave(t_end-1:t_end),time(t_end-1:t_end),0,'spline');
    T_0up=t_0up_end-t_0up;
    Hw=(max(wave(t_start:t_end))+abs(min(wave(t_start:t_end))))/2;
else
    while t_start>1 && wave(t_start)>0
        t_start=t_start-1;
        wave(t_start)=calc_wave_irr(time(t_start),x,stepf,frq_wave,k_wave,phi_wave,↙
S_w,heading);
    end
    t_0up=interp1(wave(t_start:t_start+1),time(t_start:t_start+1),0,'spline');
    while t_end<length(time) && wave(t_end)<0
        t_end=t_end+1;
        wave(t_end)=calc_wave_irr(time(t_end),x,stepf,frq_wave,k_wave,phi_wave,S_w,↙
heading);
    end
    t_0up_end=interp1(wave(t_end-1:t_end),time(t_end-1:t_end),0,'spline');
    T_0up=t_0up_end-t_0up;
    Hw=(max(wave(t_start:t_end))+abs(min(wave(t_start:t_end))))/2;
end
%Calculating zero upcrossing frequency
frq_0up=2*pi./T_0up;
end
```

```
function [Beta] = calc_Beta_instant(D,h_R,pt_p)
%Calculates Beta loss factor for one specific moment
    R=D/2;
    h_prop=h_R-pt_p(3);
    if h_prop/R <= -0.48
        Beta=0;
    elseif h_prop/R >= 1.3
        Beta=1;
    else
        Beta=1-0.675*(1-0.769*h_prop/R)^1.258;
    end
end
```



```
function [RAO_h]=calc_centec_h(RAO,set_heading,heading)
% Calculates RAO for given heading based on RAO for a set of headings
    RAO_perm=permute(RAO,[2,1,3]);%now we have heading, frq,speed
    RAO_h=squeeze(interp1(set_heading,RAO_perm,heading,'spline',0));
end
```



```
function [eta_D] = calc_eta_D(x,z,J,U,U_max,U_min,Ua,M,Lpp,pt_p,z1,frq_surge,↙
heading_surge,U_surge,heading,frq_Radd,Phi_AW,U_Radd,U_data,t_still,w_still,R_still,↙
T_still,Tpeak,Hs,prob_s,dist_state,reg,stepf,frq_wave,k_wave,phi_wave_irr,time_wave,↙
stept,Heading_sea,frq,RM_c_p,z5,rho,g,epsilon)
%Calculates the propeller specific efficiency for a given sea state,
%scatter or route
%   Removing the parameters not of interest otherwise function is not working with↙
fmincon
[eta_D] = calc_eta_D_and_more(x,z,J,U,U_max,U_min,Ua,M,Lpp,pt_p,z1,frq_surge,↙
heading_surge,U_surge,heading,frq_Radd,Phi_AW,U_Radd,U_data,t_still,w_still,R_still,↙
T_still,Tpeak,Hs,prob_s,dist_state,reg,stepf,frq_wave,k_wave,phi_wave_irr,time_wave,↙
stept,Heading_sea,frq,RM_c_p,z5,rho,g,epsilon);
end
```

```
function [eta_D] = calc_eta_D_and_more(x,z,J,U,U_max,U_min,Ua,M,Lpp,pt_p,z1,↙
frq_surge,heading_surge,U_surge,heading,frq_Radd,Phi_AW,U_Radd,U_data,t_still,↙
w_still,R_still,T_still,Tpeak,Hs,prob_s,dist_state,reg,stepf,frq_wave,k_wave,↙
phi_wave_irr,time_wave,stept,Heading_sea,frq,RM_c_p,z5,rho,g,epsilon)
%Calculates the propeller specific efficiency for a given sea state or
%yourney
% This avoids confusion later on
frq_RAO=frq;
%unpacking of propeller properties
AeA0=x(1);
PD=x(2);
D=x(3);
%calculating rmp for service speed in still water
[~,~,~,~,n] = check_service_speed_attainable(x,z,1,2,1,2,T_still,J,rho,Ua);
%total probability/measurements
prob_tot=sum(prob_s,'all');
%defining some distances
l_zone=length(dist_state);
l_Hs=size(Hs,2);
l_Tp=size(Tpeak,2);
%set up vectors for storage
eta_Dz=zeros(1,l_zone);
time_z=eta_Dz;
%iteration over all zones
for zone=1:l_zone
    eta_Ds=zeros(l_Hs,l_Tp);
    Uavg_s=zeros(l_Hs,l_Tp);
    %iteration over all sea states
    for h=1:l_Hs
        for tp=1:l_Tp
            %limiting to the states with high occurance
            if prob_s(zone,h,tp)/prob_tot>0.05
                %Defining the sea state
                head=Heading_sea(zone,h,tp);%180 is head waves
                if reg==1
                    lambda_div_L=Tpeak(zone,tp); %value to compare with Taskar
                    H_w=Hs(zone,h); %wave amplitude
                    S_w=H_w;
                    lambda_wave=lambda_div_L*Lpp;
                    frq_wave=sqrt(2*pi*g/lambda_wave); %rad/s
                    k_wave=frq_wave.^2/g;
                    Tpeak(zone,tp)=2*pi/frq_wave;
                    phi_wave=0;
                else
                    phi_wave=phi_wave_irr;
                    S_w=model_waves_irr(Hs(zone,h),Tpeak(zone,tp),frq_wave);%↙
generating wave spectrum
                end
                %getting the RAO for the right heading
                z1h=calc_centec_h(z1,heading_surge,head);
                z5h=calc_centec_h(z5,heading,head);
                RM_c_ph=calc_centec_h(RM_c_p,heading,head);
                Phi_AW_h=calc_centec_h(Phi_AW,heading,head);
                %determing an estimate of starting speed based on average added↙
```

```
restistance en KT polynomials
                U_est=U;
                count=1;
                U_est_old=U_est(1)+2*U_est*epsilon;
                while  count<2000 && abs(U_est-U_est_old)/U_est>epsilon
                    U_est_old=U_est;
                    Radd_avg= calc_Radd_avg(frq_wave,stepf,S_w,frq_Radd,Phi_AW_h,↙
U_Radd,U_est,reg);
                    U_est=estimate_U(U_est,U_est_old,U_data,t_still,w_still,R_still,↙
Radd_avg,rho,D,PD,AeA0,z,n,J);
                    U_est=(U_est+U_est_old)/2;
                    count=count+1;
                end
                %do the time simulation
                [Rtot,Q_efft,U_t,~,t_start,t] = simulate(stept,U_est,n,head,Lpp,M,↙
pt_p,z1h,frq_surge,U_surge,U_data,w_still,t_still,PD,AeA0,D,z,R_still,frq_Radd,↙
Phi_AW_h,U_Radd,stepf,frq_wave,k_wave,phi_wave,RM_c_ph,z5h,frq_RAO,reg,time_wave,↙
Tpeak(zone,tp),S_w,U_max,U_min,epsilon,g,rho);
                %starting time for averages
                start=max(0*60/stept,t_start);
                %Calculating the averages
                Uavg_s(h,tp)=mean(U_t(start:t));
                %Calculating effective power
                P_E=U_t.*Rtot;
                %Calculating delivered power at the shaft
                P_D=n*2*pi*Q_efft;
                %Calculating propeller specific efficiency eta_D for sea state s
                eta_D_fl=P_E(start:t)./P_D(start:t);
                eta_Ds(h,tp)=mean(eta_D_fl);
                if reg==1
                    frq_wave=[0.0005:stepf:1.5]';
                end
            else
                prob_s(zone,h,tp)=0;
            end
        end
    end
    % Calculating delivered efficiency for a zone/scatter, average speed in
    % the zone for a route and the estimated time the ship would sail in
    % the zone
    eta_Dz(zone)=sum(squeeze(prob_s(zone,:,:)).*eta_Ds,'all')/sum(squeeze(prob_s↙
(zone,:,:)),'all');
    Uavg_zone=sum(squeeze(prob_s(zone,:,:)).*Uavg_s,'all')/sum(squeeze(prob_s↙
(zone,:,:)),'all')
    time_z(zone)=dist_state(zone)/Uavg_zone;
end
eta_D=sum(time_z.*eta_Dz)/sum(time_z);
%this should avoid the memory problems
evalin('base','save(''eta_D'')');
evalin('base','clear');
evalin('base','load(''eta_D'')');
end
```

```
function [eta_D] = calc_eta_Dstill(x,U,Ua,Rstill,U_data,n,rho,z)
%Calculates the delivered efficiency in still water
%   input is propeller,
%   ship and advance speed,
%   propeller rps
%   still water resistance data
% Unpacking propeller char
AeA0=x(1);
PD=x(2);
D=x(3);
% Calculate advance coefficient
J=Ua/(n*D);
% Calculate effective power
if length(U_data)==1
 P_E=U*Rstill;
else
P_E=U*interp1(U_data,Rstill,U,'spline');
end
% Calculate KQ
KQ=calc_KQ_poly(J,PD,AeA0,z);
% Calculate delivered power
P_D=KQ*n^3*D^5*2*pi*rho;
% Calculate delivered efficiency
eta_D=P_E/P_D;
end
```



```
function [mot]=calc_mot_instant(time,x,stepf,frq,k_wave,phi_wave,S_RAO,reg,heading)
% Calculates the instanteous motion
%NOTE when regular wave, S_RAO is amplitude, frequencies are encounter frequencies
if reg==1
    Ampl=abs(S_RAO);
    phi=angle(S_RAO);
    mot=Ampl.*cos(frq*time-phi+k_wave*cos(heading/180*pi)*x);
else
    phi=angle(S_RAO); % Phases of motion amplitude
    mot=sum(sqrt(2*abs(S_RAO).*stepf).*cos(frq*time-phi-phi_wave'-k_wave*cos↙
(heading/180*pi)*x));
end

end
```

```
function [c,ceq] = calc_prop_still_invalid(x,z,Draft,Lpp,pt,n_min,n_max,P_min,P_max,↙
T_still,J,Ua,p_a,rho,g)
% Returns two values
%- c1 is negative if required engine speed is higher than minimal
%- c2 is negative if required engine speed is lower than maximal
%- c3 is negative if P_D is higher than minimal
%- c4 is negative if P_D is lower than maximal
%- c5 is negative if Burril 5% cavitation criterion fullfilled
%- the second value (ceq) should be given but not used thus empty is returned
% Checking if the service speed is attainable
[c1,c2,c3,c4,n] = check_service_speed_attainable(x,z,n_min,n_max,P_min,P_max,↙
T_still,J,rho,Ua);
% Checking cavitation
c5 = check_cav(x,Draft,Lpp,pt,Ua,n,T_still,p_a,rho,g);
c=[c1,c2,c3,c4,c5];
ceq=[];
end
```

```
function [Radd_avg] = calc_Radd_avg(frq_wave,stepf,S_w,frq_Radd,Phi_AW,U_Radd,U,reg)
% Calculates the average added resistance of the wave spectrum
%in case of regular waves S_w_interp=H_w
if reg==1
    Phi_AW_frq=interp1(frq_Radd,Phi_AW,frq_wave,'spline');
    if U<U_Radd(end)
        Phi=interp1(U_Radd, Phi_AW_frq,U,'spline',0);
    else
        Phi=Phi_AW_frq(end);
    end
    if Phi<0
        Phi=0;
    end
    Radd_avg=S_w^2*Phi;
else
    Phi_AW_U=frq_Radd;
    for f=1:length(frq_Radd)
        if U<U_Radd(end)
            Phi_AW_U(f)=interp1(U_Radd, squeeze(Phi_AW(f,:)),U,'spline',0);
        else
            Phi_AW_U(f)=  squeeze(Phi_AW(f,end));
        end
    end
    Phi_AW_interpU=interp1(frq_Radd,Phi_AW_U,frq_wave,'spline',0);
    %R_add average for spectrum
    S=2*Phi_AW_interpU.*S_w*stepf;
    Radd_avg=sum(S);
end
```

```
function [Radd]=calc_Radd_instant(frq_Radd,Phi_AW,frq_reg,U_Radd,U,Hw)
% Calculates added resistance based on a 'quasi' regular wave to imitate
% the fluctuates in sea state
%The procedure is proposed by Faltinsen et al. (1980) and used by Taskar(2016)
    if frq_reg>frq_Radd(end)
        Phi_AW_frq=squeeze(Phi_AW(end,:));
    else
    Phi_AW_frq=interp1(frq_Radd,squeeze(Phi_AW(:,:)),frq_reg,'spline');
    end
    if U<U_Radd(end)
        Phi=interp1(U_Radd, Phi_AW_frq,U,'spline',0);
    else
        Phi=Phi_AW_frq(end);
    end
    if Phi<0
        Phi=0;
    end
    Radd=Hw^2*Phi;
end
```



```
function [RAO_U]=calc_RAO_U(RAO,U_set,U)
% Calculates RAO for given speed
    if length(U_set)==1
        RAO_U=RAO;
    else
    RAO=RAO';
    RAO_U=interp1(U_set,RAO,U,'spline');
    end
end
```

```
function [eff_0prop] = calc_sol_still_eff_0(x,J,T,Ua,rho,z)
% Calculates open water efficiency for a given thurst and propeller
% Unpacking propeller char
AeA0=x(1);
PD=x(2);
D=x(3);
% Calculating the required KT/J^2 to deliver the required thrust
KT_div_J2_req=T/(D^2*rho*Ua^2);
% Calculating the KT/J^2 and efficiency curve of the propeller
[~,~,KT_div_J2,~,eff_0,indexJmax]=calc_poly(PD,J,AeA0,z);
KT_div_J2=squeeze(KT_div_J2);
eff_0=squeeze(eff_0);
indexJmax=squeeze(indexJmax);
% Finding open water efficiency for where the KT/J^2 polynomial is equal to the↙
required KT/J^2
eff_0prop=interp1(KT_div_J2(1:indexJmax),eff_0(1:indexJmax),KT_div_J2_req,'spline',↙
0);
end
```



```
function [S_prop_c] = calc_S_prop(S_w,frq_wave,frq_RAO,RM_c_p)
% Calculates motion spectrum
index=find(frq_wave>frq_RAO(end),1);
RM_interp=frq_wave;
if isempty(index)==0
    RM_interp(index:end)=complex(1*cos(pi),1*sin(pi));
    if index>1
    RM_interp(1:index-1)=interp1(frq_RAO,RM_c_p,frq_wave(1:index-1),'spline',0);
    end
else
    RM_interp=interp1(frq_RAO,RM_c_p,frq_wave,'spline',0);
end
S_prop_c= RM_interp.^2.*S_w;
end
```

```
function [T,Q] = calc_T_andQ(Beta,t_s,n,D,U_a,PD,AeA0,z,rho)
% Calculates the effective thrust and torque including ventilation losss.
%KT and KQ are calculated with KT and KQ polynomials of the B-series
% J is the vector of the J values for which there are points in the KT polynomials↙
in the matrix
    m=0.83; %less torque loss than thrust loss of factor Beta see fatilsen (1980)
    J=U_a/(n*D);
    KTmax=calc_KT_poly(0,PD,AeA0,z);
    KQmax= calc_KQ_poly(0,PD,AeA0,z);
    Jzero=fzero(@(x) calc_KT_poly(x,PD,AeA0,z),1);
    KQmin=calc_KQ_poly(Jzero,PD,AeA0,z);
    if J<0
        KT= KTmax;
        KQ= KQmax;
    else
        KT= calc_KT_poly(J,PD,AeA0,z);
        KQ= calc_KQ_poly(J,PD,AeA0,z);
    end
    if KT<0
        KT=0;
        KQ=KQmin;
    end
    T=(1-t_s)*Beta*KT*rho*n^2*D^4;
    Q=max(Beta^m*KQ*rho*n^2*D^5,KQmin*rho*n^2*D^5);
end
```



```
function [U] = calc_U(T_eff,Uold,stept,M,Rtot)
% Calculates the speed based on the dynamic equation for surge (1st law of Newton)
    U=stept/M*(T_eff-Rtot)+Uold;
end
```

```
function [Ua,V_fl_s1,V_fl_s2,factor] = calc_Ua_instant(w_p,U,frq_reg,frq_e_reg,z1,z5,pt,Lpp,heading,g,t_0up,time,Hw,rho)
% Calculates the advance speed in waves
%Principle of calculations of Radd used to determin Ua:
%    between each zero upcrossing the wave is modelled as a regular wave

% Calculating factor alpha
    alpha = calc_table_alpa(frq_reg,heading,Lpp,g);
% Calculating wave number
    k_wave = frq_reg.^2/g;
% Calculate the terms of V_fluct in frequency domain
    [V_fl_ct] = (1-w_p)*U; %_ct for constant term
    [V_fl_s1] = -(1-w_p)*frq_e_reg*abs(z1)*sin(frq_e_reg*(time-t_0up)-angle(z1));%first oscillating term of V_fluct
    [V_fl_s2] = alpha*frq_reg*Hw*exp(-k_wave*(-pt(3)))*cos(heading*pi/180)*cos(frq_e_reg*(time-t_0up)-k_wave*pt(1)*cos(heading*pi/180));
    delta_p=-rho/4*frq_e_reg^2*abs(z5)^2*pt(1)^2;
    [V_mean]=U*sqrt(1-delta_p/(0.5*rho*U^2));
    factor=V_mean/U;
% Calculaing Ua
    Ua=(V_fl_ct+V_fl_s1+V_fl_s2)*factor;
end
```



```
function [wave]=calc_wave_irr(time,x,stepf,w_wave,k_wave,phi_wave,S_w,heading)
% Calculates wave height in time domain for given wave spectrum
% Input:
% - time vector [s)]
% - x location of wave from the origin
% - stepsize of the frequency
% - wave frequencies to be used
% - phase between the wave frequencies
% - wave spectrum
% - l_s is number of sea states for which the wave height has to be
% Calculations
l_t=length(time);
% Calculate amplitude of each wave frequency
A=sqrt(2*abs(S_w).*stepf).*ones(1,l_t);
% Calculate pase each wave frequency in time and space domain
B=cos(w_wave.*time-phi_wave'.*ones(1,l_t)-k_wave*x*cos(heading/180*pi)*ones(1,l_t));
wave=sum(A.*B,1);
end
```

```
function [wave]=calc_wave_reg(time,x,w_wave,k_wave,H_w,heading)
% Calculating waveheight of regular wave
l_t=length(time);
l_d=length(x);
l_frq=length(w_wave);
w_wave1 = repmat(w_wave,1,l_d,l_t);
k_wave1 = repmat(k_wave,1,l_d,l_t);
time1 = repmat(time,l_frq,1,l_d);
time1=permute(time1,[1,3,2]);
x1 = repmat(x,l_frq,1,l_t);
wave=squeeze(H_w.*cos(w_wave1.*time1-k_wave1*cos(heading/180*pi).*x1));
end
```



```
function [z] = calc_z_c_angle(H_w,z_i,frq_zi,frq_wave)
% Calculates complex amplitude (distance) for a given RAO in regular wave
g=9.81;
k=frq_wave^2/g;
[frq_min,index]=min(frq_zi);
if frq_wave<frq_min
    z=H_w*complex(k.*cos(angle(z_i(index))),k.*sin(angle(z_i(index))));
else
    z=H_w*interp1(frq_zi,z_i,frq_wave,'spline',0);
end
end
```



```
function [z] = calc_z_c_dist(H_w,z_i,frq_zi,frq_wave)
% Calculates complex amplitude (distance) for a given RAO in regular wave
[frq_min,index]=min(frq_zi);
if frq_wave<frq_min
    z=H_w*complex(1.*cos(angle(z_i(index))),1.*sin(angle(z_i(index))));
else
    z=H_w*interp1(frq_zi,z_i,frq_wave,'spline',0);
end
end
```

```
function [c] = check_cav(x,Draft,Lpp,pt,Ua,n,T_still,p_a,rho,g)
%returns (Ae/A0)_min - Ae/A0
%(Ae/A0)_min  is the minimal ratio required accordiding to Burril 5% cavitation
% Unpacking propeller char
AeA0=x(1);
PD=x(2);
D=x(3);
% Calculating p_0-p_v
p_0p_v=p_a+rho*g*(Draft+pt(3)+0.0075*Lpp);
% Computing stagnation pressure
q=1/2*rho*(Ua^2+(0.7*pi*n*D)^2);
sigma_R=p_0p_v/q;
% Calculating Ae/A0 min
A0=pi*D^2/4;
AeA0_min=T_still/(A0*(1.067-0.229*PD)*(0.3*sqrt(sigma_R)-0.03)*q);
c=AeA0_min-AeA0;
end
```

```
function [c1,c2,c3,c4,n_theo] = check_service_speed_attainable(x,z,n_min,n_max,↙
P_min,P_max,T_still,J,rho,Ua)
% Unpacking propeller char
AeA0=x(1);
PD=x(2);
D=x(3);
% Calculating the required KT/J^2 to deliver the required thrust
KT_div_J2_req=T_still/(D^2*rho*Ua^2);
% Calculating the KT/J^2 curve of the propeller
[~,KQ_poly,KT_div_J2,~,~,indexJmax]=calc_poly(PD,J,AeA0,z);
KT_div_J2=squeeze(KT_div_J2);
KQ_poly=squeeze(KQ_poly);
indexJmax=squeeze(indexJmax)+1;
% Finding J for where the KT/J^2 polynomial is equal to the required KT/J^2
J_theo=interp1(KT_div_J2(1:indexJmax),J(1:indexJmax),KT_div_J2_req,'spline',0);
% Calculating the theoretical engine speed to deliver the required thrust.
n_theo=Ua/(J_theo*D);
% Finding KQ for where the KT/J^2 polynomial is equal to the required KT/J^2
KQ_theo=interp1(KT_div_J2(1:indexJmax),KQ_poly(1:indexJmax),KT_div_J2_req,'spline',↙
0);
% Calculating the theoretical delivered power
P_theo=KQ_theo*rho*n_theo^3*D^5*2*pi;
% Verify if n is withing the engine speed limits, both should be negative
c1= n_min-n_theo;
c2= n_theo-n_max;
% Verify if P is withing the engine power limits, both should be negative
if P_min==P_max
    c3=-1;
    c4=-1;
else
    c3=(P_min-P_theo)/(P_max-P_min);
    c4= (P_theo-P_max)/(P_max-P_min);
end
end
```

```
function [U_est] = estimate_U(U,U_data,t_still,w_still,R_still,Radd,rho,D,PD,AeA0,z,↙
n,J)
% Estimates the ship speed for a given propeller and ship resistance
% Getting the char for the given speed
t=interp1(U_data,t_still,U,'spline');
w=interp1(U_data,w_still,U,'spline');
Rstill=interp1(U_data,R_still,U,'spline');
Rtot=Rstill+Radd;
% Required thrust to maintain the given speed
T=Rtot/(1-t);
% Calculating required KT
KT=T/(rho*D^4*n^2);
% Calculating KT polynomial
[KT_poly,~,~,~,~,indexJmax] = calc_poly(PD,J,AeA0,z);
KT_poly=squeeze(KT_poly);
% Calculating advance coefficient for required KT
if KT>KT_poly(1)
    J_work=J(1);
else
    J_work=interp1(KT_poly(1:indexJmax),J(1:indexJmax),KT,'spline',0);
end
% Calculating advance speed for calculated advance coefficient
Ua=J_work*n*D;
% Calculating ship speed
U_est=Ua/(1-w);
end
```

```
% Selects the optimal propeller in still water and in the optimal in waves as↙
defined in main_setup_shipname
close all
clear
clc
% Start of the optimisation
main_setup_KVLCC2
% Initial guess of propeller
x0_still=[0.432,0.47,9.86];
% Boundary constraints
nonlcon=@(x)calc_prop_still_invalid(x,z,Draft,Lpp,pt_p,n_min,n_max,P_stillmin,↙
P_stillmax,T_still,J,Ua,p_a,rho,g);
A = [];
b = [];
Aeq = [];
beq = [];
lb=[AeA0min, PDmin, Dmin];
ub=[AeA0max, PDmax, Dmax];
% Selecting optimal propeller in still water
eta_0fun=@(x) 1/calc_sol_still_eff_0(x,J,T_still,Ua,rho,z);
options = optimoptions↙
(@fmincon,'Algorithm','sqp','Display','iter','PlotFcn','optimplotfval');
[opt_still,eta_0max] =fmincon(eta_0fun,x0_still,A,b,Aeq,beq,lb,ub,nonlcon,options);
eta_0max=1/eta_0max;
% Calculating the propeller rps
[~,~,~,~,n_stillopt] = check_service_speed_attainable(opt_still,z,n_min,n_max,↙
P_stillmin,P_stillmax,T_still,J,rho,Ua);
% Calculating the delivered efficiency in still water for the selected propeller
eta_Dstill = calc_eta_Dstill(opt_still,U,Ua,R_still,U_data,n_stillopt,rho,z);
% Calculating eta_D for the optimal propeller in still water
eta_optDstill = calc_eta_D(opt_still,z,J,U,U_max,U_min,Ua,M,Lpp,pt_p,z1,frq_surge,↙
heading_surge,U_surge,heading,frq_Radd,Phi_AW,U_Radd,U_data,t_still,w_still,R_still,↙
T_still,Tpeak,Hs,prob_s,dist_state,reg,stepf,frq_wave,k_wave,phi_wave_irr,time_wave,↙
stept,Heading_sea,frq,RM_c_p,z5,rho,g,epsilon);
% Selecting optimal propeller in sea state(s) water
eta_Dfun=@(x)1/calc_eta_D(x,z,J,U,U_max,U_min,Ua,M,Lpp,pt_p,z1,frq_surge,↙
heading_surge,U_surge,heading,frq_Radd,Phi_AW,U_Radd,U_data,t_still,w_still,R_still,↙
T_still,Tpeak,Hs,prob_s,dist_state,reg,stepf,frq_wave,k_wave,phi_wave_irr,time_wave,↙
stept,Heading_sea,frq,RM_c_p,z5,rho,g,epsilon);
[opt_wave,eta_Dmax]=fmincon(eta_Dfun,opt_still,A,b,Aeq,beq,lb,ub,nonlcon,options);
eta_Dmax=1/eta_Dmax;
% Calculating the propeller rps
[~,~,~,~,n_optwave] = check_service_speed_attainable(opt_wave,z,n_min,n_max,↙
P_stillmin,P_stillmax,T_still,J,rho,Ua);
% Calculating the open water efficiency in still water
eta_0wave=1/eta_0fun(opt_wave);
% Calculating the delivered efficiency in still water for the selected propeller
eta_Dwave = calc_eta_Dstill(opt_wave,U,Ua,R_still,U_data,n_optwave,rho,z);
```

```
% Initializing ship characteristics
% General constants
rho=1025; % density of sea water[kg/m^3]
g=9.81; %[m/s^2]
p_a=101.325*10^3; % [Pa] atmospheric pressure
% General model properties
Lpp=320; %[m]
B=58; %[m] breath of vessel
Draft=20.8; %[m]
Cb=0.8098; %taken from Taskar
m=312291.3*10^3; %[kg] mass of the ship obtained by delftship
m_add=m/(pi*sqrt(rho*Lpp^3/m)-14); %[kg] added mass for surge
M=m+m_add; %total mass for dynamic ship model
S=26978 ; %[m^2] wetter surface
pt_p = [-Lpp*0.98/2, 0, -0.045*Lpp]; %Given in Hamid "CFD verification and↙
validation of added resistance and motions of KVLCC2 with fixed and free surge in↙
short and long head waves"
Ukn_service=15.5; %[knts]
U=Ukn_service*0.514; %[m/s]
U_min=0; % simulation limit
U_max=100*0.514; % an upper limit to avoid errors shooting up to infinite speed
nRPM_max=110; % [rpm] maximal engine speed based on data engines MAN
nRPM_min=76; % [rpm] minimal engine speed based on data engines MAN
MCR=3.5*10^7; % P_E\0.5
P_stillmax=0.9*MCR;
P_stillmin=0.6*MCR;
n_max=nRPM_max/60; % [rps]
n_min=nRPM_min/60; % [rps]
z=4; %number of blades
mBeta=0.83; %less torque loss than thrust loss of factor Beta see fatilsen (1980)
% Getting the RAO ect except for surge
read_RAO_KVLCC2
% Getting the surge RAO based on the graph given in Taskar (2016)
RAO_surge
% Getting the added resistance data
read_Radd_KVLCC2
% Getting still water properties (still water resistance, wake factor, thrust↙
reduction factor)
versionyear=version('-release');
year=str2double(versionyear(1:4));
if year==2020
    read_still2020_KVLCC2
elseif year==2019
    read_still2019_KVLCC2
else
    fprintf('Matlab version might not be compabitble, it is advised to use 2019 or↙
2020 version')
    read_still2019_KVLCC2
end
Ukn_data=Dat_still(:,1);
U_data=Ukn_data*0.514;
R_still=Dat_still(:,2)*10^3;
w_still=Dat_still(:,3)./Dat_still(:,3)*0.375;
t_still=Dat_still(:,4);
```

```
% Calculting thrust, wake factor and advance speed at service speed in still water
T_still=interp1(U_data,R_still./(1-t_still),U,'spline');
ws=interp1(U_data,w_still,U,'spline');
Ua=(1-ws)*U;
% Setting up boundaries
J=0.05:0.01:2; % Starts not with 0 because we divide be J later on
PDmin=0.5; % Based on KT graph available
PDmax=1.4;
AeA0min=0.40;
AeA0max=1.00;
Dmax=2/3*Draft;
Dmin=Draft*0.3;
% Calculating RAO of relative motion at propeller
[RM_c_p] = calc_rel_mot_point(z3,z4,z5,frq,k_RAO,pt_p,heading);%_p is means at↙
propeller axis
% Defining trip parameters
reg=0; %defines if a regular waves or not for the whole simulation
read_in_sea_state_with_prob
% Hs=[5.5]; %specific wave height in case of irregular waves, wave amplitude for↙
regular waves
% Tpeak=[9.5]; %peak to peak period in case of irregular waves, lambda/L for regular↙
waves
% prob_s=[10^5]; %give in matrix format: Nzones x NHs x NTpeak
dist_state=[1]*10^3; %distance to cover in the sea state/zone
Heading_sea=[180]*ones(length(dist_state),length(Hs),length(Tpeak)); %in degrees,↙
give in matrix format: Nzones x NHs x NTpeak
prob_s=permute(repmat(prob_s,[1,1,2]),[3,1,2]);
prob_s=prob_s(1,:,:);
% Defining simulation parameters
epsilon=0.001; %[m/s] error margin of the speed
stept=0.1; % [s] stepsize for time
seconds=20*60; %time of waves
time_wave=(0:stept:seconds);
stepf=0.0005; %[rad/s] stepsize for frequencies of wave spectrum (irr waves)
frq_wave=[0.0005:stepf:1.5]'; %frequency range of irr wave spectrum
k_wave=frq_wave.^2/g;
phi_wave_irr=rand(1,length(frq_wave))*2*pi; %random phase shift between different↙
regular waves
```

```
function [S_w]=model_waves_irr(Hs,Tpeak,frq)
% Makes a spectrum of waves according to ISSC
    l_w=length(frq);
    l_s=length(Hs);
    w_peak=2*pi./Tpeak; %rad/s
    S_w=zeros(l_s,l_w);
    for i=1:l_s
       S_w(i,:)=0.313*Hs(i).^2.*w_peak(i).^4.*exp(-1.25*(w_peak(i)./frq).^4)./(frq.↙
^5);
    end
    S_w=S_w';
end
```

```
function [Rtot,Q_efft,U_t,time_run,t_start,t] = simulate(stept,U,n,heading,Lpp,M,↙
pt_p,z1,frq_surge,U_surge,U_data,w_still,t_still,PD,AeA0,D,z,R_still,frq_Radd,↙
Phi_AW,U_Radd,stepf,frq_wave,k_wave,phi_wave,RM_c_p,z5,frq_RAO,reg,time_run,Tpeak,↙
S_w,U_max,U_min,epsilon,g,rho)
%Simulates the ship with given propeller in specific sea state
%Note S_w is used as H_w for regular waves because less double coding
% Setting up variable size
l_t=length(time_run);
U_t=zeros(1,l_t);
Q_efft=U_t;
Rtot=U_t;
X=U_t; % Distance ship has sailed (X-position)
% Start at 2 peak tot peak periods from zero time this ensures the past zero-↙
upcrossing has no negative time
t_start=round(2*Tpeak/stept);
if reg==1
    t_start=1;
    t_0up=t_start;
    frq_0up=frq_wave;
    Aw=S_w;
end
% Initial variable values
U_t(t_start)=U; %[m/s] estimated start velocity, not perfect because only takes into↙
account the effect of added resistance
t=t_start;
% Loop for time simulation stops before end of time because the next zero upcrossing↙
should be before the end time
while time_run(t)<time_run(end)-2*Tpeak
    if t>t_start
        U_t(t)=U_t(t-1);
        X(t)=X(t-1)+U_t(t-1)*stept;
    end
    count=0;
    U_old=U_t(t)+2*epsilon*U_t(t)+1; %plus one is to avoid problems when U_t(t) is↙
close to zero
    % Calculate the wave height out of interest
    if reg==1
        H_w=calc_wave_reg(time_run(t),X(t),frq_wave,k_wave,S_w,heading);
    elseif reg==0
        H_w=calc_wave_irr(time_run(t),X(t),stepf,frq_wave,k_wave,phi_wave,S_w,↙
heading);
        % Calculate the 'quasi' regular wave properties of the sip
        [t_0up,frq_0up,Aw] = calc_0upcrossing(time_run,t,X(t),stepf,frq_wave,k_wave,↙
phi_wave,S_w,heading);
    end
    % Iterations to approximate the ship speed in each time step
    while abs(U_old-U_t(t))/U_t(t)>epsilon && U_t(t)<U_max && U_t(t)>=U_min &&↙
count<2000 %iterate for every timestep until speed is constant for the time step or↙
when speed is higher than max for wich we have data or lower than the data lower↙
limit
        % Calculate encounter frequency or quasi regular wave
        frq_0up_e=calc_frq_e(frq_0up,U_t(t),heading,g);
        % Getting the RAO for the right speed
        RM_c_pU=calc_RAO_U(RM_c_p,U_Radd,U_t(t));
```

```
        z1U=calc_RAO_U(z1,U_surge,U_t(t));
        z5U=calc_RAO_U(z5,U_Radd,U_t(t));
        % Surge amplitude complex for quasi regular wave
        Surge_c=calc_z_c_dist(Aw,z1U,frq_surge,frq_0up);
        % Pitch amplitude complex for regular wave
        Pitch_c=calc_z_c_angle(Aw,z5U,frq_RAO,frq_0up);
        % Relative motion spectrum/amplitude
        if reg==1
            S_prop_c=calc_z_c_dist(S_w,RM_c_pU,frq_RAO,frq_wave);
        elseif reg==0
            S_prop_c = calc_S_prop(S_w,frq_wave,frq_RAO,RM_c_pU);
        end
        % Calucalting relative position of the propeller shaft at time t
        h_R=calc_mot_instant(time_run(t),X(t),stepf,frq_wave,k_wave,phi_wave,↙
S_prop_c,reg,heading);
        % Calculating loss factor beta (ventilation)
        Beta=calc_Beta_instant(D,h_R,pt_p);
        % Calculating wake and thrust reduction factor
        w_s=interp1(U_data,w_still,U_t(t),'spline');
        t_s=interp1(U_data,t_still,U_t(t),'spline');
        % Calculating advance speed
        [U_at,~,~,~]= calc_Ua_instant(w_s,U_t(t),frq_0up,frq_0up_e,Surge_c,Pitch_c,↙
pt_p,Lpp,heading,g,t_0up,time_run(t),Aw,rho);
        % Calcultating the effective thrust and torque
        [T_efft,Q_efft(t)]=calc_T_andQ(Beta,t_s,n,D,U_at,PD,AeA0,z,rho);
        % Calculating total resistance
        Rstill=interp1(U_data,R_still,U_t(t),'spline');
        Radd_e=calc_Radd_instant(frq_Radd,Phi_AW,frq_0up,U_Radd,U_t(t),Aw);
        Rtot(t)=Rstill+Radd_e;
        % Calculating the speed of the vessel
        U_old=U_t(t);
        if t==t_start
            U_sol=calc_U(T_efft,U_t(t),stept,M,Rtot(t));
        else
            U_sol=calc_U(T_efft,U_t(t-1),stept,M,Rtot(t));
        end
        U_t(t)=(U_sol+U_old)/2;
        count=count+1;
    end
    t=t+1;
end
t=t-1;% Counted one too much, now t is last index of calculations in loop
% Reducing the used memory
clearvars -except Rtot Q_efft T_efft U_t U_at Beta time_run t_start t
end
```